Feasibility study for fresh water storage in saline aquifers by means of the Fresh Storage Saline Extraction well, with a focus on the Red Sea coast, Egypt

Graduation project Marloes van Ginkel

Delft University of Technology

Faculty of Civil Engineering and Geosciences

Delft University of Technology mentors

Prof.dr.ir.Th.N. Olsthoorn

Dr.ir.M. Bakker

Dr.ir.L.C. Rietveld

Dutch Egyptian Consortium Aquifer Storage Recovery

DEC ASR mentor

Drs.E. Smidt

Delft, December 2007

Preface and Acknowledgement

This report presents the results of the graduation project carried out to complete the master program Water Management at Delft University of Technology, faculty of Civil Engineering and Geosciences. The graduation project, performed for the Dutch Egyptian Consortium Aquifer Storage Recovery (DEC ASR), investigates the feasibility of fresh water storage in saline aquifers by means of Fresh Storage Saline Extraction (FSSE) wells.

The examination committee guiding this project consisted of prof.dr.ir.Th.N. Olsthoorn and dr.ir.M. Bakker of the Geohydrology group of the Water Resources section of the TU Delft, dr.ir.L.C. Rietveld as the third TU Delft- supervisor, and drs.E. Smidt as external member and project team leader of the DEC ASR.

Hereby I would like to thank all committee members for the opportunity they gave me to do this project, and for their enthusiasm and the support and advices they gave me during my graduation.

My time in Egypt was very pleasant and useful due to the good company of Evert Witkop and the continuous good care of Dr. Raouf Darwish, Dr. Salah Rashwan, Prof. Dr. Abdul Shata and Dr. Safaa Moustafa Mouhamed Soliman. Dr. Raouf Darwish organized two very interesting field trips which were also nice and pleasant. Dr. Salah Rashwan was a good teacher in Egyptian water management. Dr. Abdul Shata taught me about the Egyptian geology. And Dr. Safaa Moustafa Mouhamed Soliman taught me the basics of groundwater flow modeling with Visual MODFLOW. I am grateful to the management of the Egyptian Research Institute for Groundwater, Dr. Ahmed Khater and Dr. Nahed El Arabi, for giving me the opportunity to work at their institute. I have worked together with the Egyptian Research Institute for Groundwater for two weeks and I like to thank my colleagues, too many to mention everybody individually.

I would like to thank the directors and engineers of the drinking water plants El Gouna, Nefertary, Port Ghalib, Equinox and Cataract for their hospitality and time, their explanation on the plant operations and for all the information they have provided so kindly.

Special thanks for Christian Langevin for his quick responses on all my burning modeling questions regarding SEAWAT. To Joris Meijerink for his help with my Matlab struggles. And to Ed Veling for his help on the analytical solution.

Finally I would like to express my gratitude to my family, boyfriend, house mates, 4.93 room mates and all my wonderful friends for giving me all the love and support I needed to complete this project.

Delft, 12/12/07,

Marloes van Ginkel

Summary

This research is a feasibility study to determine whether fresh water storage in saline aquifers is possible by means of a Fresh Storage Saline Extraction (FSSE) well. The focus is on the situation prevailing along the Egyptian Red Sea coast, where fresh water is produced for tourist resorts by desalination of local groundwater, mostly as saline as seawater. Storing fresh water in the subsurface during low demand periods and recovering it in periods of high demands increases the efficiency of desalination in this area. However, subsurface storage of the fresh desalinated water is a challenge due to the lower density of this water compared to the ambient salt groundwater. This density difference causes the stored fresh water to float up to the ceiling of the aquifer and spread out to be lost within weeks if just left to its own. However, it can be kept in place around the well by continuous pumping of salt water from below the stored cone-shaped bubble using the same well (FSSE-well).

This report analyses FSSE-well storage systems from the point of view of groundwater hydraulics to examine their geohydrologic feasibility and to learn how to successfully apply such systems in practice. The research is performed for the Dutch Egyptian Consortium Aquifer Storage Recovery. The analysis was done by means of deriving a mathematical solution to the problem followed by numerical modeling of representative situation using SEAWAT.

The results of the research show that it is possible to store fresh water in and recover it from a saline aquifer by means of a FSSE-well. The fresh water bubble can be kept in place around the well by continuous extraction of salt water at a limited rate of about 10% of normal extraction rates. Separate screens are necessary to resist the establishment of a seepage face causing continuous mixing with salt water. The salt water extraction rate and the radius of the bubble can be calculated with an analytical formula derived in this research.

An interface is created between the injected fresh water and the salt water in the aquifer. During storage periods 4% fresh water is lost per month due to hydrodynamic dispersion for the cases considered. It is possible to infiltrate and recover the water in different injection-storage-recovery cycles. The recovery efficiency increases in successive cycles. The recovery efficiency in the first cycle is 50%, in the second cycle 67% and in the third cycle 80% for the cases considered.

The storable and recoverable volume is dependent on the characteristics of the aquifer. FSSE-wells favor thick aquifers (in the order of 20-30 m). Heterogeneity of the aquifer may be critical and needs to be determined in the field. Ambient groundwater flow has a substantial influence on the recovery efficiency. It is possible to recover the bubble after an unmanaged period of no pumping in the order of one week (calamity or maintenance) for the case considered. A field experiment should be carried out before FSSE-wells can be used on large scale. It is to be recommended to investigate the advantages of fresh water storage combined with subsurface energy storage or wastewater storage.

Storing fresh water by means of FSSE-wells is an innovative way of making use of the economic settings and the groundwater physics that go with the density differences between fresh and salt water. The application of FSSE-wells could increase the sustainability of desalination plants.

Table of contents

1 Introduction

This research is on the feasibility of storage of fresh water in saline aquifers to reduce the costs of desalination for potable water production. The underlying assumption is that storing fresh water in the subsurface during periods of low demand and recovering it in periods of high demands increases the sustainability of desalination of brackish or salt water.

The focus is on the Egyptian Red Sea coast area, where, like other arid coasts, tourist resorts are booming and need fresh water. Because no fresh water is available, it is produced by desalination of local groundwater, which is generally about as saline as seawater. Because of strong seasonal demand fluctuations and the high costs of these plants, water storage can save money. Subsurface storage has the benefit of the large space available and the absence of evaporation and sunlight heating. Subsurface water storage may also be substantially cheaper than water storage above ground using expensive manmade tanks of steel or concrete. However, subsurface storage of the fresh desalinated water is a challenge due to the lower density of this water compared to the ambient salt groundwater. This density difference causes the stored fresh water to float up to the ceiling of the aquifer and spread out to be lost within days to weeks if just left to its own. However, it can be kept in place around the well by continuous pumping of salt water at a limited rate from below the stored cone-shaped bubble using the same well (FSSE-well, Figure 4, page 8). This continuous pumping of salt water is no loss in these systems as the fresh water produced from it is sold to the consumer also in low demand times. Hence, storage of fresh water in saline aquifers to bridge demand variations is theoretically feasible in these settings, where a base demand is always there to consume the fresh water that is produced from the continuous pumping necessary to keep the stored water trapped around the wells. Therefore, this way of storing fresh water is an innovative way of making use of the economic settings and the groundwater physics that go with the density differences between fresh and salt water.

This report analyses these systems from the point of view of groundwater hydraulics to examine their geohydrologic feasibility and to learn about the operations and design criteria necessary to make such systems a success in practice. Although important, economics are not the focus of this report. Where an economic analysis is necessary results of relevant studies will be used.

The research is performed for the Dutch Egyptian Consortium Aquifer Storage Recovery (DEC ASR). End 2006, Smidt Groundwater BV took the initiative to assemble Dutch and Egyptian experts to realize subsurface storage of desalinated water to improve the efficiency of desalination plants in tourist resorts along the Egyptian Red Sea and Mediterranean coasts. This initiative builds on twenty years experience with artificial recharge in Egypt. A consortium was formed comprised of Dutch and Egyptian companies and institutions: Van Essen Instruments (A Schlumberger Company), Waternet, Kiwa Water Research, SG Consultancy and Mediation, Darwish Consultants Engineers, and the Egyptian Research Institute for Groundwater. Goal of the first phase of this project is identifying locations and interests in Egypt, and carrying out a feasibility study that should lead to a pilot location in a second phase of the project. A grant has been obtained from the Netherlands' Partners for Water Fund of the agency of the Dutch Ministry of Economic affairs (EVD) for the first phase of the project. This phase started January

2007 and finished in September 2007. It is envisioned to carry out a pilot study in the second phase of the project.

The questions of the DEC ASR and their clients to the researcher were: What is the behavior of stored fresh water in a saline environment? What is the recovery rate and cycle efficiency? Both questions will be answered in this research.

The research was carried out at Delft University of Technology. The project locations in Egypt were visited by the researcher in April and May 2007. The daily supervisors were prof.dr.ir.Th.N. Olsthoorn and dr.ir.M. Bakker from the Geohydrology group of the Water Resources section, dr.ir.L.C. Rietveld was the external supervisor, and drs.E. Smidt was the project leader of the DEC ASR.

This report presents the results of the research. It is divided in eight chapters. This introduction is the first chapter. Chapter 2 defines the problem and study objectives. Chapter 3 describes the used geohydrological theory. Chapter 4 contains the mathematical analysis to the problem. Chapter 5 describes the numerical model set-up in SEAWAT while its results are presented in Chapter 6. Chapter 7 contains two case studies of Nefertary and Port Ghalib, Red Sea coast. Finally, the conclusions and recommendations are in Chapter 8.

2 Problem description

This research is performed in the framework of the DEC ASR. The objective of this consortium is to realize ASR to improve the economic efficiency of desalination plants in tourist resorts along the Egyptian Red Sea and Mediterranean Coasts. In section 2.1 the ASR principle is explained. In section 2.2 the characteristics of Egypt are described especially the tourism sector and their fresh water availability. The problem is outlined in section 2.3 and the research question is described in section 2.4.

2.1 Aquifer Storage Recovery

In situations with seasonal fluctuations in water availability and water demand, storage could be used to bridge peak demands. Adequate storage may be the key to sustainable water management, by overcoming water shortages and especially during drought spells. There may be sufficient overall amounts of water available in many cases; however, storage is necessary to be able to use it [Pyne, 2007]. When water is stored in an aquifer with the purpose to extract it later, the storage principle is called ASR, or Aquifer Storage Recovery, which may be defined as the storage of water in a suitable aquifer by a well during times when water is available, and subsequent recovery of water by the same well during times when it is needed [Pyne, 2007]. This principle is shown in Figure 1.

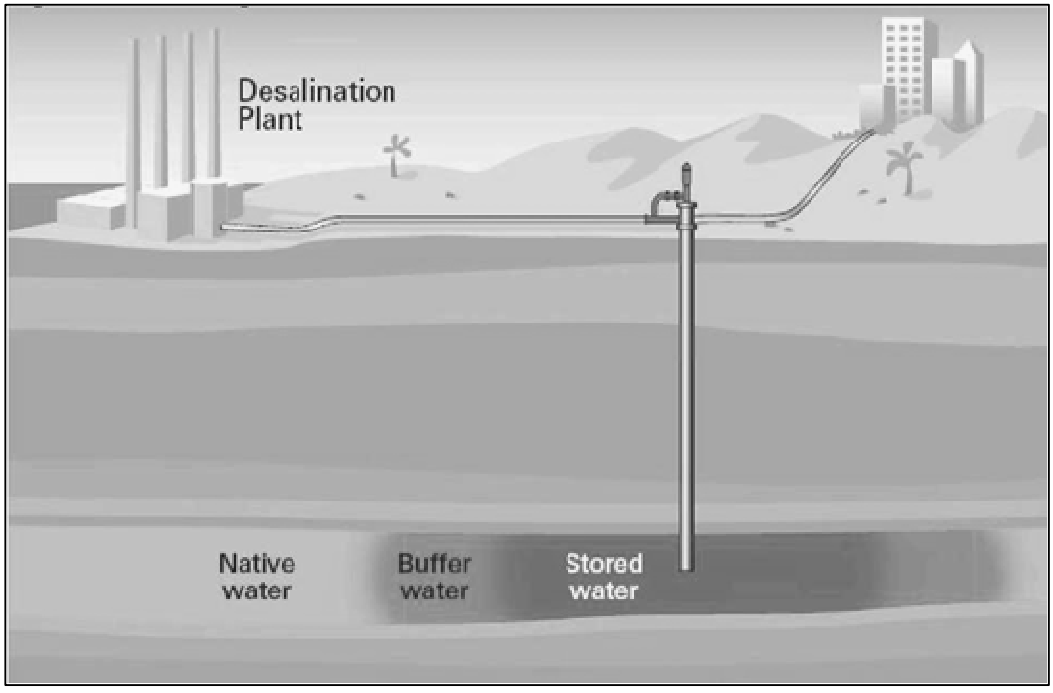

Figure 1: Aquifer Storage Recovery principle [DEC ASR, 2007], desalinated water is stored in an aquifer and used during high demand periods.

ASR is sometimes classified as a form of Artificial Aquifer Recharge. However, this term seems to become more restricted to continuous systems such as those widely used in the Netherlands by drinking water companies. In the Netherlands, river water is infiltrated after treatment in a shallow sand aquifer in the Dutch dune area along the North Sea. The water travels underground for 30 to 400 days. During that time water quality is improved by subsurface processes and pathogens are eliminated. The water is subsequently extracted and post-treated to drinking water.

ASR refers to a time-limited storage of water in aquifers. The water is injected by wells and usually extracted again at a later time by the same wells. In Florida, USA, ASR is used for seasonal storage of river water and rainwater [Buros and Pyne, 1994]. In the Netherlands, province of South Holland, a hundred or so horticulturists inject rain water from the roofs of their green houses in a shallow semi-confined brackish aquifer for use during the summer growing season. A literature study on ASR can be found in Appendix A.

2.2 Egypt

Egypt is located in the northeast corner of Africa. The country is bordered by the Mediterranean Sea in the north, Libya in the west, Sudan in the south and Israel, Palestine/Gaza and the Red Sea in the east. The total surface of Egypt is 1 million km^2 of which only 0.6% is water [Ministry of Tourism, Egypt, 2007].

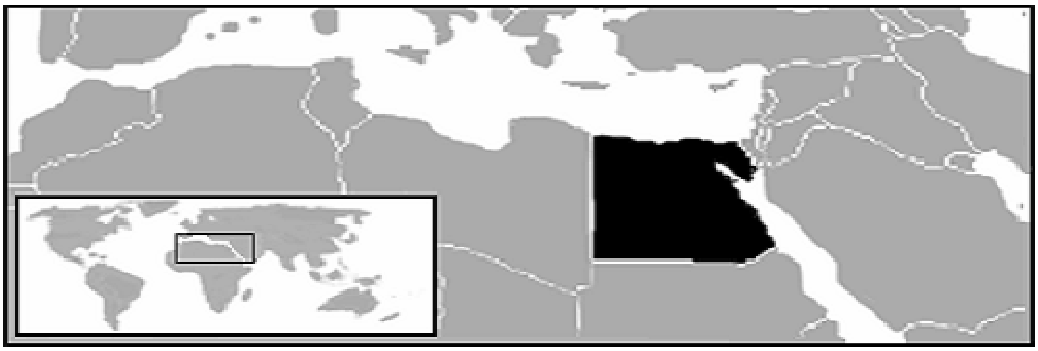

Figure 2: Location of Egypt.

The climate of Egypt is determined by its location on the border of the largest desert in the world. Its latitude position, between 22 °N and 32 °N, place it in the sub-tropical belt, although conditions on the northern coast are influenced by the presence of the Mediterranean Sea.

According to data of the FAO (2007) the mean annual temperatures in Egypt are high and register between 20 and 25 °C. Major variations occur between summer and winter temperature, as well as between coastal and inland locations. Along the Mediterranean coastal strip the temperature varies between 25-30 °C in summer and 10-18 °C in winter and the average annual rainfall varies between 100-200 mm/yr. Over the rest of Egypt the mean temperatures in summer are much higher than at the coastal strip reaching 37-42 °C. The temperatures in winter are lower with values of 5-20 °C. Over most of the interior of Egypt it is not unusual for a year to pass without any significant precipitation at all being recorded. Unfortunately, relatively little accurate information is available on evaporation and

transpiration in Egypt. The data available for class 'A' evaporation pans at Giza and Aswan [FAO, 2007] reveals maximum daily values in June of 12.9 mm at Giza and 19.3 mm at Aswan. At Aswan the annual pan loss is close to 5 m, or about double that recorded at Giza.

Egypt has a population of currently 76 million people, growing 1.80% annually [Ministry of Tourism, 2007]. 95% of the Egyptians live less than 20 km from the Nile, on its fertile banks and in the Nile valley; Cairo (around 17 million) and Alexandria (around 4.5 million).

According to the World Bank (2007) Egypt is a lower middle income country, meaning that 17% of total population lives below poverty line. The growing economy seeks to increase income from tourism. The history of the Pharaohs reaching back 3100 years, the many archeological sites and its cultural heritage make Egypt one of world's foremost cultural travel destinations [Shalaan, 2005]. Due to the beautiful beaches, unique coral reefs and marine life, the Red Sea coast has been identified as priority zone for tourism development [El-Sadek and Mabrouk, 1992].

Since the Red Sea region has been targeted for massive tourism development around 1990, the number of rooms has grown spectacularly, reaching 10,500 in the year 2000 (22% of the country) with 140,000 as the target for 2012. The majority of the resorts are in a 300km long coastal stretch with about 50-300 m coastal setback depending on the shoreline conditions [Shalaan, 2005.]. Fresh groundwater is absent or insufficient to supply the tourist areas with potable water making desalination of seawater and groundwater necessary to satisfy fresh water needs [El-Sadek and Mabrouk, 1992].

The desalination plants along the Red Sea coast typically produce water for one resort or a cluster of hotels, which have a fresh water demand of less than 1500 m^3/d, i.e. Nefertary (500 m^3/d), Equinox (300 m^3/d) and Cataract (1400 m^3/d). This situation favors the small-size Reverse Osmosis (RO) plants, with production capacities ranging between 200 and 3000 m^3/d. RO-plant capacities beyond 3000 m^3/d are limited to the main towns, i.e. El Gouna (6000 m^3/d), Hurghada, Safaga, Port Ghalib (3000 m^3/d) and Mersa Alam. The RO-desalination capacity in the Red Sea area increased from less than 20,000 m^3/d in 1980 to about 140,000 m^3/d in 2001 [Hafez and El-Manharawy, 2002].

With membrane filtration, water is pressed through an extremely thin film with small pores against the osmotic pressure, hence the name Reverse Osmosis. RO is used to remove virtually all dissolved salts and organic micro-pollutants from water. It is always preceded by a pre-treatment step to remove particulate matter. The desalinated water has an extremely low mineral content [De Moel et al., 2006]. Therefore, this so-called 'permeate' is sometimes conditioned using limestone filtration and aeration to correct its pH and remove its aggressiveness relative to metals and lime. The Egyptian drinking water standard for *Cl* is 500 ppm [Attia and Smidt, 1999]. This standard is higher than the WHO guideline for drinking water, 250 ppm [WHO, 2006] or the Dutch guideline of only 150 ppm.

Desalinated water is the most expensive source of water when compared with other more natural fresh water sources, but if natural water has to be pumped over long distances (several hundreds of kilometers) it can become just as expensive [Lamei et al., 2007]. According to Dabbagh (2001) the efficient management of desalinated water supply is becoming more and more important. While further improvements in desalination processes are certainly desirable and need to be researched and developed, it is becoming even more important that desalinated water be managed efficiently given the already large number of existing desalination plants in Egypt.

The seasonal fluctuation of fresh water demand of the hotels, villages and resorts along the Red Sea coast is large and coincides with the seasonal character of tourism. The production rates in 2006 of the 4 visited locations are shown in Figure 3. The data acquired during the field trips in April and May 2007 to the drinking water plants of El Gouna, Nefertary, Port Ghalib, Equinox and Cataract is given in Appendix B.

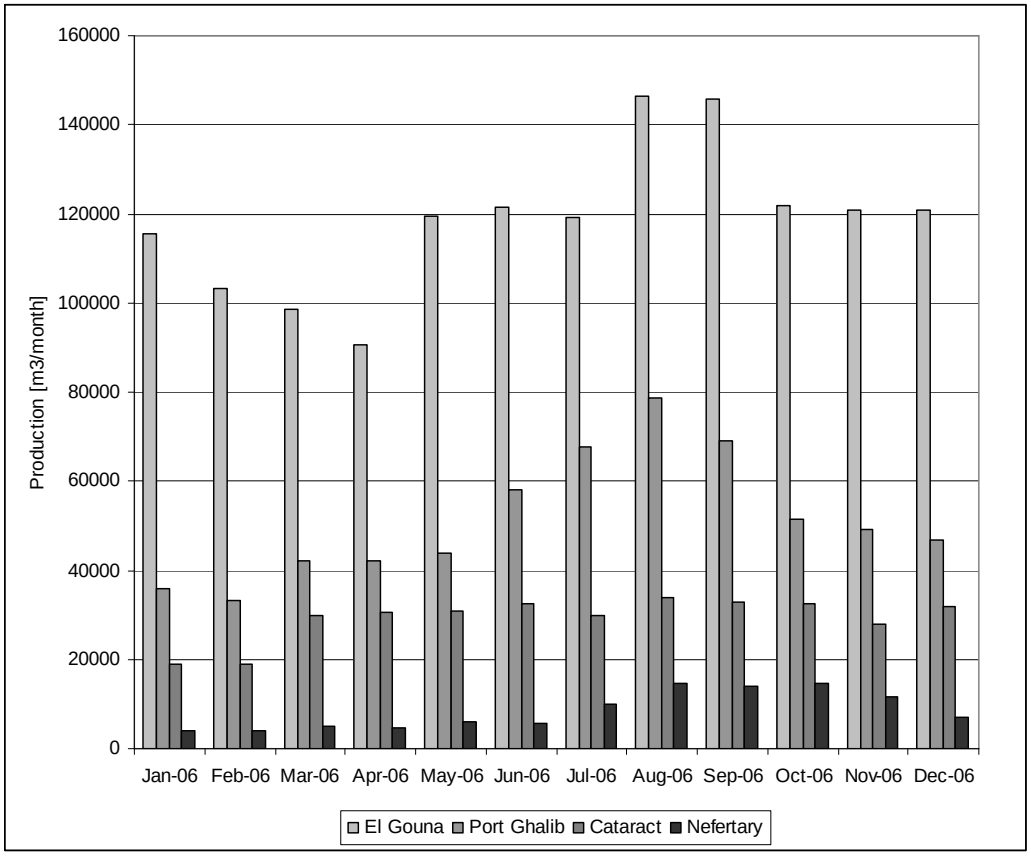

Figure 3: Production rates per location for the year 2006.

Storage could improve the efficiency of the desalination plants. Instead of increasing the production capacity every year to match peak demand, the plants may run on one even production if enough water can be stored during low demand periods for use in times of high demand. The DEC ASR has investigated the savings per unit production cost by introducing ASR in relation to desalination plant capacity. The savings for a desalination plant with a capacity of 3000 m^3/d can be 10% [DEC ASR, 2007].

2.3 Problem

Subsurface storage of desalinated water using ASR is a promising solution to improve the efficiency of the desalination plants along the Red Sea coast of Egypt. Injected fresh water displaces the native salt water in the aquifer during injection. On the fringes mixing will take place, due to diffusion and dispersion, and a mixing zone between the two water types develops, separating the injected fresh water in the bubble from the salt water in the surrounding aquifer. However, the density difference between fresh and salt water poses a challenge as it tends to float the stored fresh water upward to the top of the aquifer where it may be hard or impossible to recover at a later stage. This problem may be less evident in well-known systems with continuous recharge of fresh rainwater, causing a permanent fresh water lens to float on saline deeper water in a permanent dynamic fashion. In Egypt we only store small amounts of fresh water and further, we do not inject continuously during the storage phase. Moreover, there is no precipitation to maintain a permanent fresh water lens. Hence, under the Egyptian conditions the fresh water bubble will float up, so that the fresh water bubble will become a thin layer on top of the saline aquifer in a matter of days to weeks.

According to Bear (1978) the storage of a bubble of fresh water in a saline aquifer is possible if the interface is maintained dynamically. The essence of the matter is that a groundwater velocity difference across the interface between the stored fresh water and the present salt water must be maintained. The inclination of the interface can be calculated with the following formula:

$$\sin\alpha = \frac{\rho_s}{\rho_s - \rho_f}\frac{v_f - v_s}{k} \tag{1}$$

Where ρ_s and ρ_f are the density of the salt water and the fresh water respectively [ML^{-3}], v_s and v_f are the velocity tangential to the interface of the salt water and the fresh water respectively [LT^{-1}] and k is the hydraulic conductivity [LT^{-1}].

This implies that the inclination of the interface is maintained as long as there is a groundwater velocity difference between the stored fresh and the present salt water. The interface will be horizontal when the velocity difference equals zero, i.e. when no injection of fresh water or flow of salt water occurs. The stored water will be trapped around the well as long as we inject fresh water or extract salt water to maintain this velocity difference.

The principle of salt water extraction is visualized in Figure 4, showing an aquifer with a Fresh Storage Saline Extraction (FSSE) well with two screens. With the upper screen fresh water is injected into the aquifer. In this figure, the fresh water is in its stagnant storage phase, while salt water is being extracted with the lower screen. A velocity difference between stored fresh and present salt water is thus maintained keeping the interface in place. This looks like the technique of scavenger wells in Pakistan (Appendix A).

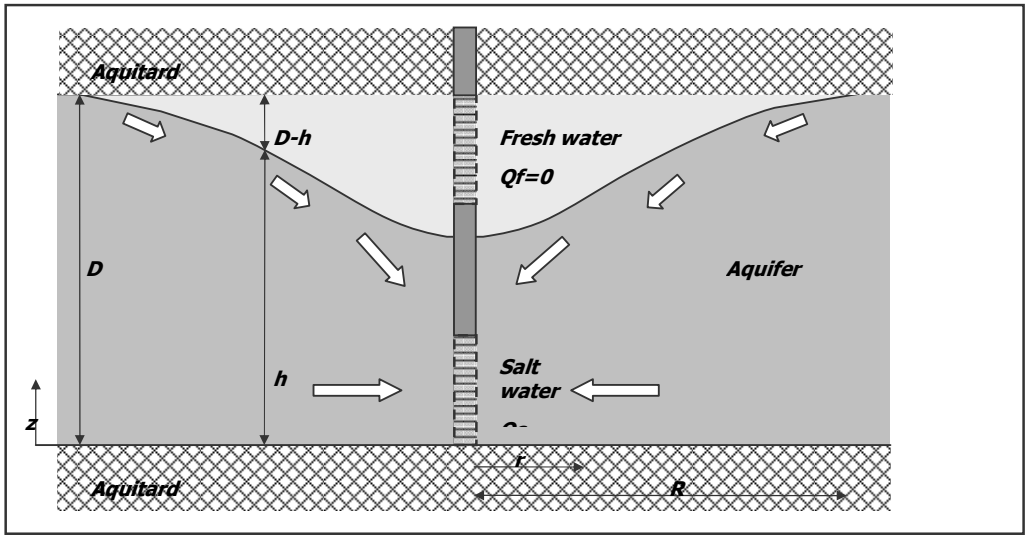

Figure 4: Fresh Storage Saline Extraction (FSSE) well in a confined aquifer during the storage phase.

2.4 Objective and research question

The objective of this research is to perform a feasibility study to determine whether fresh water storage in saline aquifers is possible by means of the Fresh Storage Saline Extraction well, with a focus on the situation prevailing along the Red Sea coast of Egypt.

The research question of this master project is whether fresh water can be stored in and recovered from a saline aquifer by means of a Fresh Storage Saline Extraction well.

The answer to the research question was sought by means of a mathematical solution to the problem followed by a numerical model built with SEAWAT.

3 Theoretical background

The basic physical theory is presented in this chapter. In the first section the hydrological cycle and occurrence of groundwater are described. In section 2 relevant properties of the aquifer are given. In the third section the basic equations of motion and for continuity of mass are derived. Section 4 gives a description of groundwater wells, steady-state flow to groundwater wells in confined and unconfined aquifers and the deviation caused by partially penetrating wells. The occurrence of fresh and salt water is described in section 5 dealing with the seepage face inside the well and the mixing processes.

3.1 Hydrological cycle and groundwater occurrence

The hydrological cycle demonstrates how water circulates from the oceans through the atmosphere and back to the sea by different paths, either overland or underground (Figure 5). These paths may range from short to long, both in terms of time and distance traveled.

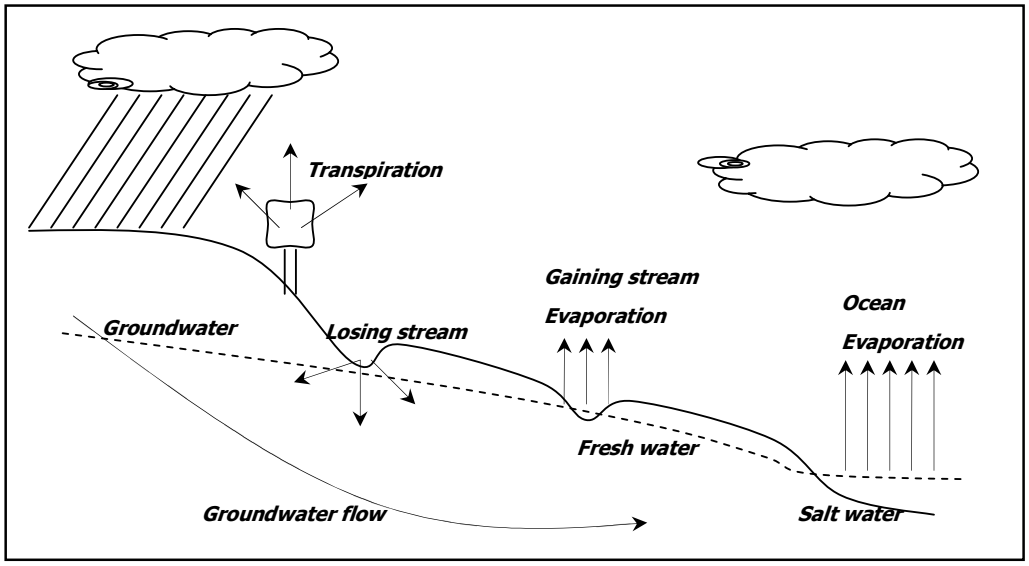

Figure 5: Hydrological cycle.

The term groundwater may be used to denote all the waters found beneath the surface of the earth [Bear, 1978]. It forms an important portion of the hydrological cycle. Water-bearing formations in the earth's crust act as a media for the transmission and as a reservoir for the storage of water.

Sources of natural recharge of groundwater are precipitation (rain, snow and ice), loosing streams, irrigation return flow, leakage from irrigation canals and artificial recharge. Seawater can originate from previous transgressions or it may also stem from evaporation in lagoons or salt lakes and from upconing due to shallow extraction or outflow.

Infiltrated water moves downward through the unsaturated zone under gravity until it reaches the saturated zone. It then moves predominantly in horizontal direction as determined by the surrounding

hydraulic situation [Fitts, 2002]. The voids in the unsaturated zone are filled with water and air; those in the saturated zone are completely filled with water.

Discharge of groundwater occurs when water emerges from the aquifer. Most natural discharge occurs as flow into surface water bodies, streams, lakes and oceans. Groundwater hardly evaporates only when it is shallow as in marshes. Pumping wells are the major artificial discharge of groundwater.

Groundwater flows through sand and gravel layers, called aquifers, which are defined as water-bearing layers for which the porosity and pore size are sufficiently large to allow transport of water in appreciable quantities [e.g. Bear, 1978]. Aquifers are separated by semi- and impermeable layers called aquitards.

3.2 Aquifer properties

The porosity of a subsurface formation n [-] is the volume of voids per volume of bulk subsurface. In this research mainly the effective porosity is used. The effective porosity of a subsurface formation n_e [-] is the volume of voids able to transmit water per volume of bulk subsurface. The hydraulic conductivity k [LT^{-1}] is the capacity of a material to transmit water. The hydraulic conductivity is proportional to the square of the effective grain size, for which often the 10% diameter is taken as determined in a sieve test. In Table 1 common porosity and hydraulic conductivity values for different aquifer materials are given.

Table 1: Aquifer properties [Fitts, 2002], porosity and conductivity values.

Aquifer material	Porosity [-]	Conductivity [m/d]
Gravel	0.15-0.35	40-60
Sand	0.20-0.45	20-40
Silt	0.35-0.50	0.1-10
Clay	0.40-0.60	0.001-0.1

3.3 Groundwater flow equations

Water always flows from regions with higher energy towards regions with lower energy. The energy per weight of water is the total head.

$$H = z + \frac{p}{\rho_w g} + \frac{v^2}{2g} \tag{2}$$

This equation describes the total head H [L] of water with elevation z [L], pressure p [$ML^{-1}T^{-2}$], the density of the fluid ρ_w [ML^{-3}], the gravitational acceleration g [LT^{-2}] and velocity v [LT^{-1}].

The three terms on the right side of equation 2 are called elevation head, pressure head and velocity head, respectively. Water always flows towards regions of lower hydraulic head. In most cases the

velocity head is generally negligible compared to the other two terms, so equation 2 may be reduced to the hydraulic head *h* [L] for groundwater flow:

$$h = z + \frac{p}{\rho_w g} \tag{3}$$

Groundwater loses energy every interval it travels. The displacement rate depends on the resistance and the loss of energy over the interval. Darcy gave an empirical formula for the relationship between flow and head gradient in 1856 (equation 4).

Uniform density

Darcy's Law in 3D in the case of uniform density and the conductivity tensor aligned with the direction of the axes is:

$$\begin{aligned} q_x &= -K_x \frac{\partial h}{\partial x} \\ q_y &= -K_y \frac{\partial h}{\partial y} \\ q_z &= -K_z \frac{\partial h}{\partial z} \end{aligned} \tag{4}$$

Where the quantity $\vec{q} = (q_x, q_y, q_z)$ is known as the specific discharge vector [LT^{-1}], and K_x, K_y, K_z [LT^{-1}] represent the components of hydraulic conductivity tensor in the respective coordinate directions.

The equation of Continuity of Mass for uniform density flow can be written as:

$$S_s \frac{\partial h}{\partial t} = -\frac{\partial q_x}{\partial x} - \frac{\partial q_y}{\partial y} - \frac{\partial q_z}{\partial z} + q_s \tag{5}$$

Where S_s [L^{-1}] is the specific storage and q_s [T^{-1}] is the fluid sink/source term.

Substitution of equation 4 for the components of the specific discharge vector in equation 5 gives:

$$\frac{\partial}{\partial x}\left(K_x \frac{\partial h}{\partial x} \right) + \frac{\partial}{\partial y}\left(K_y \frac{\partial h}{\partial y} \right) + \frac{\partial}{\partial z}\left(K_z \frac{\partial h}{\partial z} \right) + q_s = S_s \frac{\partial h}{\partial t} \tag{6}$$

Which is the governing partial differential equation for groundwater flow with uniform density and the conductivity tensor aligned with the *x,y,z*-axes.

Variable density

Fresh water head is defined as:

$$h_f = \frac{p}{\rho_f g} + z \tag{7}$$

Where *z* is elevation head [L] and ρ_f [ML^{-3}] is the fresh water density.

Darcy's Law in 3D in the case of variable density and the permeability tensor aligned with the direction of the axes is in terms of fresh water head:

$$\begin{aligned} q_x &= -K_{fx}\frac{\partial h_f}{\partial x} \\ q_y &= -K_{fy}\frac{\partial h_f}{\partial y} \\ q_z &= -K_{fz}\left(\frac{\partial h_f}{\partial z} + \frac{\rho - \rho_f}{\rho_f}\right) \end{aligned} \tag{8}$$

The terms K_{fx}, K_{fy}, K_{fz} are the equivalent fresh water hydraulic conductivities of the aquifer to the flow along the *x,y,z* directions, respectively. K_{fx} is defined by:

$$K_{fx} = \frac{k_x \rho_f g}{\mu} \tag{9}$$

Where μ is the viscosity of the water, and k_x is the intrinsic permeability in the *x*-direction. K_{fy}, K_{fz} are similarly defined using k_y, k_z.

Substitution of equation 8 for the specific discharge vector in equation 5 gives the partial differential equation for groundwater flow with variable densities and the conductivity tensor aligned with the *x,y,z*-axes:

$$\frac{\partial}{\partial x}\left(\rho K_{fx}\frac{\partial h_f}{\partial x}\right) + \frac{\partial}{\partial y}\left(\rho K_{fy}\frac{\partial h_f}{\partial y}\right) + \frac{\partial}{\partial z}\left(\rho K_{fz}\left(\frac{\partial h_f}{\partial z} + \frac{\rho - \rho_f}{\rho_f}\right)\right) = \rho S_s \frac{\partial h_f}{\partial t} + n_e \frac{\partial \rho}{\partial C}\frac{\partial C}{\partial t} - \rho_s q_s \tag{10}$$

Where ρ [ML^{-3}] is the density of the groundwater, ρ_f [ML^{-3}] is the fresh water density, and ρ_s [ML^{-3}] is the density of the water added or removed, S_s [L^{-1}] is the specific storage, n_e represents aquifer porosity, C [ML^{-3}] is the solute concentration, q_s [T^{-1}] is the fluid sink/source term. The term $\rho S_s \left(\partial h_f / \partial t\right)$ describes the rate of mass per unit volume of aquifer due to storage effects, the term $n_e \partial\rho\partial C / \partial C\partial t$ describes the rate of mass per unit volume of aquifer due to changing solute

concentration, and $\rho_s q_s$ gives the rate at which mass is added or removed, per unit of volume, by sources or sinks.

3.4 Groundwater wells

Extraction of groundwater from a well results in a cone of depression of the head around the well. The opposite happens when injecting water. The amount of depression is called drawdown, which diminishes with distance from the well [e.g. Fitts, 2002]. Groundwater can occur in confined, semi-confined and unconfined aquifers. A confined aquifer is completely filled and covered as well as underlain by an impervious layer; there is no free water table in the aquifer, the water is confined. A semi-confined aquifer is an aquifer covered or underlain by a semi-pervious layer and also completely filled with water. Aquifers with a free water table are called unconfined or phreatic.

3.4.1 Steady state flow to a well

The solution for radial flow to a well can be derived by combining Darcy's Law and the mass balance. The discharge of the well Q_o [L^3T^{-1}] is by convention positive for a well that removes water from the aquifer and negative for a well that injects water into the aquifer. With mass balance, this same discharge must be flowing through any cylinder at a distance *r* from the well.

$$Q_o = 2\pi r k h \frac{dh}{dr} \tag{11}$$

For unconfined flow, taking *h* upward from the assumed flat bottom of the aquifer:

$$\frac{Q_o}{2\pi k}\frac{dr}{r} = h dh \tag{12}$$

And for confined flow, in case the aquifer thickness is constant and equals *D*:

$$\frac{Q_o}{2\pi kD}\frac{dr}{r} = dh \tag{13}$$

Integrating both sides,

$$h^2 = \frac{Q_o}{\pi k}\ln(r) + C \tag{14}$$

Or for confined flow using *Ddh* in (12) instead of *hdh*:

$$h = \frac{Q_o}{2\pi kD}\ln(r) + C \tag{15}$$

The constant *C* must be obtained by applying a suitable boundary condition i.e. *h* given at a certain distance *R*.

3.4.2 Partial penetration

In the equations for flow to a well of section 3.4.1, the well penetrates the entire thickness of the aquifer. This causes the flow to be essentially horizontal. However, due to vertical flow components near the well, the flow will be three dimensional with partially penetrating wells (Figure 6).

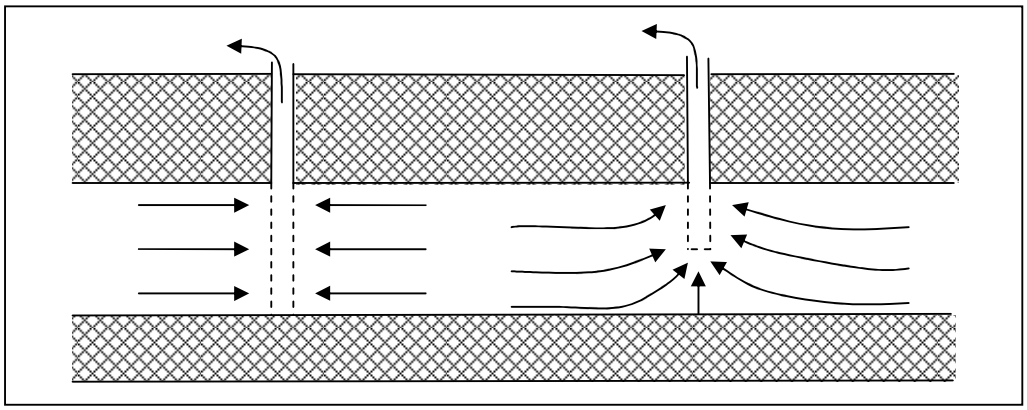

Figure 6: A fully penetrating pumping well (left) and a partially penetrating pumping well (right).

The flow close to the well will then not satisfy the equations of section 3.4.1. It causes extra drawdown in the vicinity of the well. The effect of partial penetration on the drawdown will be minimal when the radial distance from the pumping well is 1.5 times the thickness of the aquifer in isotropic aquifers. The FSSE-well used in this research consists of 2 partially penetrating wells. In the model partially penetrating wells are dealt with through sufficient vertical refinement of the model network. The influence of the partial penetration is shown in Chapter 6, Results.

3.5 Fresh and salt groundwater

Groundwater classification as fresh or saline depends on its intended use and translates to the density of the fluid [Fitts, 2002]. Fresh water contains a low concentration of dissolved salts, while salt water contains a significant concentration which is usually expressed in parts per million (the weight of salt in 1 kg water), a classification is shown in Table 2. The density of fresh water is 1000 kg/m^3. Seawater has a higher density than fresh water. The density of seawater varies between 1020-1035 kg/m^3, depending on circumstances as nearly river inflow (North Sea) or excess evaporation (Red Sea).

Table 2: Classification for water salinity based on dissolved salts [Bear, 1978].

Fresh water	<500 ppm
Brackish water	500 – 30.000 ppm
Salt water	30.000 - 50.000 ppm
Brine	>50.000 ppm

3.5.1 Seepage face

Seepage face for single density flow

A seepage face forms along a well bore when the head in the well is below the top of the open well screen. The seepage face is visualized in Figure 7. There is a small area needed to change the direction of the flow lines. The seepage face is the difference between the water table in the well and the phreatic surface at the well. Along the seepage face $p = 0$ and so the head equals z. The boundary condition is therefore $h = z$. This implies that where the water table intersects the seepage face (black dot in Figure 7) the water table, which also has $p = 0$, must be tangent to the seepage face i.e. vertical. This implies that the vertical velocity must equal $-k_z$ at this point. However, below the water table the head is constant and so the vertical specific discharge component must be zero. At the water table the vertical specific discharge suddenly changes from $-k_z$ to zero. The total specific discharge must turn from vertical at the top of the seepage face to zero below it. This is only possible in a smooth way if the horizontal flow component at the water table in the well has infinite value as is shown in Figure 7.

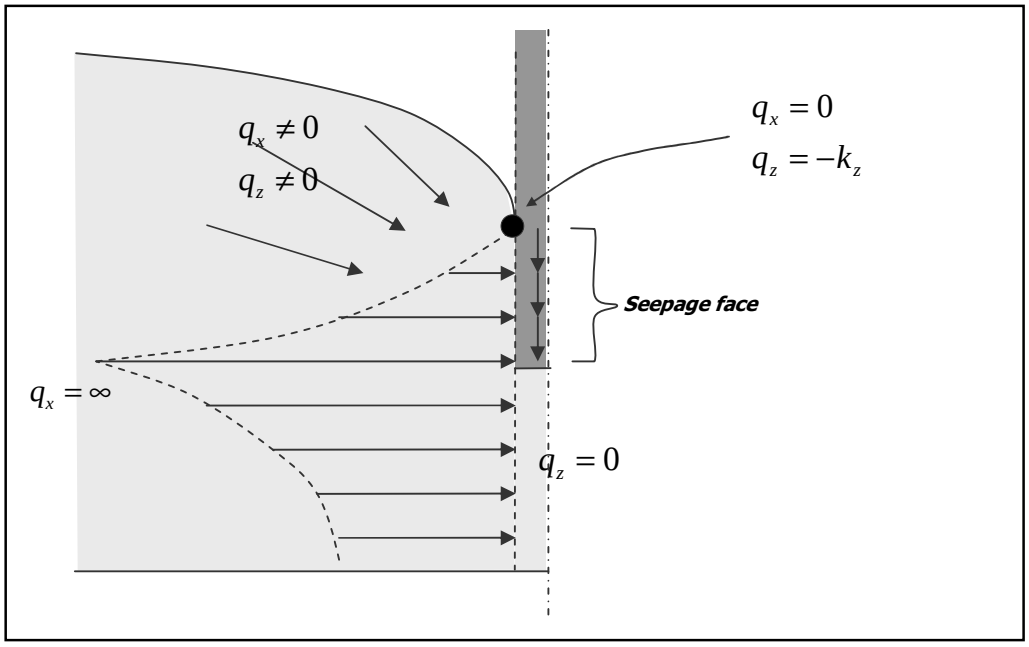

Figure 7: Radial symmetric cross section of a well with an open well screen and a seepage face along the well bore.

Seepage face for fresh and salt water

The seepage flow is an important characteristic when designing storage of fresh water floating on salt water. In the case of fresh water floating on salt water a seepage face develops naturally as it does with any fluids having a different density and velocity difference across their interface [Olsthoorn, 2007]. As an important consequence, also for so-called scavenger wells, in case of an open well screen incoming salt water will continuously mix with resident fresh water (Figure 8).

Therefore, the design of a FSSE-well storage system requires a blind length of casing at the elevation of the interface to prevent inflow of salt water directly into the fresh water. Even then there is still the risk that the interface inside the well descends into the lower screen. To prevent this, there should be a packer inside the casing to completely separate the fresh and the salt water.

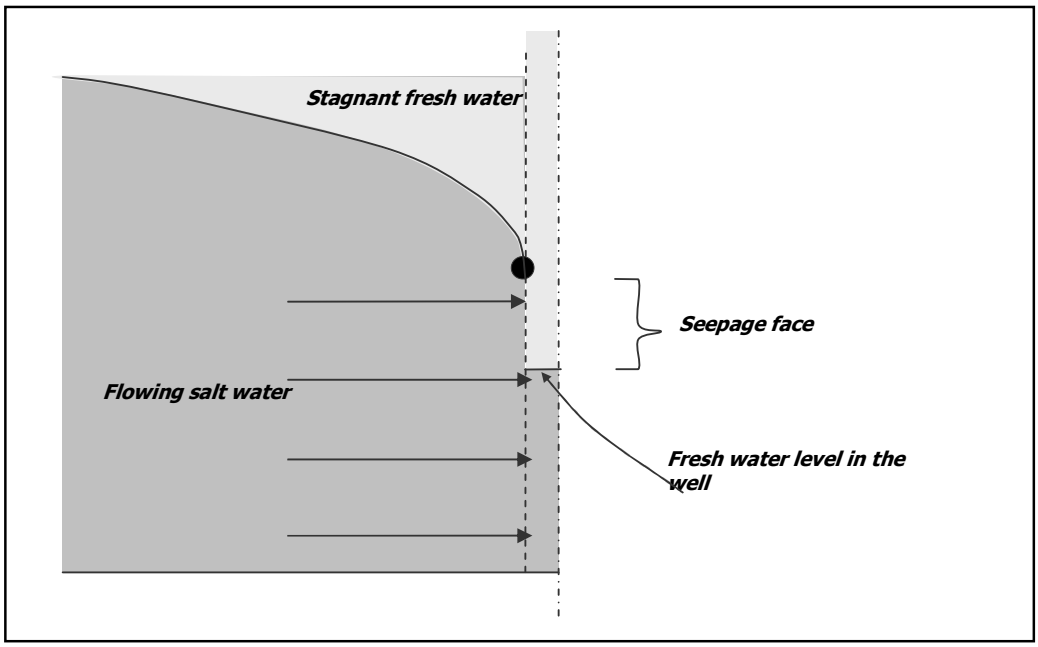

Figure 8: Radial symmetric cross section of a well with an open well screen, with a fresh-salt water interface and a seepage face along the well bore.

3.5.2 Fresh-salt water interface: a mixing zone

For the studied situation, fresh water is injected into a saline aquifer. The fresh water displaces the native salt water in the aquifer. A mixing zone will develop at that interface, separating the injected fresh water in the bubble from the salt water in the surrounding aquifer. This mixing zone is the result of the transport processes diffusion and dispersion.

Advection

The main transport mechanism is advection. When groundwater flows, solutes flow along with the water possibly delayed by sorption and ion exchange, which are ignored here as salinity is de facto determined by *Cl* which does not adhere to grain surfaces. The amount of solute transported by advection then follows from Darcy's Law as the product of specific volume flux q [LT^{-1}] times the solute concentration C [ML^{-3}]:

$$\vec{F}_{adv} = C\vec{q} \tag{16}$$

Where $\vec{F}_{adv}$ is the advective solute flux [$ML^{-2}T^{-1}$].

Advection may change the shape of a polluted region, but the concentration remains unchanged. The plume size grows linearly with time $(\Delta x = vt)$ if there is only advection.

$$\frac{\partial C}{\partial t} = -\nabla \vec{F}_{adv} \tag{17}$$

On micro scale the displacement is more complicated. Instead of straight flow lines, we observe a highly variable flow along curved flow lines. Reasons for this variability are: the velocity in the middle of a pore is higher than at the grain surface; not all pores have the same diameter; and not all pores have the same direction [i.e. Boekelman et al., 2002]. Consequently, the solute displaces irregularly and mixing occurs by molecular diffusion and mechanical dispersion.

Molecular diffusion

Molecular diffusion is due to random movement of ions [Oude Essink, 2001]. It will smooth concentration gradients even without any flow occurring. The relation between the diffusive flux and the concentration gradient is given by Fick's Law:

$$\vec{F}_{dif} = -nD_d \nabla C \tag{18}$$

The change of concentration with time for diffusion can be written with the formula:

$$\frac{\partial C}{\partial t} = -\nabla \vec{F}_{dif} \tag{19}$$

Where $\vec{F}_{dif}$ is the diffusive mass flux [$ML^{-2}T^{-1}$], n is the porosity of the aquifer, D_d is the coefficient of molecular diffusion corrected for the pore structure [L^2T^{-1}] and C [ML^{-3}] the solute concentration.

The process is driven by differences in concentration, independent of flow. The standard deviation of the spread σ of an initially sharp concentration front increases with time t according to:

$$\sigma = \sqrt{2D_d \Delta t} \tag{20}$$

Mechanical dispersion

Mechanical dispersion is due to the flow in a homogeneous medium. The process occurs due to the different magnitude and orientation of the velocity in the pores. Not all particles travel over the same distance or in the same direction. The result is a more intense mixing [Oude Essink, 2001]. The dispersion coefficient is proportional to the magnitude of the velocity of the groundwater. The relation between the dispersive flux of solute mass and the concentration gradient is given by:

$$\vec{F}_{dis} = -nD_m \nabla C \tag{21}$$

Where $\vec{F}_{dis}$ is the dispersion mass flux [$ML^{-2}T^{-1}$], n the porosity of the aquifer, D_m is the coefficient of mechanical dispersion [L^2T^{-1}] and C [ML^{-3}] is the solute concentration.

The change of concentration with time due to dispersion can be written with the formula:

$$\frac{\partial C}{\partial t} = -\nabla \vec{F}_{dis} \tag{22}$$

The dispersion coefficient is proportional to the magnitude of the velocity of the groundwater. The standard deviation of the spread σ in longitudinal and transversal direction of an initially sharp concentration front increases with time t according to:

$$\sigma_L = \sqrt{2a_L \vec{v} t} \text{ and } \sigma_T = \sqrt{2\alpha_T \vec{v} t} \tag{23}$$

Where $\vec{v}$ is the groundwater velocity $\vec{v} = \vec{q} / n_e$. The parameters α_L and α_T are the longitudinal and transversal dispersivity. In general longitudinal dispersivity is five to ten times higher than the transversal dispersivity.

Hydrodynamic dispersion

Both dispersion and diffusion have a smoothing influence on differences in concentration. Hydrodynamic dispersion is the combined effect of the two processes. The hydrodynamic dispersion coefficient is expressed by $D_h = D_d + D_m$. The hydrodynamic dispersion is an important characteristic when designing fresh water floating on salt water. A mixing zone of brackish water will develop. The hydrodynamic dispersion may be estimated in terms of the standard deviation of the dispersion front, using $\alpha_L \vec{v} >> D_d$:

$$\sigma = \sqrt{2\left(D_d + \alpha_L \vec{v}\right) t} = \sqrt{2\alpha_L \vec{v} t} \tag{24}$$

Which after flowing over a distance L becomes:

$$\sigma = \sqrt{2\alpha_L L} \tag{25}$$

Equation of Solute Transport

The equation of solute transport describes the transport of solutes and the change in density. The equation of solute transport is a combination of the previous equations which described the change of concentration with time for advection, diffusion and dispersion (equations 17, 19, 22). Hence, it is also known as the advection-dispersion equation. This partial differential equation can be written as:

$$\frac{\partial C}{\partial t} = \frac{\partial}{\partial x_i}\left(D_{ij} \frac{\partial C}{\partial x_j} \right) - \frac{\partial}{\partial x_i}\left(C v_i \right) + \frac{q_s C_s}{n_e} + \sum R_e \qquad (26)$$

Where C is the dissolved concentration of species [ML^{-3}], v_i is the linear pore water velocity [LT^{-1}], D_{ij} is the hydrodynamic dispersion tensor [L^2T^{-1}], q_s is the source or sink flux [LT^{-1}], C_s is the concentration of the source or sink flux [ML^{-3}] and $\sum R_e$ is the chemical reaction term [$ML^{-3}T^{-1}$].

4 Mathematical analysis

In this chapter a mathematical analysis is given of the principles of the FSSE-well. Section 4.1 contains an analysis of the flow to a FSSE-well. In section 4.2 the analytical solution is derived.

4.1 Analysis of flow to FSSE-well

To analyze this type of storage analytically FSSE-wells are considered in an unconfined (Figure 9) and in a confined aquifer (Figure 10) in radial symmetric cross section. There are 2 partially penetrating well screens with a certain distance between them to prevent the occurrence of a seepage face within the well screen (section 3.5.1). In the figures the fresh water bubble is in its storage phase. It is assumed that a given volume of desalinated water *V* has been injected and does not change during the storage period.

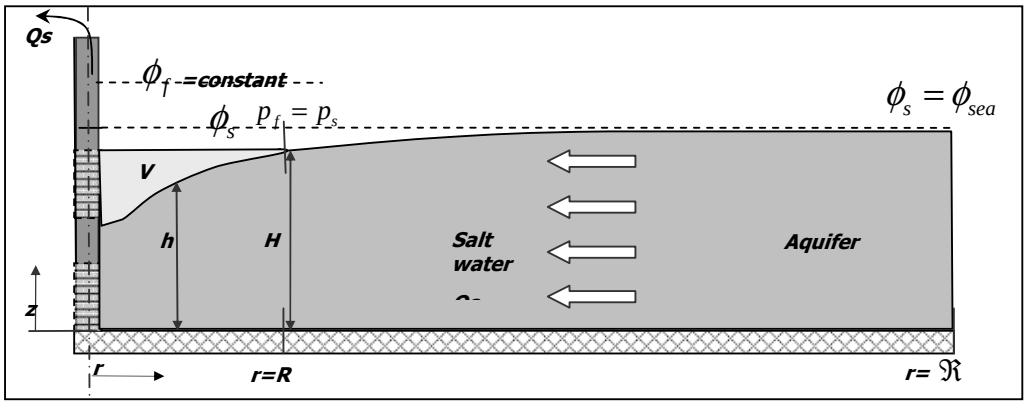

Figure 9: Radial symmetric cross-section of a FSSE-well in an unconfined aquifer.

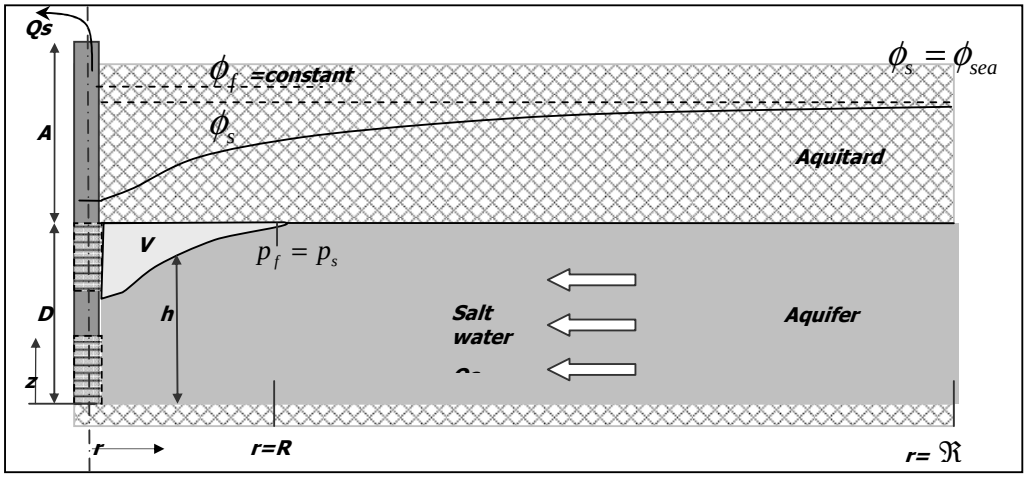

Figure 10: Radial symmetric cross-section of a FSSE-well in confined aquifer.

Two situations can be distinguished:

- $0 < r < R$: The situation can be seen as unconfined flow with the bottom of the bubble as the free salt water table.
- $R < r < \Re$: The situation can be seen as standard unconfined or confined flow as derived in section 3.4.1.

The analytical solution for the salt water head *h* for $0 < r < R$ is given in the following section.

4.2 Analytical solution

To analyze this type of flow analytically a radially symmetric cross section with the well in its center is considered. The analysis below considers only the fresh water bubble during its storage period. It is assumed that a given volume of desalinated water has been injected and does not change during the storage period. This situation is assumed steady state; the salt groundwater flow Q_s [L^3T^{-1}] towards the well is constant at any distance $r < R$ [L] and further given by Darcy's Law:

$$Q_s = 2\pi rkh\frac{d\phi_s}{dr} \tag{27}$$

Where *k* is the horizontal conductivity [LT^{-1}], *h* the distance of the saline water table above the base of the aquifer [L] and ϕ_s the salt water head [L].

The fresh water pressure is equal to the salt water pressure at $r = R$.

$$\left(\phi_f - H\right)\rho_f = \left(\phi_s - H\right)\rho_s \tag{28}$$

Where *H* [L] is the static fresh water head measured relative to the base of the aquifer.

At $r < R$ where the fresh water pressure equals the salt water pressure along the interface it follows that $\left(\phi_f - h\right)\rho_f = \left(\phi_s - h\right)\rho_s$. The salt water head can then be written as:

$$\phi_s = \frac{\rho_f}{\rho_s}\phi_f + \frac{\rho_s - \rho_f}{\rho_s}h \tag{29}$$

With $\upsilon_s = \left(\rho_s - \rho_f\right)/\rho_s$ it follows that $\frac{d\phi_s}{dr} = \upsilon_s\frac{dh}{dr}$. Substitution in Darcy's Law:

$$Q_s = 2\pi rk\upsilon_s h\frac{dh}{dr} \tag{30}$$

This equation may be solved by integration:

$$hdh = \frac{Q_s}{2\pi k\upsilon_s}\frac{1}{r}dr \tag{31}$$

$$h = \sqrt{\frac{Q_s}{\pi k \upsilon_s} \ln r + C} \tag{32}$$

And solve for C by applying as boundary condition for the unconfined case at $r = R, h = H$, the distance of the salt water table above the base of the aquifer *h*, becomes:

$$h = \sqrt{H^2 + \frac{Q_s}{\pi k \upsilon_s} \ln\left(\frac{r}{R}\right)} \tag{33}$$

Or for the confined case with as boundary condition at $r = R, h = D$,

$$h = \sqrt{D^2 + \frac{Q_s}{\pi k \upsilon_s} \ln\left(\frac{r}{R}\right)} \tag{34}$$

The volume of the fresh water bubble V can be calculated by integration of its thickness between the well radius r_w and R, with the following formula:

$$V = 2\pi n_e \int (D - h)\, r dr \tag{35}$$

Yielding

$$V = 2\pi n_e \int_{r_w}^{R} \left(D - \sqrt{D^2 + \frac{Q_s}{\pi k \upsilon_s} \ln\left(\frac{r}{R}\right)} \right) r dr = 2\pi n_e \int_{r_w}^{R} \left(a - \sqrt{b \ln cr} \right) r dr \tag{36}$$

Where for the unconfined case $a = H$, $b = Q_s / (\pi k \upsilon_s)$ and $c = \exp\left(H^2 \pi k \upsilon_s / Q_s R\right)$ and for the confined case $a = D$ and $c = \exp\left(D^2 \pi k \upsilon_s / Q_s R\right)$.

The result of this integral is:

$$V = \frac{1}{4} \pi n_e \left[\left(a - \sqrt{b \ln cr} \right) 4r^2 + \left(2\sqrt{2}\sqrt{b} r^2 \right) F(x) \right]_{r_w}^{R} \tag{37}$$

With $F(x)$ the Dawson function which is defined as:

$$F(x) = e^{-x^2} \int_0^x e^{t^2} dt \tag{38}$$

With $x = \sqrt{2}\sqrt{\ln cr}$

The fresh water volume V was calculated for different salt water extraction discharges Q_s and radii of the fresh water bubble R. The equation is also solved by numerical integration. The answer of the analytical solution fits the numerical solution as can be seen in Figure 11. The Matlab script is given in Appendix C.

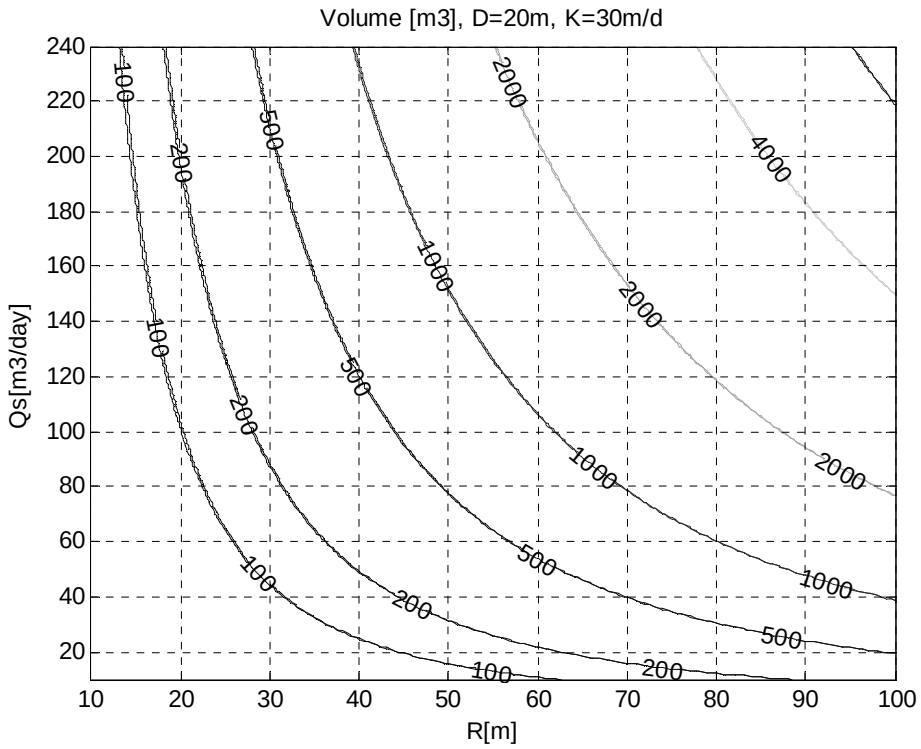

Figure 11: Computed volumes in storage for different Q_s and R, with D = 20 m and K = 30 m/d, analytical solution (fluent line) and numerical integration (dotted line).

The analytical solution is used as a guideline in this research. The analytical solution does not exist when the distance of the salt water table, representing the fresh-salt water interface, above the base of the aquifer h decreases below the bottom of the aquifer. Hence, there is a maximum value for the salt water discharge Q_s depending on the thickness of the aquifer. For an aquifer with 20 m thickness Q_s is maximum 240 m^3/day. There is also a restriction to the radius of the fresh water bubble of 100 m for the given situation. This determines a maximum value for the fresh water volume stored. For an aquifer with thickness 20 m, salt water extraction flow 240 m^3/day and radius 100 m, the fresh water volume can maximum be 6,000 m^3 as can be seen in Figure 11. In reality fresh water will enter the salt water screen when the interface is decreased below the thickness of the aquifer. Because this phenomenon is undesirable the restrictions of the analytical solution are used in this research.

5 Numerical modeling

The goal of the modeling effort is to find out how a fresh water bubble in a saline aquifer, stored by means of a FSSE-well, can be recovered; how it behaves under different circumstances (conductivity, depth, heterogeneity, ambient groundwater flow and calamity); and what the recovery rate is.

To accomplish the goal a groundwater model has been constructed using the numerical groundwater program SEAWAT, using Visual MODFLOW as a graphical user interface. This program can simulate and predict the hydraulic behavior of a groundwater system in response to injection and recovery of water with different density.

In this chapter the setup of the numerical model is described. In section 5.1 the data and assumptions are given. Section 5.2 gives a description on the computer code SEAWAT. In section 5.3 the model setup is outlined. The model parameters, boundary and initial conditions are given in section 5.4 and the spatial and temporal discretizations are described in section 5.5.

5.1 Concept of the model

This research is performed in the framework of the DEC ASR. The consortium focuses on desalination plants in tourist resorts along the Egyptian Red Sea coast. The model parameters are based on the data collected during the field trips in April and May 2007 to the drinking water plants of El Gouna, Nefertary, Port Ghalib, Equinox and Cataract in Egypt. The geography of the area along the Red Sea coast is described in section 2.2 and Appendix B contains detailed descriptions of the areas.

The area is characterized by a warm dry climate. There is no natural recharge. The desalination plants are located at maximum 5 km land inward, but four of them are within 1 km land inward. The salinity of the local groundwater is equal that of the Red Sea (42000 ppm) and the aquifers are connected to the sea. The thicknesses of the aquifers typically range from 5 to 30 m and the heads in the confined aquifers range from 10 to 60 m below ground surface. The aquifer material consists of gravelly sand, rocks, and limestone with sand (previous coral reefs), with *K*-values ranging from 10 to 50 m/d [Shata, 2007].

The model is a generalized prototype of the situation in the five locations in Egypt. The distance to sea of this model is 1,000 m, the salinity of the aquifer is 42,000 ppm, the thickness of the aquifer is 20 m and the hydraulic conductivity of the aquifer is 30 m/d. In this research only confined aquifers are considered, because it appeared to be numerically impossible to simulate the behavior of the bubble in an unconfined aquifer (dry cells). The initial head is 35 m.

5.2 SEAWAT

SEAWAT [Guo and Langevin, 2002] makes it possible to simulate 3D variable density transient groundwater flow. SEAWAT couples the flow and transport equations of two widely used codes (MODFLOW [McDonald and Harbough, 2000] and MT3D [Zheng and Wang, 1999]) with some modifications to include density effects.

The governing flow equation in SEAWAT is [Guo and Langevin, 2002]:

$$\frac{\partial}{\partial x_i}\left[\rho K_{fx}\left(\frac{\partial h_f}{\partial x_i}+\frac{\rho-\rho_f}{\rho_f}\frac{\partial L}{\partial x_i}\right)\right]+\frac{\partial}{\partial y_j}\left[\rho K_{fy}\left(\frac{\partial h_f}{\partial y_j}+\frac{\rho-\rho_f}{\rho_f}\frac{\partial L}{\partial y_j}\right)\right]$$

$$+\frac{\partial}{\partial z_k}\left[\rho K_{fz}\left(\frac{\partial h_f}{\partial z_k}+\frac{\rho-\rho_f}{\rho_f}\frac{\partial L}{\partial z_k}\right)\right]=\rho_s S_f\frac{\partial h_f}{\partial t}+n_e\frac{\partial \rho}{\partial C}\frac{\partial C}{\partial t}-\rho_s q \qquad (39)$$

Where x, y, z [L] are coordinate axes, i, j, k are column, row and layer indices respectively, K_f is equivalent fresh water hydraulic conductivity [LT^{-1}], h_f is equivalent fresh water head [L], t is time [T], L is the cell centre elevation [L], ρ is the density of the groundwater [ML^{-3}], ρ_f is the fresh water density [ML^{-3}], S_f is equivalent fresh water specific storage [L^{-1}], n_e is effective porosity [-], C is solute concentration [ML^{-3}], ρ_s is fluid density of source or sink water [ML^{-3}] and q_s is the volumetric flow rate of sources and sinks per unit volume of aquifer [T^{-1}].

For the flow equation the Algebraic Multigrid Methods for Systems Solver (SAMG) Package is used for all the simulations in this research. The advantages of this solver over other solvers are the rapid execution times and the scalability of the time step to the convergence criterion. This means that the time step size is scaled during the running process. The convergence criterion is set to $1e^{-4}$ m for the head change.

The transport equation is [Guo and Langevin, 2002]:

$$\frac{\partial C^k}{\partial t}=\frac{\partial}{\partial x_i}\left(D_{ij}\frac{\partial C^k}{\partial x_j}\right)-\frac{\partial}{\partial x_i}\left(C^k v_i\right)+\frac{q_s C_s^k}{n_e}+R_n \qquad (40)$$

Where C^k is dissolved concentration of species k [ML^{-3}], D_{ij} is the hydrodynamic dispersion tensor [L^2T^{-1}], v_i is linear pore water velocity [$L\,T^{-1}$], C_s^k is concentration of the source or sink flux for species k [ML^{-3}] and R_n is the chemical reaction term [$ML^{-3}\,T^{-1}$].

In this research the Method of Characteristics (MOC) is used as the numerical method to solve the transport equation (equation 40). The MOC method uses a conventional particle tracking technique based on a mixed Eulerian-Lagrangian method for solving the advection term. The dispersion,

sinks/source mixing and chemical reaction terms are solved with the finite difference method. The MOC technique tracks a large number of moving particles forward in time, and keeps track of the concentration and position of each particle. The main advantage of the MOC method is that it is virtually free of numerical dispersion. The MOC method is further described in Appendix D.

5.3 Model set-up

The model is a generic prototype of the situation representative for the five visited locations in Egypt. The modeled area is a cylinder with a radius of 1,000 m, the aquifer is confined with a thickness of 20 m, the salinity of the native groundwater is 42,000 ppm, the initial salt water head is 35 m and a hydraulic conductivity is 30 m/d. The FSSE-well is located in the center of the cylinder, the well radius is 1 m. The sea is the boundary at $\Re$ = 1,000 m with a constant head of ϕ_s = 35 m.

To minimize calculation time a radially symmetric cross section model is used. This means that every grid cell at a distance *r* from the well represents a cylindrical ring. To model this with a standard model and user interface the characteristics of the aquifer (hydraulic conductivity K_x, K_y, K_z, storage coefficients S_s, S_y and porosity values n_e, n_t) are multiplied by a factor $2\pi r$. The model set up is shown in Figure 12.

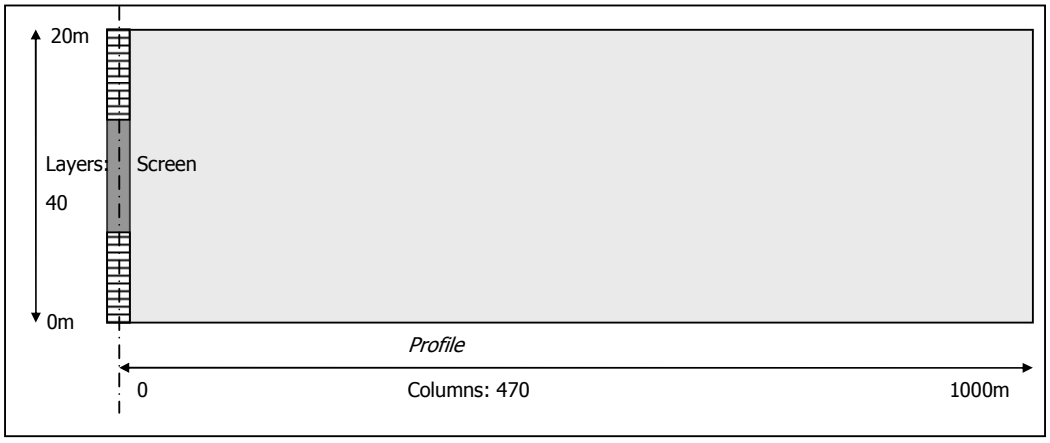

Figure 12: Model: Radially symmetric cross section profile (pie slice).

5.4 Model parameters, boundary and initial conditions

The parameters and calculation settings of the model can be found in Appendix E. A sensitivity analysis was done to compare the TVD and MOC calculation method. The TVD method has a larger root mean square error ($4.73*10^{-3}$) than the MOC method ($4.68*10^{-3}$), as was also found in theory. The MOC method will be used in this modeling.

Another sensitivity analysis was to done to find the optimal calibration criterion. A calibration criterion of $1e^{-4}$ appeared to be necessary to give a good representation of the mixing zone. A calibration criterion of $1e^{-4}$ is used in this modeling. The results of the sensitivity analyses can be found in Appendix F.

The program treats pumping wells as flux boundary conditions, such that each grid cell intersecting a well screen is assigned a specified flux [Schlumberger water services, 2006]. The pumping rate for each grid cell is calculated by the following formula:

$$Q_i = \frac{L_i K_{xi}}{\sum (LK_x)_i} Q_T$$

Where Q_i is the discharge from layer *i* to a particular well in a given stress period [L^3T^{-1}], Q_T is the well discharge in that stress period [L^3T^{-1}], L_i is the screen length in layer *i* [L], K_{xi} is the hydraulic conductivity in the x-direction in layer *i* [LT^{-1}], and $\sum (LK_x)_i$ represents the sum of the products of screen length and hydraulic conductivities in the *x*-direction of all layers penetrated by the well.

Visual MODFLOW does not take into account velocity differences along the well screen length, i.e. a higher velocity at the upper and bottom part of the screen.

The head is specified at *r* = $\Re$ = 1,000 m, where ϕ_s = 35 m. The initial head in the aquifer is specified at ϕ_s = 35 m.

5.5 Spatial and temporal discretization

The mesh consists of 470 by 40 cells. The grid size in *x*-direction is 0.5 m for the first 150 m and 5 m for the following 850 m. The grid Peclet number imposes that the dimension of the cell should not exceed a few times the magnitude of the longitudinal dispersivity (α_H = 0.1) as otherwise numerical dispersion will occur [Oude Essink, 2001].

The grid size in *y*-direction is 0.3 m. The thickness of the cross section is 1 m, the program needs at least 3 rows. A grid size sensitivity analysis was done, the results can be found in Appendix F.

The total simulation time is 200 days. The initial step size is 0.1 day. The SAMG Package of SEAWAT automatically scales down the time step size to meet the convergence criterion during the model run.

6 Results

This chapter contains the results of the modeling. In section 6.1 the numerical solution is verified by comparing it with the analytical solution. In section 6.2 the behavior of the fresh water is simulated while stored for prolonged times. Section 6.3 shows how the fresh water bubble is trapped around the well during managed storage by means of the FSSE-well. In section 6.4 the recovery of the bubble is simulated. Section 6.5 shows the behavior of the bubble during several injection-recovery cycles. The influence of the thickness of the aquifer, the conductivity and the heterogeneity of the aquifer are discussed in sections 6.6, 6.7 and 6.8. The behavior of the bubble during a calamity and by ambient groundwater flow is given in sections 6.9 and 6.10.

6.1 Head in saline aquifer

The model was compared to the analytical solution of section 4.2. Figure 13 gives the results for the head in a confined saline aquifer for a fully penetrating well, with a screen length of 20 m, and a partially penetrating well, with a screen length of 5 m at the bottom of the aquifer. Partial penetration of the well results in an extra lowering of the piezometric head (section 3.4.2). Beyond r = 50 m (2 times the thickness of the aquifer) the head is equal to the head for a fully penetrating well (Figure 13).

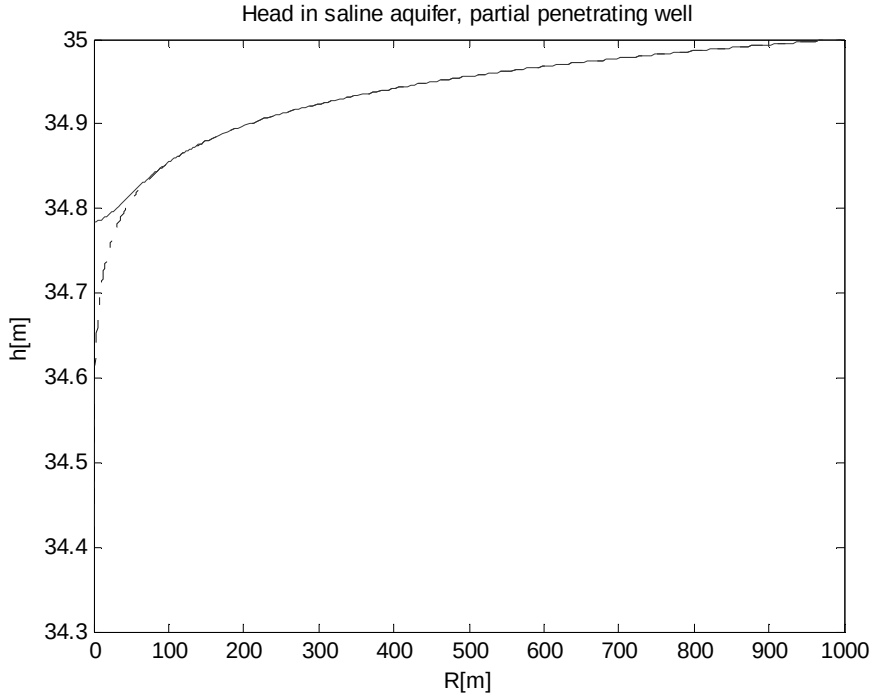

Figure 13: Head result for a fully (fluent line) and partially (dotted line) penetrating well in a confined aquifer calculated with SEAWAT.

Figure 14 compares the numerically and analytically calculated heads for fully penetrating wells. The numerical solution (the dots in Figure 14) tends to have a lower value than the analytical solution.

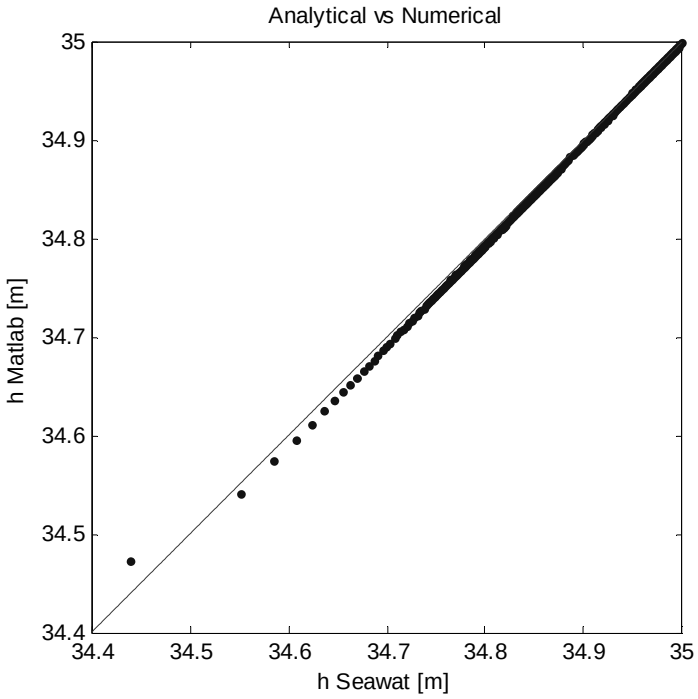

Figure 14: Head comparison analytical (fluent line) vs numerical (dots).

The dots in Figure 14 represent the heads in the cell center. The reason which introduces an error in the comparison of numerically and analytically calculated heads is the schematized radial symmetric cross section (Figure 15). Every grid cell at a distance *r* from the well represents a cylindrical ring. In the analytical model pie slices as in the first figure of Figure 15 are used, but in the numerical model the pie slices are schematized by blocks as in the second figure of Figure 15. This introduces an error especially in the vicinity of the well (compare grid cell areas).

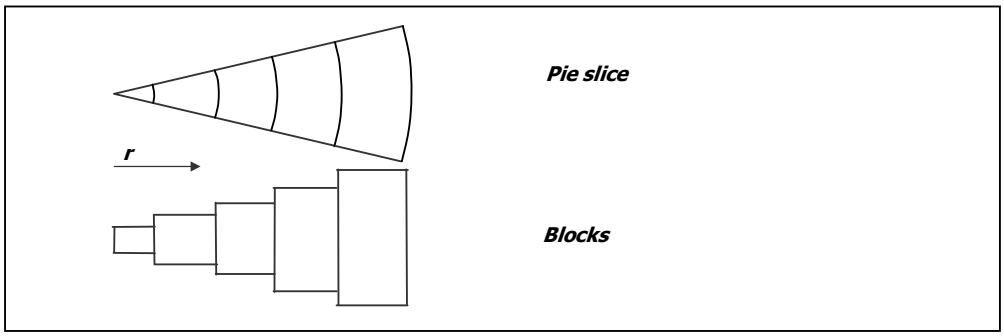

Figure 15: Schematization of the radial symmetric cross section model.

6.2 Floating up of fresh water

In Chapters 1 and 2 was mentioned that the density difference between fresh and salt groundwater causes the fresh water to float up to the ceiling of the aquifer and spread out such that it may be hard or impossible to recover at a later stage. A model has been used to examine this buoyancy of fresh water in a saline aquifer. Details of the model have been given in sections 5.3, 5.4 and 5.5.

Fresh water is injected by a partially penetrating well with 5 m screen at the top of the aquifer at the left vertical boundary representing the center of an axially symmetric flow system. The injection rate Q_f is 100 m^3/d. After 60 days continuous injection, it stopped after which a prolonged 140 days storage period followed without injection and extraction. Figure 16 shows the result of the modeling effort. After 200 days the fresh water bubble has a radius of 105 m and a thickness of only 4 m.

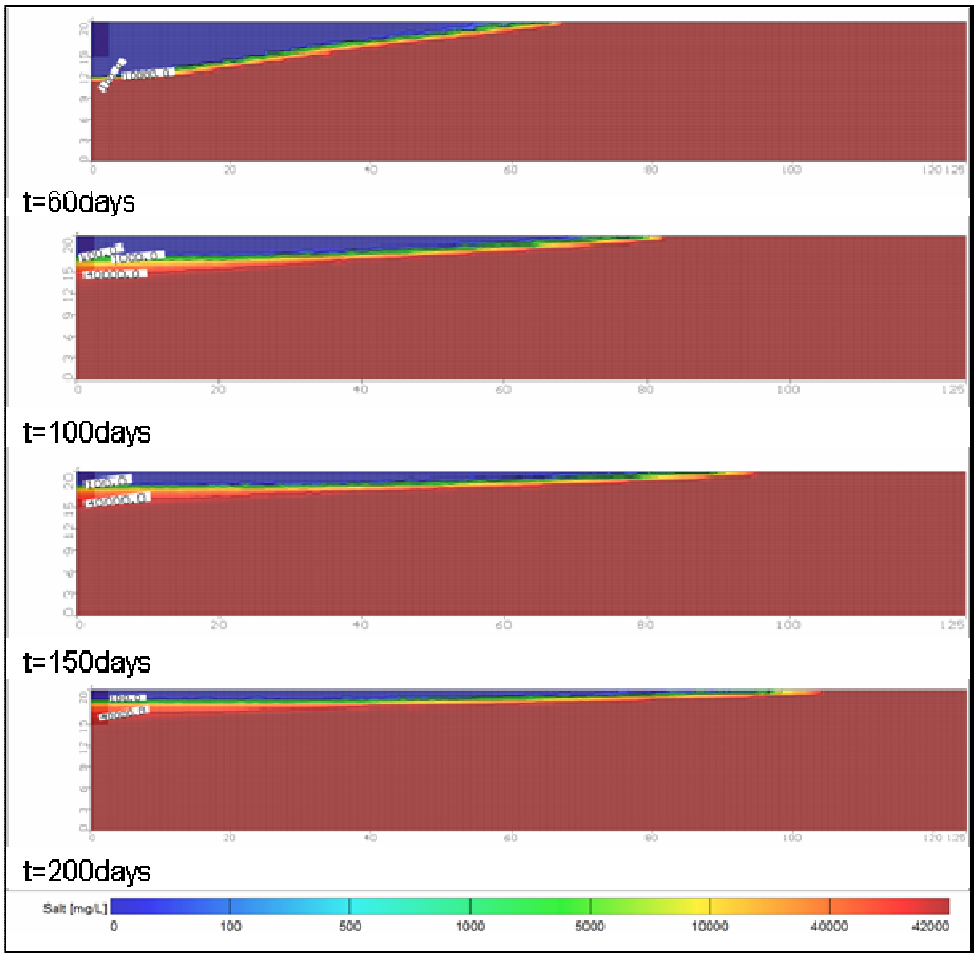

Figure 16: Fresh water bubble floats up and becomes a flat pancake during unmanaged storage (SEAWAT result). 60 days is the end of the injection period after which 140 days of storage was simulated without injection and extraction.

Conclusion

During unmanaged storage the lower density of the fresh water compared to the ambient saline groundwater causes the stored fresh water to float up to the ceiling of the aquifer and spread out to be lost within weeks.

6.3 Storage of the fresh water bubble

The principle of the FSSE-well is that stored fresh water is kept in place around the well by continuous pumping of salt water from below the stored bubble, to maintain the necessary velocity difference across the fresh-salt water interface. A model has been used to examine the storage of the bubble by means of a FSSE-well.

Fresh water is injected by a partially penetrating well with 5 m screen at the top of the aquifer at the left vertical boundary representing the center of an axially symmetric flow system. The injection rate Q_f is 100 m^3/d. After 60 days continuous injection, it stopped.

The following phase is a storage phase. The radius of the fresh water bubble after 60 days is 60 m. During the storage phase, the velocity difference across the interface between fresh and salt water is maintained by continuous salt water extraction using a partially penetrating well of 5 m screen at the bottom of the aquifer. To keep the bubble in place, without loss of fresh water in the saline screen, the extraction flow is set to 240 m^3/d. Figure 11 shows that in this case the radius of the bubble will become 95 m.

The modeling results are given in Figure 17 showing the fresh water bubble trapped in its place. The thickness of the bubble near the well stays about 5 m while in Figure 16 it reduced to 2 m.

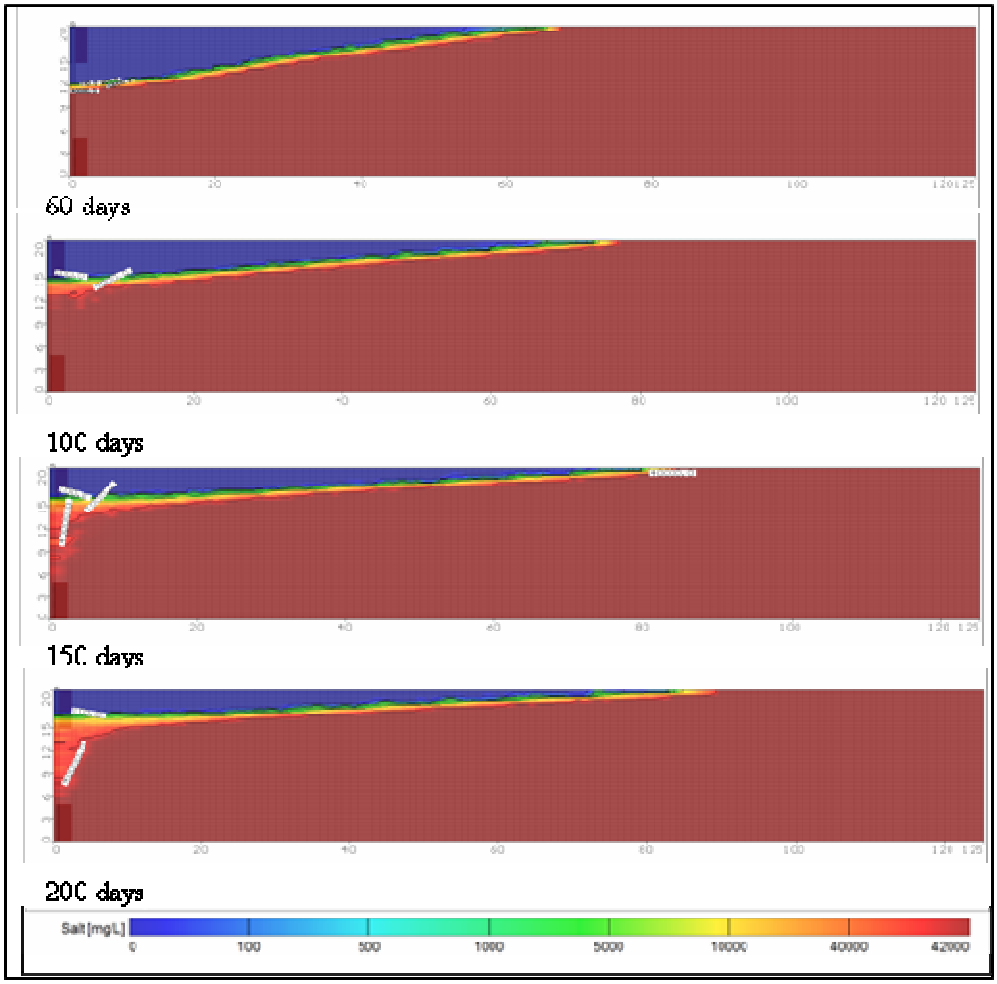

Figure 17: Fresh water bubble during managed storage (SEAWAT result), 60 days is the end of the injection period after which 140 days of storage was simulated with a salt water extraction of 240 m^3/d in the lower screen.

The initial thickness of the mixing zone after 60 days injection can be approximated with the formula for the standard deviation of the mixing front, $\sigma = \sqrt{2\alpha_T R}$ where α_T is the transversal dispersivity (α_T = 0.1) and R is the radius of the bubble (95 m), which equals 4.5 m.

Mixing between fresh and salt water during injection, storage and recovery is often considered a loss, however storing an initial value of water may be considered an investment and as such be added to the overall investment of the plant. The mixing zone is equivalent to the walls of a storage basin above ground as it kind of prevents losses from subsequent injection-storage-recovery cycles. In this view recovery of subsequent storage cycles will increase and approach 100% in most aquifer-storage-recovery wells [Pyne, 2007].

However, a 100% recovery is never achievable because the standard deviation of the mixing front σ and thus the thickness of the mixing zone increases with time, according to formula 41.

$$\sigma = \sqrt{2D_h t} \tag{41}$$

During storage periods more fresh water will be lost due to hydrodynamic dispersion, which is represented in Figure 18. Figure 18 was computed by integrating the amount of fresh water available in storage (SEAWAT result) having a salinity of less than 100 ppm, 500 ppm and 1000 ppm, respectively. The loss of fresh water volume is about 4% per month.

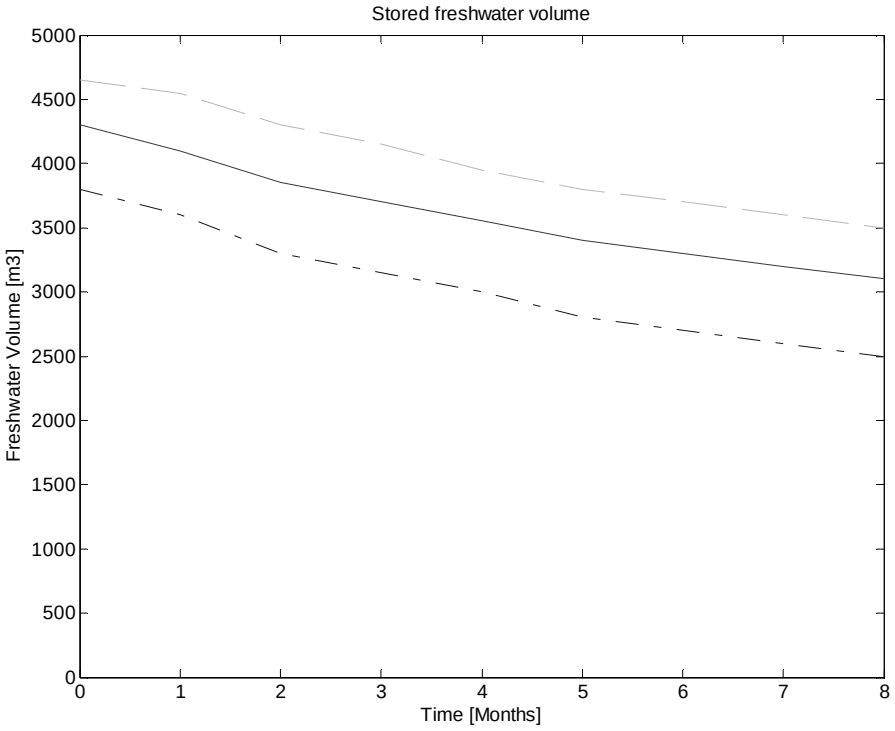

Figure 18: Decrease in stored fresh water volume in months (SEAWAT results) for different levels of acceptable recovery concentrations in ppm. The point-dotted line gives the volume with a maximum recovery concentration of 100 ppm, the fluent line gives the volume with a maximum recovery concentration of 500 ppm and the dotted line gives the volume with a maximum recovery concentration of 1,000 ppm.

Conclusion

The fresh water bubble can be kept around the well by means of a FSSE-well. The necessary salt water extraction to keep the bubble in place, without loss of fresh water in the saline screen, and the radius of the bubble can be calculated with the analytical solution (section 4.2) or red from Figure 11.

Mixing between fresh and salt water is often considered a loss; however the mixing zone can be considered an investment which can be used during following injection-storage-recovery periods. During storage periods 4% fresh water is lost per month due to hydrodynamic dispersion.

6.4 Recovery of bubble of fresh water

Section 6.3 shows that fresh water can be stored in a saline aquifer by means of a FSSE-well, but important questions are: How can fresh water be recovered and what is the recovery efficiency for a fresh water quality of 500 ppm (Egyptian drinking water standard)? The results of several model simulations to analyze this are given in this section.

Model 1: Q_s during recovery is Q_s+Q_f

During the recovery phase of an injection-storage-recovery cycle a velocity difference across the fresh and salt water interface must be maintained when v_f-v_s is outward. Injection is thus possible, without simultaneous extraction of salt water. However, extraction of the fresh water requires maintaining the velocity difference across the interface. Therefore, a first design proposal is adding the extraction rate of the fresh water to that of the salt water. This means if the extraction of the fresh water is Q_f and the salt water extraction to keep the bubble in place during the storage period is Q_s, the salt water extraction during the recovery of fresh water should be increased to Q_f+Q_s.

The recovery phase has been simulated with a fresh water extraction rate Q_f of 100 m^3/d. The salt water flow during recovery is 340 m^3/d. The interface near the well reaches the bottom of the fresh water screen after 5 days, when a fresh water volume of 500 m^3 has been recovered. The total injected fresh water volume was 6,000 m^3. The recovery efficiency is therefore 8%, showing that most of the fresh water remains in the aquifer (Figure 19).

The mixing zone is small and therefore the recovery efficiency for fresh water qualities of 100 ppm and 1,000 ppm are almost equal to the recovery efficiency of 500 ppm, 7% and 8% respectively. In this research only recovery efficiencies for a fresh water quality of 500 ppm will be given.

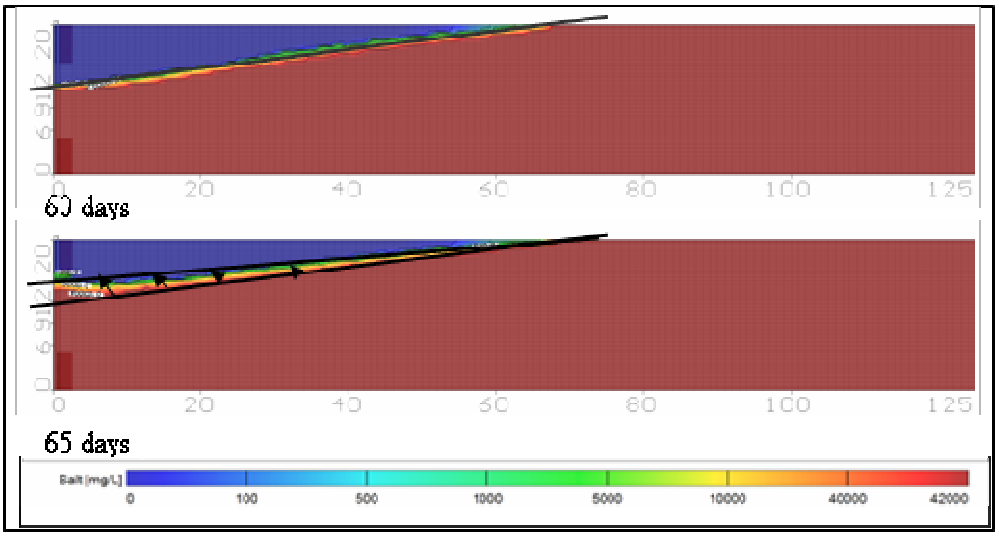

Figure 19: Fresh water bubble during recovery with Q_f = 100 m^3/d, Q_s = 340 m^3/d (SEAWAT results), 60 days is the end of the injection period after which a fresh water recovery was simulated with a salt water extraction of 340 m^3/d with the lower screen. The interface reaches the bottom of the fresh water screen after 5 days.

When extracting fresh water, the interface will move in the direction of the fresh water screen (Figure 19). But, due to the shape of the bubble, with radius>>height, the interface will reach the bottom of the fresh water screen while most of the stored fresh water is still in the aquifer at larger distances from the well. Figure 20 shows the amount of fresh water versus the radius of the bubble and the velocity over the radius. As can be seen, the fresh water is almost stagnant beyond r = 20 m. Three-quarters of total volume therefore hardly moves and will thus not be recovered.

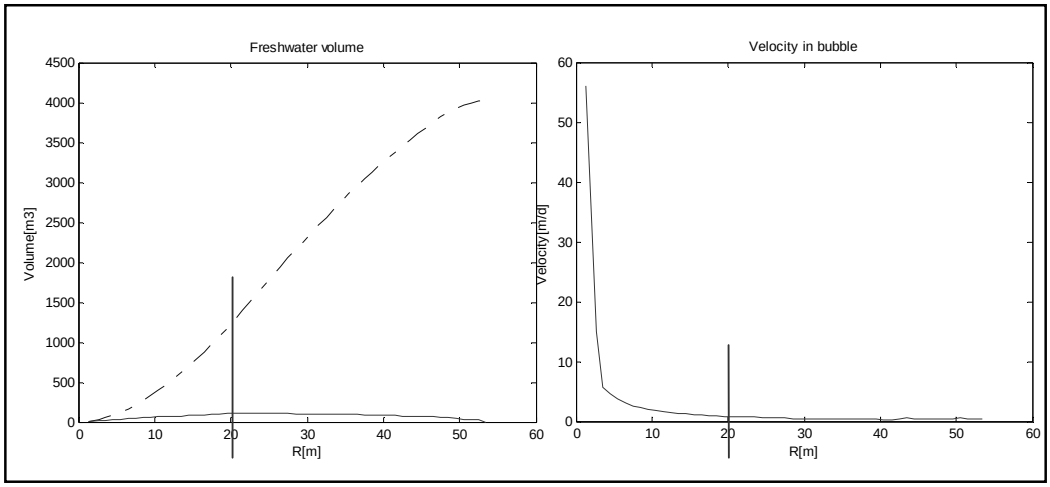

Figure 20: Fresh water volume over radius (fluent line: volume of the grid cell, dotted line: total volume over the radius) and velocity in the bubble over radius.

As soon as the interface reaches the bottom of the fresh water screen, recovered fresh water will be mixed with salt water. Recovery will then have to stop, while most fresh water remains in the aquifer. To recover most of the fresh water it seems necessary to change the shape of the bubble, i.e. increase the inclination of the interface to keep most fresh water closer to the well and to facilitate its recovery by increasing the thickness of the fresh water bubble near the well. The radius of the bubble can be decreased by increasing the salt water extraction rate.

Model 2: Q_s during recovery is 4* Q_s during storage

In the following model the salt water extraction is four times higher than necessary to keep the bubble in place, Q_s is 2,000 m^3/d. The fresh water extraction rate is the same as during the previous simulation. The result is a velocity increase near the edge of the bubble (Figure 21).

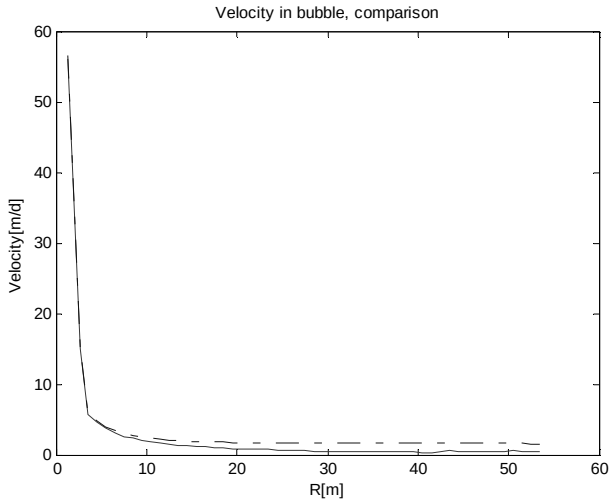

Figure 21: Comparison of velocity in the bubble (fluent line: Q_s = 340 m^3/d, dotted line: Q_s = 2,000 m^3/d).

The simulation results are shown in Figure 22. After 60 days of fresh water injection, fresh water recovery starts. The interface now reaches the salt water screen 30 days later, after which a fresh water volume of 3,000 m^3 has been recovered, which is 50% of injected volume (6,000 m^3). The recovery efficiency for the first cycle is therefore 50%.

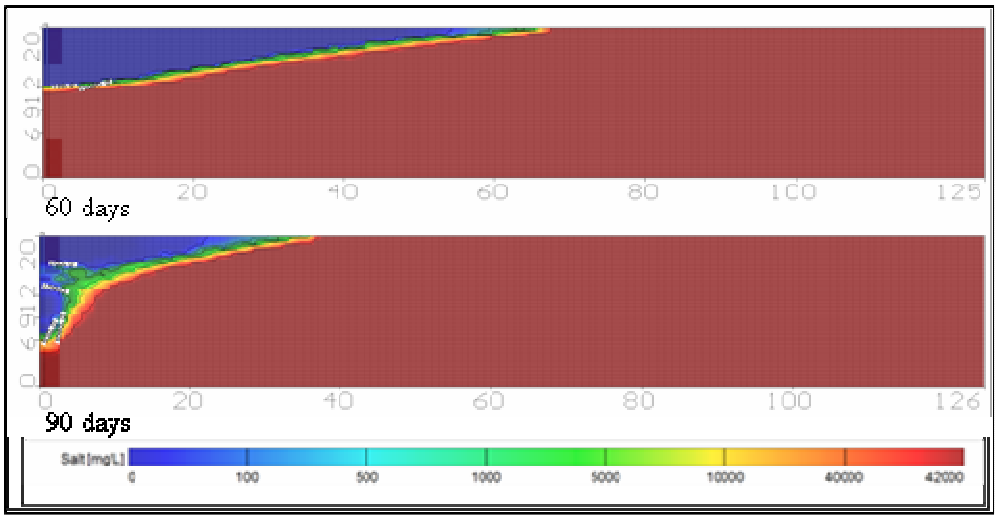

Figure 22: Fresh water bubble during recovery with Q_f = 100 m^3/d, Q_s = 2,000 m^3/d (SEAWAT results), 60 days is the end of the injection period after which a fresh water recovery was simulated. The interface reaches the bottom of the fresh water screen after 30 days.

The restriction of the analytical solution (section 4.2) is that the salt water extraction rate may not exceed a certain value, because then the salt water table decreases below the bottom of the aquifer. In that case the analytical solution does not exist. The head in the aquifer during recovery is given in Figure 23. The maximum lowering of the head along the well is 12 m. The water table in the well is

lower due to the seepage face in the well. The well is filled with fresh water. Fresh water is lost by the salt water screen.

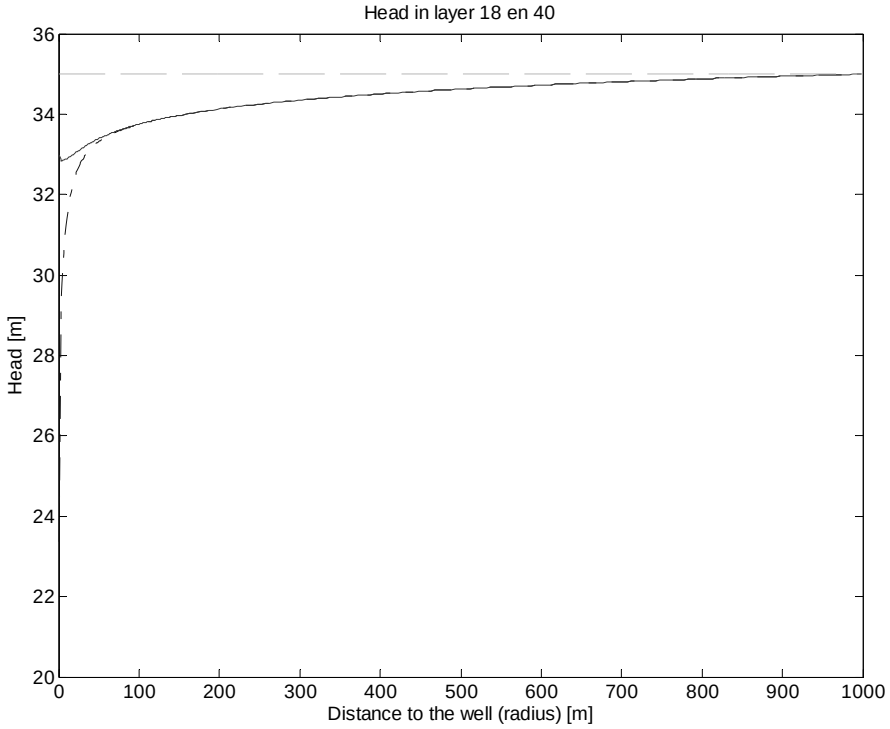

Figure 23: The head in layer 18 (fluent line) and layer 40 (point-dotted line) during fresh water recovery with a fresh water recovery rate of 100 m^3/d and a salt water extraction rate of 2,000 m^3/d. Modflow gives equivalent fresh water head.

Model 3: Recovery after a storage period

In the following model fresh water is recovered after a storage period of 100 days. The salt water extraction discharge Q_s is 2,000 m^3/d. To drive the fresh water closer to the well before recovery starts, the rate of the salt water extraction is increased 5 days before the onset of fresh water recovery (at t = 155 days).

The results of the simulation are shown in Figure 24. A volume of 2,500 m^3 has been recovered when salt water reaches the fresh water screen after 25 days, which is 40% of injected volume (6,000 m^3).

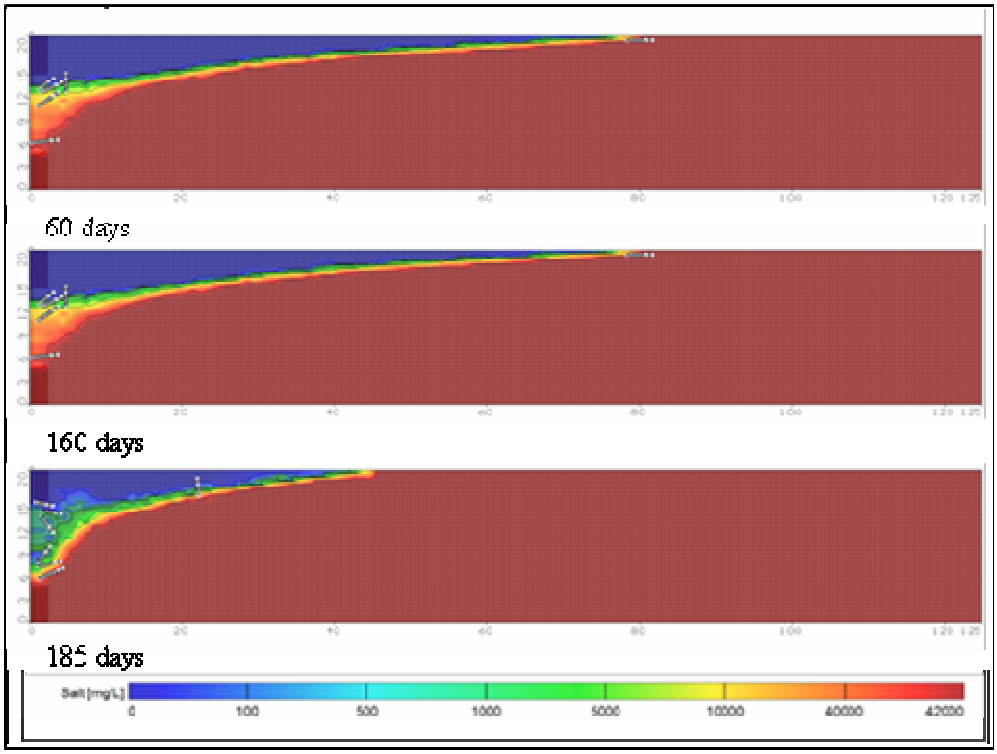

Figure 24: Fresh water bubble (SEAWAT results), 60 days is the end of the injection period after which 100 days of storage was simulated with a salt water extraction of 240 m^3/d at the lower screen. At t = 160 d fresh water recovery was simulated with fresh water extraction of 100 m^3/d and salt water extraction of 2,000 m^3/d. The interface reaches the bottom of the fresh water screen after 25 days.

Conclusion

The recovery efficiency for the first cycle without storage is 50% and after 100 days storage 40%. After a storage period it is necessary to increase the rate of the salt water extraction some days before the onset of fresh water recovery. This is to drive the fresh water in stock closer to the well before recovery starts.

6.5 Injection-recovery cycles

It is important to know what the influence of injection-recovery cycles is on the recovery efficiency. According to the theory stated in section 6.3 the recovery efficiency increases after the first cycle, because the invested mixing zone can be used in the following period.

To verify this theory a model has been used in which several injection-recovery cycles were simulated. Table 3 shows the operating scheme of the FSSE-well. Cycles of one month are not realistic and this simulation is only used to verify the theory. The operation of a FSSE-well with more realistic seasonally operating cycles is given for the Port Ghalib case in Chapter 7.

Table 3: Time table for the operation of the FSSE-well.

Time	Phase	Qs [m^3/d]	Qf [m^3/d]
0-60 days	Injection	0	100
60-90 days	Recovery	-2000	-100
90-120 days	Injection	0	100
120-140 days	Recovery	-2000	-100
140-170 days	Injection	0	100
170-200 days	Recovery	-2000	-100

The behavior of the fresh water bubble during injection-recovery cycles is shown in Figure 25. In the first recovery cycle (t = 60-90 days) it is possible to extract fresh water for 30 days before salt water reaches the fresh water screen. The recovery efficiency of the first recovery cycle is therefore 50%. The recovery efficiency of the second cycle is 67%. The recovery efficiency of the third cycle is 80%.

Conclusion

It is possible to infiltrate and recover the water in successive injection-recovery cycles. The mixing zone can be used several times. The recovery efficiency increases in successive cycles. The recovery efficiency is 50% in the first cycle, 67% in the second cycle and 80% in the third cycle.

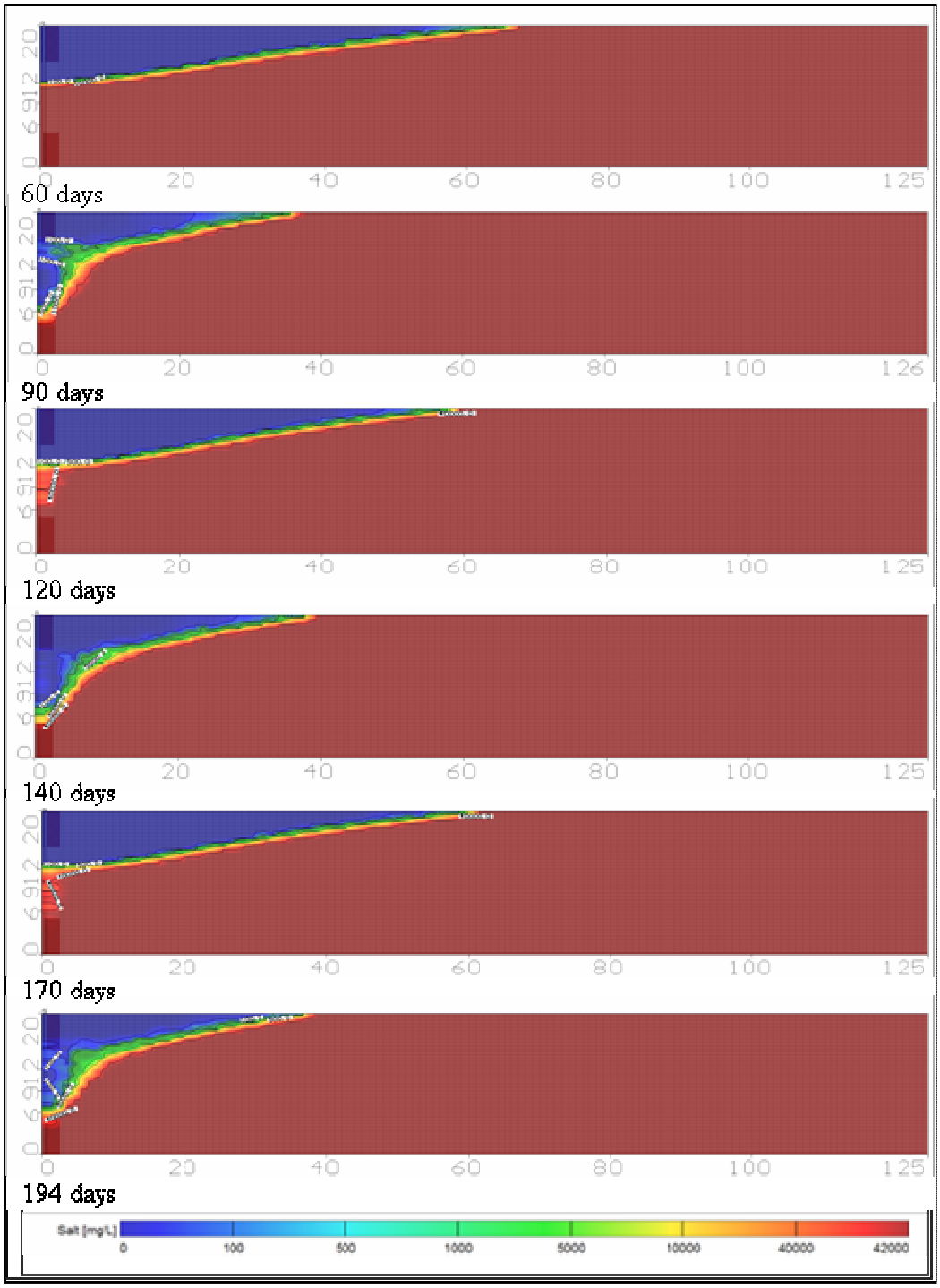

Figure 25: Fresh water bubble during injection-storage-recovery cycles (SEAWAT results). 60 days is the end of the injection period after which fresh water recovery was simulated until the interface reaches the bottom of the fresh water screen after 30 days. At *t* = 90 d a second fresh water injection period starts and at *t* = 120 d a subsequent fresh water recovery period. The interface reaches the bottom of the fresh water screen after 20 days. At *t* = 140 d a third fresh water injection period starts and at *t* = 170 d a subsequent fresh water recovery period. The interface reaches the bottom of the fresh water screen after 24 days.

6.6 The influence of aquifer thickness on recovery

In a thinner aquifer the salt water head will decrease below the bottom of the aquifer when the fresh water bubble is stored and kept in place with the same extraction discharge as in a thicker aquifer. The bottom of the bubble will reach the salt water screen, and fresh water will be lost in the salt water screen.

Figure 26 shows analytically computed storage volumes for different Q_s and R, with K = 30 m/d and varying D-values. According to the analytical solution, the salt water discharge in an aquifer of 10 m depth may not exceed 100 m^3/d without loss of fresh water in the salt water screen, the radius can maximally be 30 m. Consequently, a maximum volume of 500 m^3 can be stored without loss of fresh water in the salt water screen. In an aquifer of 20 m depth a fresh water bubble with a radius 100 m and a volume of 6,000 m^3 can be captured with a salt water extraction rate Q_s is 240 m^3/d. In an even thicker aquifer of 30 m depth a maximum volume of 30,000m^3 with a radius 200 m can be captured with a salt water extraction discharge Q_s of 450 m^3/d.

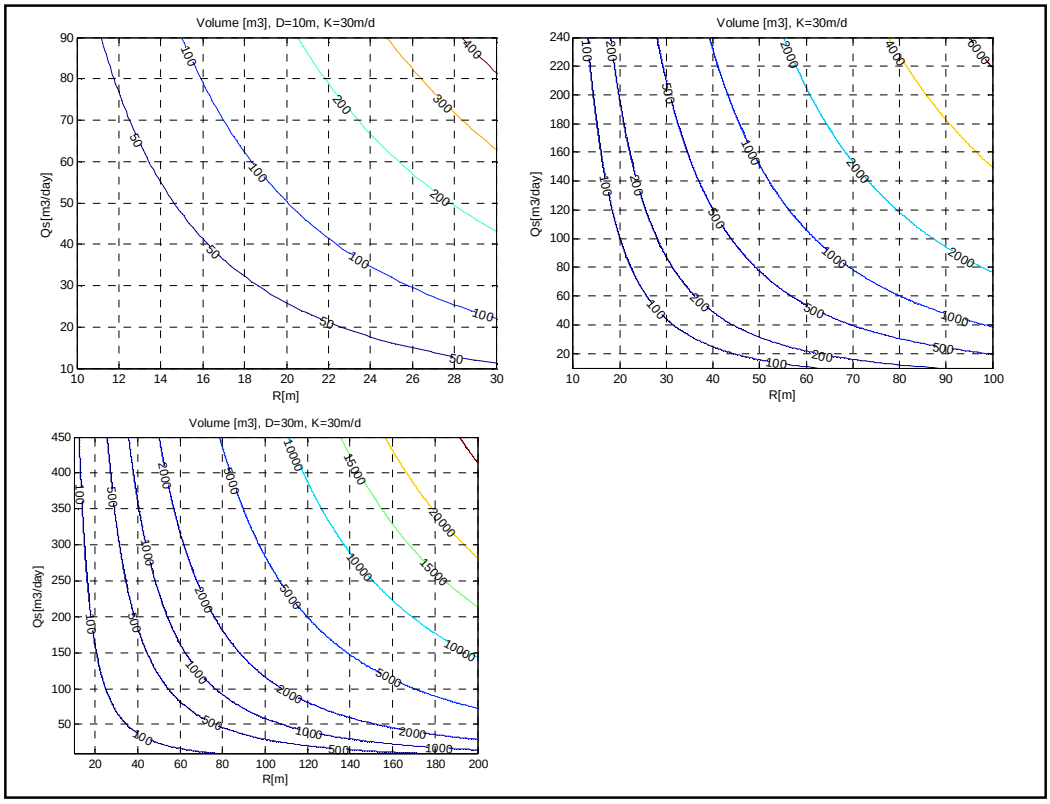

Figure 26: Analytical computed volumes in storage for different Q_s and R, with K = 30 m/d and varying D-values.

Conclusion

In thicker aquifers the salt water extraction can be larger than in thinner aquifers. Due to the larger extraction rate more water can be kept in place. It is attractive to store the water in a thicker aquifer. However in a thinner aquifer you can completely displace the native salt water. This is the conventional

ASR operation. Examples can be found in Appendix A; in Abu Dabi a large scale ASR field is constructed at the moment.

6.7 The influence of the conductivity on recovery

As stated in section 3.2 the hydraulic conductivity *K* is the capacity of a material to transmit water. If *K* increases the aquifer transmits water more easily. What is the influence of the conductivity on the shape of the bubble and the salt water extraction discharge to keep the fresh water around the well? Fracture flow is beyond the scope of this research because porous medium variations of porosity are relatively small compared to variations in conductivities.

According to Figure 27 a volume of 2,000 m^3 can be stored in a bubble with a radius of 60 m, salt water extraction discharge Q_s of 200 m^3/d, aquifer depth 20 m and hydraulic conductivity 30 m/d. When the conductivity is 10 m/d instead of 30 m/d a volume of more than 6,000 m^3 can be stored in the same bubble. When the conductivity of the aquifer is 50 m/d only 1,000 m^3 can be stored in this bubble.

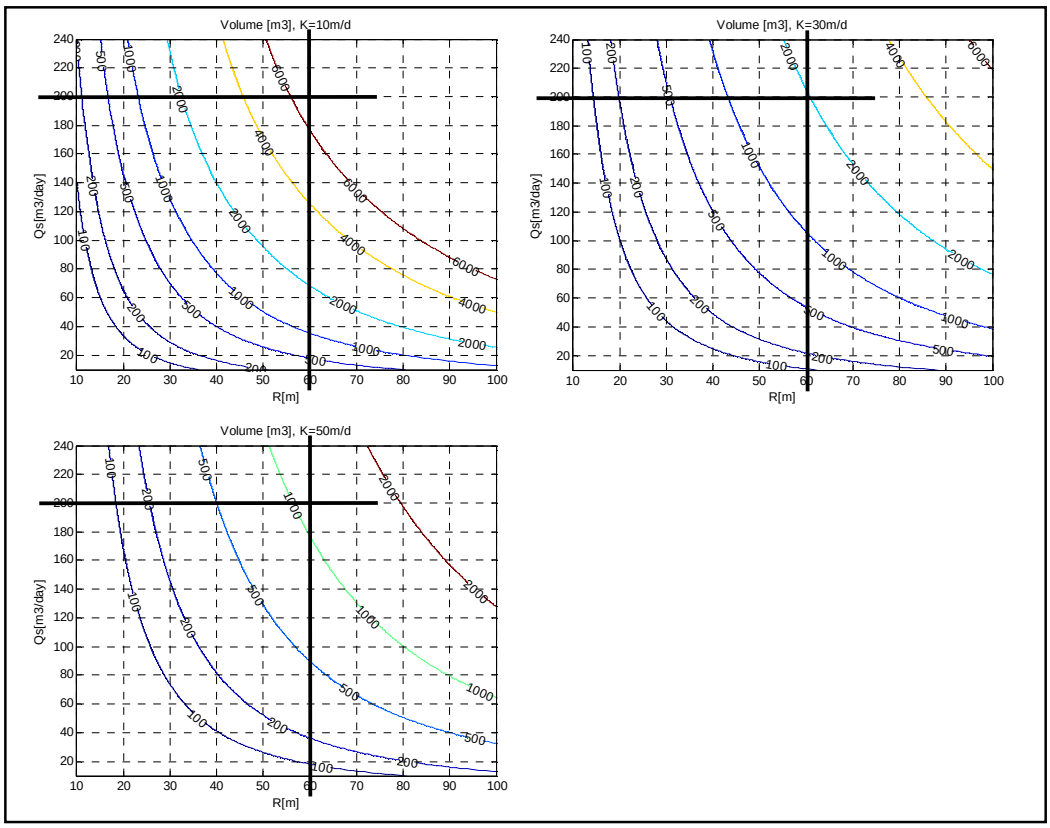

Figure 27: Analytical computed volumes in storage for different Q_s and R, with aquifer thickness 20 m and varying K-values.

Conclusion

For a larger *K*-value a larger radius is needed to store the same volume. To keep a more extended bubble on its place a larger salt water extraction discharge is needed.

6.8 The influence of heterogeneity on recovery

Aquifers are often heterogeneous, containing thin gravel and clay layers or fractures of sand and limestone. Models were used to investigate the influence of heterogeneity on the behavior of the bubble and the recovery efficiency.

To simulate a layered aquifer rather than a homogeneous one a model has been constructed in which the 5th layer from above had a ten times higher *K*-value than the surrounding aquifer, representing a gravel layer of 0.5 m thickness. After 60 days fresh water injection, a storage phase started from t = 60-150 d. At day 150 the recovery phase started.

Figure 28 shows the results for injection-storage-recovery. The water moves preferentially through the gravel layer. After 60 days the bubble has reached its final volume. The mixing zone at the top is larger than in the model of section 6.3 (Figure 17). The salt water flow was increased 5 days before fresh water recovery starts. The result at t = 150 d shows that the water moves more easily through the gravel layer. The mixing zone increases along the bottom edge of the bubble during the recovery phase. Salt water reaches the fresh water screen after 5 days recovery. The recovery efficiency after a storage period of 90 days is 8%.

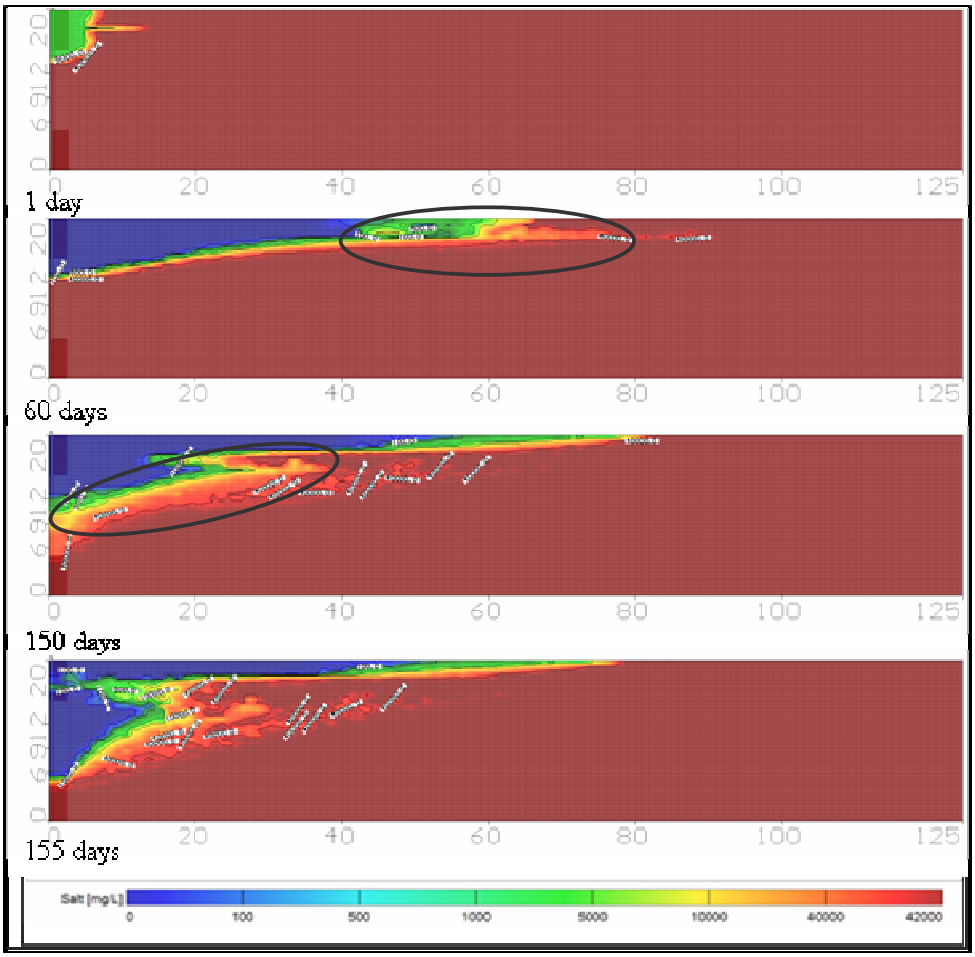

Figure 28: Fresh water bubble during injection, storage and recovery in heterogeneous aquifer with a gravel layer in the 5th layer from above (SEAWAT results). 60 days is the end of the injection period after which a 90 days storage period was simulated. At *t* = 150 d fresh water recovery starts and salt water reaches the fresh water screen after 5 days through the gravel layer.

Another model has been used to investigate the behavior of the bubble in an aquifer with a clay layer in the middle of the aquifer. Figure 29 shows the results. The clay layer separates the fresh water from the salt water screen. A volume of 3,000 m^3 is recovered. The recovery efficiency after a storage period of 90 days is 50% for the first cycle, which is equal to the recovery efficiency for immediate recovery for the normal situation without a clay layer. This is a very good result. But, is it necessary to use a FSSE-well in this situation? Maybe the application of the conventional ASR technique is more favorable.

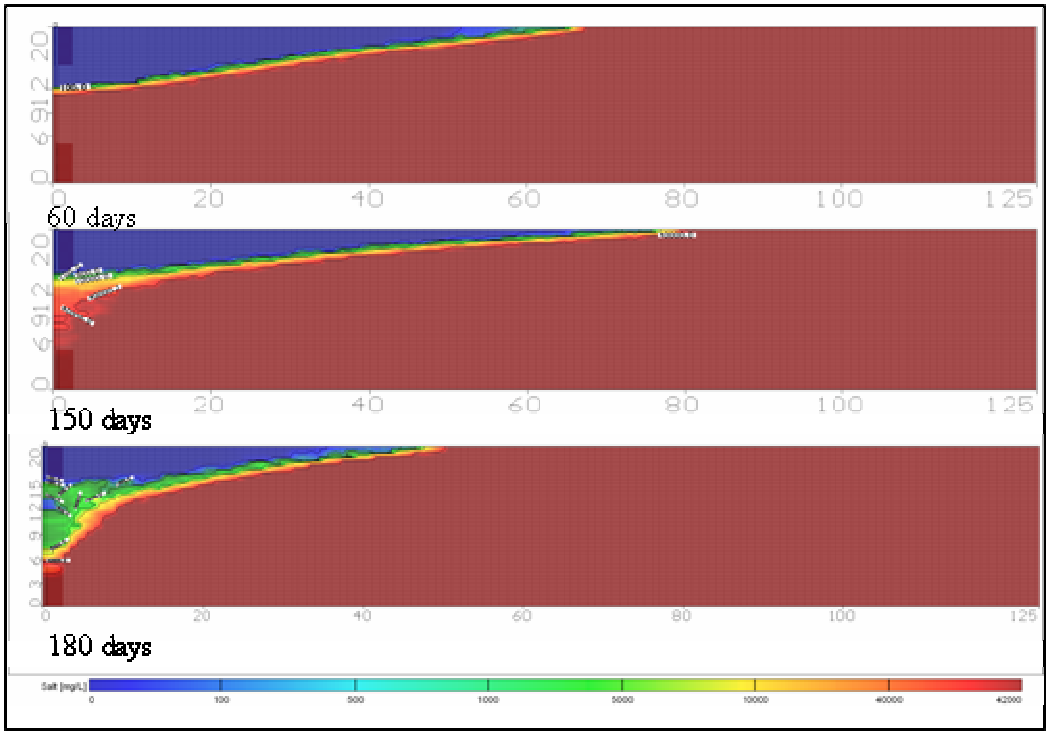

Figure 29: Fresh water bubble during injection, storage and recovery in heterogeneous aquifer with a clay layer in the middle of the aquifer (SEAWAT results). 60 days is the end of the injection period after which 90 days of storage was simulated. At *t* = 150 d fresh water recovery starts with a fresh water extraction of 100 m^3/d and salt water extraction of 2,000 m^3/d. Salt water reaches the fresh water screen after 30 days at the bottom of the screen.

Conclusion

Heterogeneity can have a negative and a positive influence on the recovery efficiency of the FSSE-well. When the aquifer is intersected by a gravel layer in the upper part, in the fresh water bubble, the mixing zone is increased and the recovery efficiency is very low (after a storage period of 90 days 8%). But, when the aquifer is intersected by a clay layer in the middle of the aquifer, just below the fresh water bubble, the recovery efficiency is very high (after a storage period of 90 days 50%). Hence, heterogeneity of the aquifer needs to be determined in the field, it may be critical.

6.9 Calamities

An important question is what will happen if the salt water pump should stop for a while, i.e. due to maintenance or failure. Clearly, the fresh water bubble will float up (section 6.2), but is it still possible to get it back to its original form and recover it?

A model has been used in which there was no pumping for 10 days, after 60 days fresh water injection to create the bubble. The results are shown Figure 30. It was possible to recover the bubble with a salt water rate of 240 m^3/d after this time. Compared to Figure 17 the mixing zone beneath the fresh water well screen is larger than in the normal situation, but the radius of the bubble is the same.

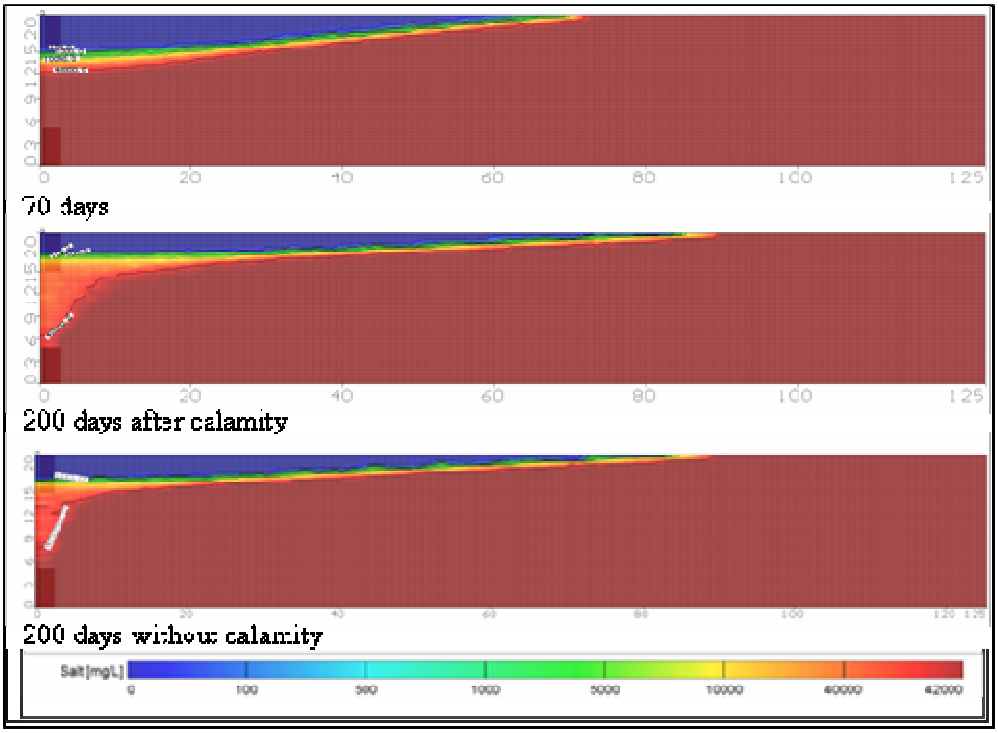

Figure 30: Fresh water bubble during a 10 days unmanaged storage period after injection (*t* = 0-70 d) and subsequent recovery, compared with the result of section 6.3 without calamity (SEAWAT results).

After a pumping stop for 1 month or more it is not possible to pull the bubble back from the ceiling of the aquifer to the FSSE-well with a salt water discharge of 240 m^3/d.

Conclusion

It is possible to recover the bubble after an unmanaged period of no pumping in the order of one week (calamity or maintenance) in which the bubble has floated to the ceiling of the aquifer. But after a period of 1 month it is impossible to recover the fresh water with the normal salt water extraction discharge.

6.10 Ambient groundwater flow

The FSSE-wells will always be used in a well field comprising several wells. During the storage phase all FSSE-wells extract salt water with a capacity of 240 m^3/d. The FSSE-wells act as mirror wells on each other and there is no influence of ambient groundwater flow due to extraction of wells. An important question is what will happen when 1 FSSE-well in the well field starts recovering the fresh water with a salt water extraction of 2,000 m^3/d. To analyze this situation 2D models have been constructed.

The 2D cross section model is 200 m long and the thickness of the aquifer is 20 m (Figure 31). A FSSE-well is located in the center of the cross-section; the well radius is 1 m. This well is part of a FSSE-well gallery. The other wells of the FSSE-well gallery are located in a line parallel to the model, left and right of the well in the model, with a mutual distance of 200 m. All wells are in the storage phase. The mesh consists of 400 by 40 cells; the grid-size in *x*- and *y*-direction is 0.5 m (Figure 31).

The analytical solution for a 2D situation is:

Darcy: $q = -k\upsilon_s h\frac{dh}{dx}$ (42)

Where q is the salt water discharge [L^2T^{-1}] and $\upsilon_s = \left(\rho_s - \rho_f\right)/\rho_s$.

Which, after integration and with as boundary condition at $x = R, h = D$, yields:

$$h = \sqrt{D^2 + \frac{2q}{K\upsilon_s}(R - x)} \quad (43)$$

The stored fresh water volume can then be calculated by integration of the thickness of the fresh water bubble between the well radius and *R* with the following formula:

$$V = 2n_e\int_{r_0}^{R}\left(D - h\right)dr \quad (44)$$

With a radius of the bubble of 60 m and a fresh water volume of 100 m^2 the salt water rate to keep the bubble in its place is 2.4 m^2/d. Fresh water is injected with a capacity of 2.5 m^2/d for 40 days. After 40 days storage the fresh water is recovered in 20 days with a fresh water extraction rate of 2.5 m^2/d and a salt water extraction rate during recovery of 15 m^2/d. The recovery efficiency is 50%. Figure 31 gives the results of the 2D model without ambient groundwater flow.

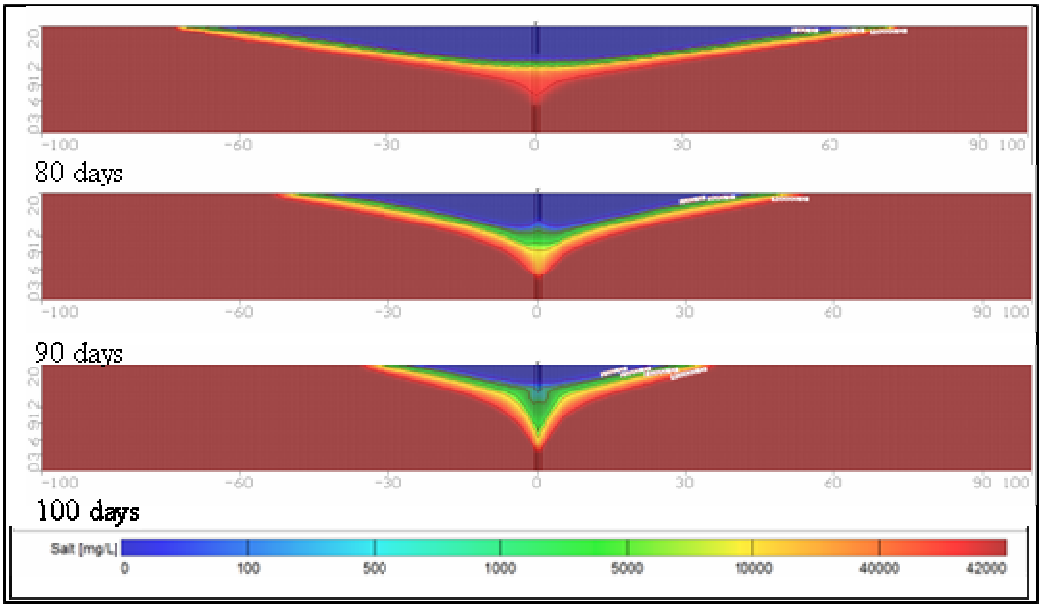

Figure 31: 2D model for FSSE-well (SEAWAT results). 40 days is the end of the fresh water injection period after which a storage period of 40 days starts. At *t* = 80 d the fresh water recovery phase starts.

In the following model simulation the influence of the groundwater velocity is investigated and compared to the results without ambient groundwater flow. The mutual distance between wells in a well field will be 200 m. In this simulation the FSSE-well directly left from the well in the model starts fresh water recovery with a salt water extraction rate of 2,000 m^3/d at t = 50 d. The velocity of the groundwater below the FSSE-well in the model, due to the abstraction of 2,000 m^3/d in a neighboring FSSE-well, is 0.53 m/d:

$$v_s = \frac{Q}{2\pi r D n_e} \tag{45}$$

Figure 32 shows the results of the 2D model with ambient groundwater flow. The neighboring FSSE-well starts extracting at t = 50 d and extracts for 40 days which results in a groundwater velocity below the FSSE-well in the model of 0.53 m/d. The displacement of the bubble is visualized in Figure 32. At t = 90 d the recovery period of the FSSE-well in the model starts. The recovery efficiency is 15%. Ambient groundwater flow has a significant influence on the recovery efficiency.

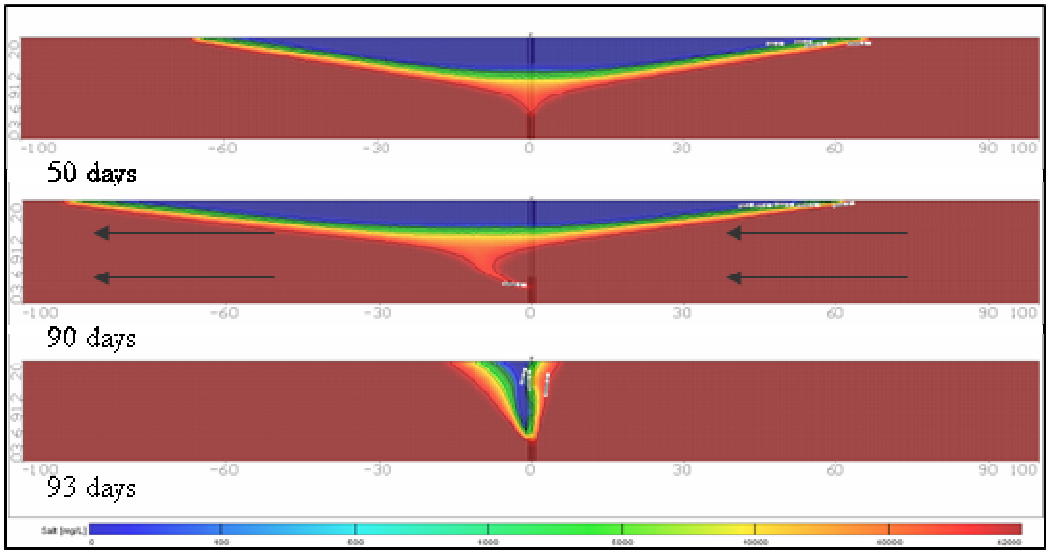

Figure 32: 2D model of a FSSE-well (SEAWAT results). 20 days is the end of the fresh water injection period after which a storage period of 70 days starts. A neighboring well at distance of 200 m left from the well in the model starts extraction at *t* = 50 d and extracts for 40 d with an extraction rate of 2,000 m^3/d, which results in a groundwater velocity of 0.53 m/d. At *t* = 90 d the fresh water recovery phase of the well in the model starts, the interface reaches the fresh water screen after 3 days.

Conclusion

Ambient groundwater flow has an influence on the recovery efficiency. The recovery efficiency after a storage period of 80 days, with an ambient groundwater flow of 0.53 m/d due to fresh water recovery of a FSSE-well in the neighborhood for 40 days, is 15%, compared to 50% without ambient groundwater flow.

7 Applications in Egypt

In this chapter the application of FSSE-wells in the plants of Nefertary and Port Ghalib is discussed. Section 7.1 describes the possibilities in Nefertary. Section 7.2 outlines the possibility of FSSE-well application in Port Ghalib. Section 7.3 gives an example for the operating scheme of a combined extraction-FSSE-well well-field in Port Ghalib.

7.1 Nefertary

Nefertary hotel is located 20 km south of Safaga along the main highway from Cairo via Hurghada to Mersa Alam. The drinking water plant Nefertary produces water for the hotel. The drinking water plant is owned by the American company Ridgewood. There are two pumping wells with a capacity of 60 m^3/h and one injection well for the hyper saline brine water with a capacity of 40 m^3/h. The total capacity of the plant is 500 m^3/day. The efficiency of the plant is 33%. The wells are located 350 m land inward, 12 m above mean sea level (Figure 33). A detailed description can be found in Appendix B.

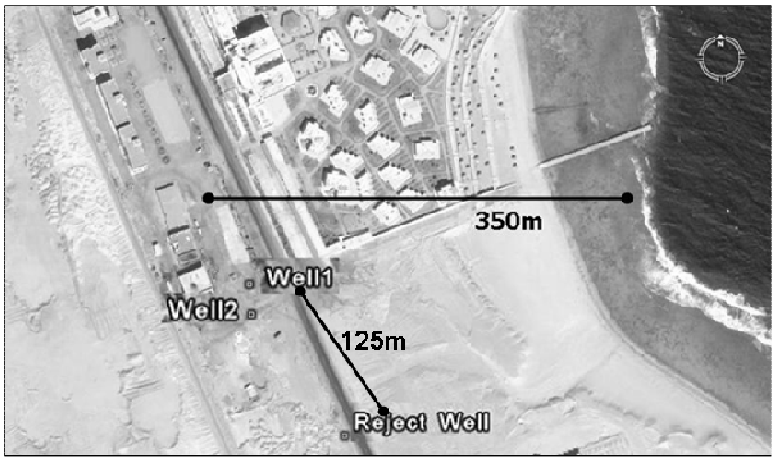

Figure 33: Nefertary area - hotel and drinking water plant with 2 extraction wells and 1 injection well [Google earth].

There are two aquifers in Nefertary at a depth of 20 m and 30 m below ground surface. The aquifers both have a thickness of 6 m. There is a period of low production at the desalination plant. Therefore the question was raised if the capacity of the plant could be used to store the produced fresh water underground and recover it via a FSSE-well. Our model and analysis indicate that it is probably not needed and less feasible to use a FSSE-well in this situation (section 6.6). Instead it is possible to use the conventional techniques (Aquifer Storage Recovery) here, by which the native salt water in the aquifer is completely displaced. By using this storage technique also another problem in Nefertary can be solved.

During the functioning of the wells the quality of the extracted water deteriorated. The original salinity was 42,000 ppm, equal to Red Sea water, but increased to 62,000 ppm. The complete system of pumping wells and injection wells has been functioning for about one and a half year. Egyptian laws do

not allow to pump the hyper saline water directly to the sea close to the coral reefs. Only highly expensive long pipelines far out of the influence zone of the reefs can be accepted. The increase in salinity in the case of Nefertary indicates a short circuit between extraction and injection wells. This has been shown also in the modeling. The problem can be limited by increasing the distance between the wells. This can be done in different ways: by increasing the distance physically by building the injection well a few hundred meters further away, by constructing the injection screen in the deepest aquifer and the extraction screens in the highest aquifer or by the constructing of a barrier between the two extraction wells and the injection well.

By means of the conventional ASR technique, fresh water is injected in the aquifer and the native water is displaced, thus creating a fresh water barrier underground which will turn off the hyper saline flow paths to the extraction wells. A numerical model was constructed to examine the influence of such a screen. Further details of this numerical model can be found in Appendix B.

7.2 Port Ghalib

Port Ghalib is a new built city on the Red Sea coast of Egypt. The city is located 60 km north of Marsa Alam along the main highway from Cairo via Hurghada to Marsa Alam. The city is still in the construction phase. The lay-out of the area of the drinking water plant is given in Figure 34.

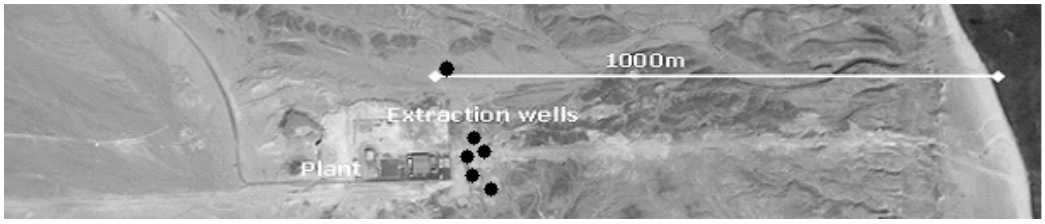

Figure 34: Port Ghalib plant and extraction well field. There are 6 wells. The plant is located 1 km land inward [Google earth].

The existing total capacity of the drinking water plant is 3,000 m^3/day. The recovery of the membranes is 40%. There are 6 extraction wells, each with a pump capacity of 100 m^3/h. The wells are located 1 km land inward, 40 m above mean sea level. The hyper saline brine water from the desalination plant is pumped directly to sea by a pipeline at 500 m off the shore.

Table 4 gives additional information about the extraction wells.

Table 4: Information on the well field: amount, discharge rates, TDS rate, depth, screen length and static level.

Wells	Extraction wells
Amount	6
Discharge (m^3/h)	100
TDS-rate (ppm)	41,250
Depth (m)	150
Screen length (m)	48
Static level	40

Salt water extraction data for the years 2003-2006 were given by the plant manager of Port Ghalib (Figure 35). These data show an annual growth rate of 5%. This growth rate is used here to predict the necessary salt water extraction for the coming years. Maximum salt water extraction in 2006 was 80,000 m^3/month, maximum salt water extraction in 2007 was 86,500 m^3/month. Figure 35 gives the salt water extraction according to an annual growth rate of 5% per year for the years 2003-2010.

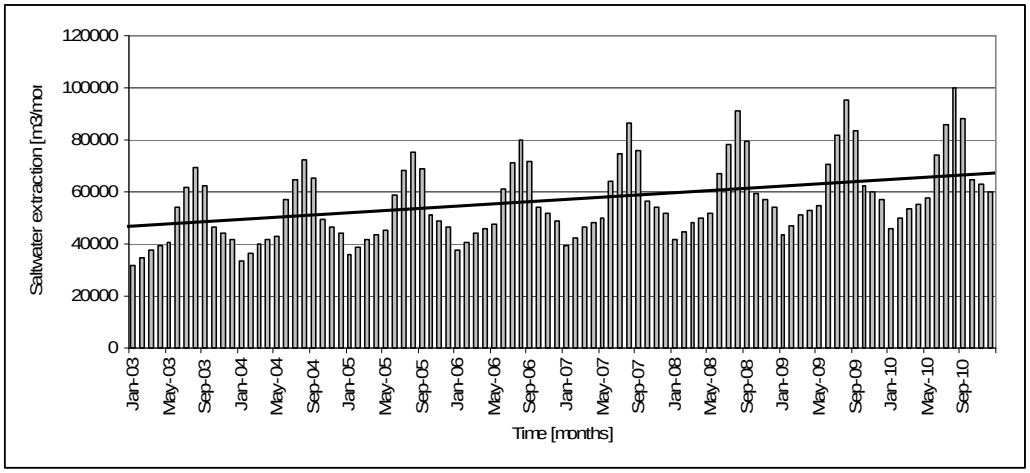

Figure 35: Port Ghalib salt water extraction [m^3/month] for the years 2003-2006. The salt water extraction has been extended to 2010 using a 5% growth rate for the years 2007-2010.

FSSE-wells aim to bridge peak demands for stored fresh water. When, for example, the salt water extraction in the coming years may not exceed the maximum extraction of 2007 (86,500 m^3/month) 1 FSSE-well is needed in 2008 to bridge the demand in August (1 FSSE-well can store a volume of 3,000 m^3 fresh water). In 2009 3 FSSE-well can be used to bridge the demand in July, August and September. In 2010 4 wells are needed to bridge the high demand in July, August and September. In Table 5 different maximum production rates are given together with the necessary number of FSSE-wells to bridge the peak demands in summer.

Table 5: Different maximum production rates, together with the necessary number of FSSE-wells to bridge the peak demands in summer.

Max production	86,500 [m^3/month]	80,000 [m^3/month]	70,000 [m^3/month]	65,000 [m^3/month]	60,000 [m^3/month]
2008	1 FSSE-wells	3 FSSE-wells	5 FSSE-wells	8 FSSE-wells	10 FSSE-wells
2009	3 FSSE-wells	5 FSSE-wells	9 FSSE-wells	11 FSSE-wells	13 FSSE-wells
2010	4 FSSE-wells	8 FSSE-wells	12 FSSE-wells	14 FSSE-wells	16 FSSE-wells

In the following section an example is given for the operating scheme of a combined extraction-FSSE well field. The maximum production is 70,000 m^3/month.

7.3 Port Ghalib example case

In this section an example is given for the operating scheme of a combined extraction-FSSE well field. The maximum salt water extraction is 70,000 m^3/month. Figure 36 gives the salt water demand and total salt water extraction in a bar-diagram. The case is not tested in the field yet.

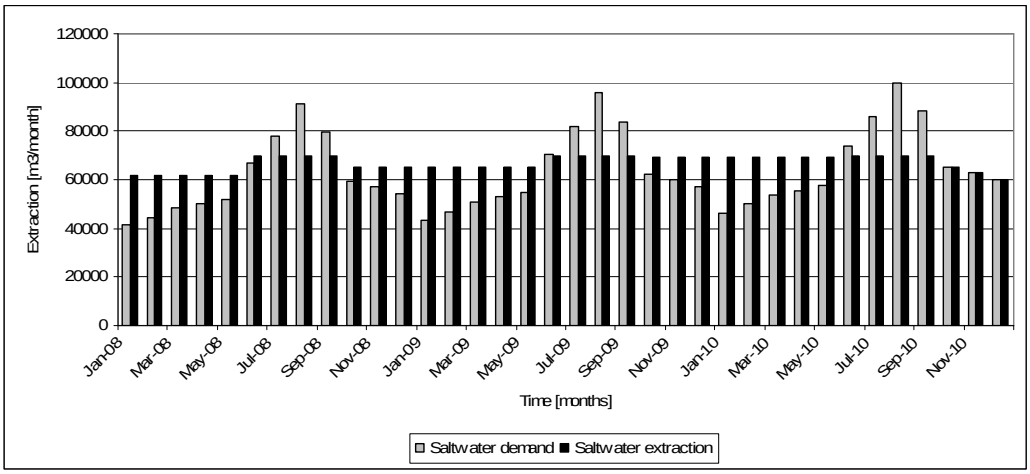

Figure 36: Salt water demand and total salt water extraction for the years 2008-2010.

This example uses the salt water extraction data of Figure 35 as the demand (the light bars in Figure 36). The dark bars are such that the peak demands are matched from storage, using a salt water extraction ceiling of 70,000 m^3/month. The production during low demand months has been made as equal as possible (dark bars of Figure 36). The difference in each month is either stored or taken from storage as shown. This provides the necessary injection and recovery rates for the simulation.

The production scheme for the years 2008-2010 by a maximum extraction of 70,000 m^3/month is shown in Table 6. The capacity of 1 extraction well is 100 m^3/h and the extraction wells are maximum 7 hours per day in operation. The production is assumed to be constant over one month.

The recovery of the membranes is 40%, requiring a salt water extraction of 2.5 times the fresh water production. In July 2008 the salt water demand is 78,000 m^3/month. A fresh water volume of 3,200 m^3 must come from storage. 1 FSSE-well can store 3,000 m^3, there is 1 FSSE-well needed in July 2008. In August 2008 the demand is 91,000 m^3/month and a fresh water volume of 8,400 m^3 must come from storage. There are 3 FSSE-wells needed in August 2008. In September 2008 the demand is 79,500 m^3/month, which equals a fresh water volume of 3,800 m^3. There is 1 FSSE-well needed in September 2008. In total 5 FSSE-wells are needed to bridge the peak demand in July, August and September 2008.

Twice the extra stored fresh water volume needed in summer 2008 was produced in the months before. One needs to inject 6,000 m^3 fresh water per FSSE-well in the months before. For five FSSE-

wells a volume of 30,000 m^3 is necessary. This volume is created by overproduction in the months January till June 2008. The production during these months is constant at 62,000 m^3/month.

The salt water extraction during the storage phase is 240 m^3/d per FSSE-well. At a certain moment all FSSE-wells produce enough to answer the salt water demand and the old extraction wells are not needed anymore (for this particular situation this happens from November 2009 on). During recovery of the stored water a FSSE-well yields 2,000 m^3 fresh water per day. This is more than needed for the production. A solution for this extra water must be found.

In summer 2009 a fresh water volume of 20,600 m^3 is needed. The 5 FSSE-wells used in 2008 can be used again. The recovery of these wells is 67%, a volume of 15,000 m^3 fresh water must be injected in the months before, 10,500 m^3 can be recovered from these wells. 4 extra FSSE-wells are needed. Therefore a volume of 24,000 m^3 fresh water must be injected in the months before. The extra fresh water volume is produced in the months October 2008 till May 2009. The production during these months is constant at 65,000 m^3/month.

In June, July, August and September 2010 a fresh water volume of 27,200 m^3 is needed to bridge the peak demand. The recovery rate of the 5 FSSE-wells originating from 2009 is 80%, the recovery rate of the 4 FSSE-wells originating from 2010 is 67%. 20,000 m^3 can be stored in the old FSSE-wells. 3 extra FSSE-wells are needed.

The radius of a bubble is 100 m. The mutual distance between two wells is 200 m. After three years 12 FSSE-wells are in operation. A 3 by 4 FSSE-well field can be used with an area of 600 * 800 m^2.

A model has been used to simulate the behavior of one of the FSSE-wells for this example case. This well is assumed to be taken into operation in January 2008 and used during the following three years of the example 2008-2010. At the beginning of the storage phase, the simulated FSSE-well is the first well in the well field used for storage. And at the beginning of the subsequent recovery phase the simulated FSSE-well is the first from which fresh water is recovered. This well thus has the longest storage periods of the wells in the field. The maximum storage period is 220 days in the winter of 2009-2010. The last column of Table 6 gives the operation of this FSSE-well. Figure 37 gives the result of the simulation.

Figure 37: Fresh water bubble during a 3 year simulation of subsequent injection-storage-recovery cycles (SEAWAT results). At 1 January 2008 the well is taken into operation, fresh water is injected with an injection rate of 100 m^3/d. 1 March is the end of the injection period after which a storage period of 4 months starts in which salt water is extracted with a extracting rate of 240 m^3/d. At 25 June 2008 the salt water extraction discharge is increased to 2000 m^3/d in order to increase the inclination of the interface. At 1 July 2008 fresh water is recovered with a recovery rate of 100 m^3/d till the 1 August 2008. In August and September the bubble is 'empty' and the salt water extraction rate is 240 m^3/d. At 1 October 2008 a second fresh water injection period starts and at 5 December 2008 the bubble is full again. A subsequent storage period follows from December till 25 June 2009. Fresh water is recovered from 1 July till 1 August 2009. A third fresh water injection period starts at 1 October 2009 and the bubble is full again at 5 November 2009. The bubble is stored from 5 November till 9 June 2010. The fresh water is recovered from 14 June 2010 till 10 July 2010.

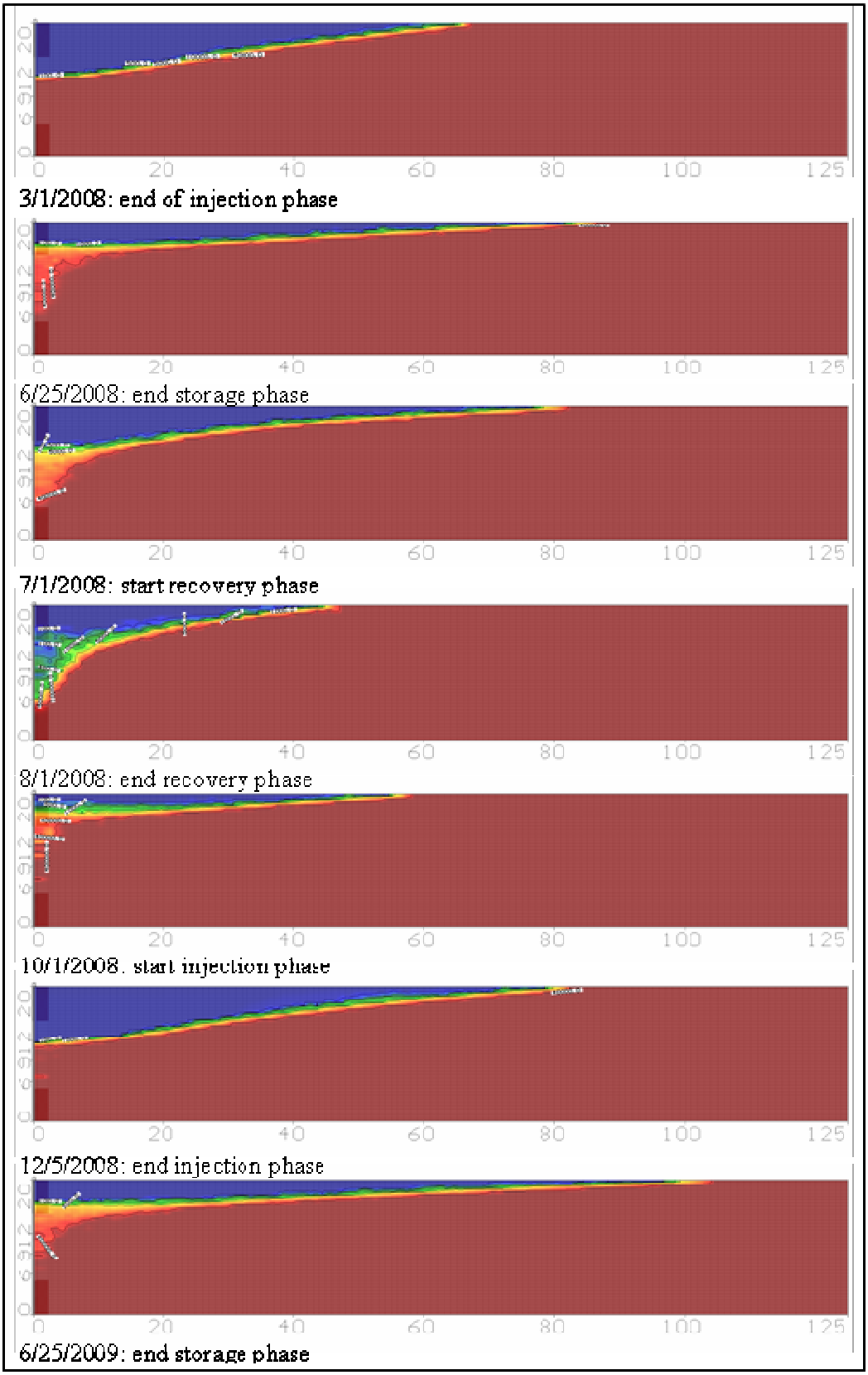
3/1/2008: end of injection phase
6/25/2008: end storage phase
7/1/2008: start recovery phase
8/1/2008: end recovery phase
10/1/2008: start injection phase
12/5/2008: end injection phase
6/25/2009: end storage phase

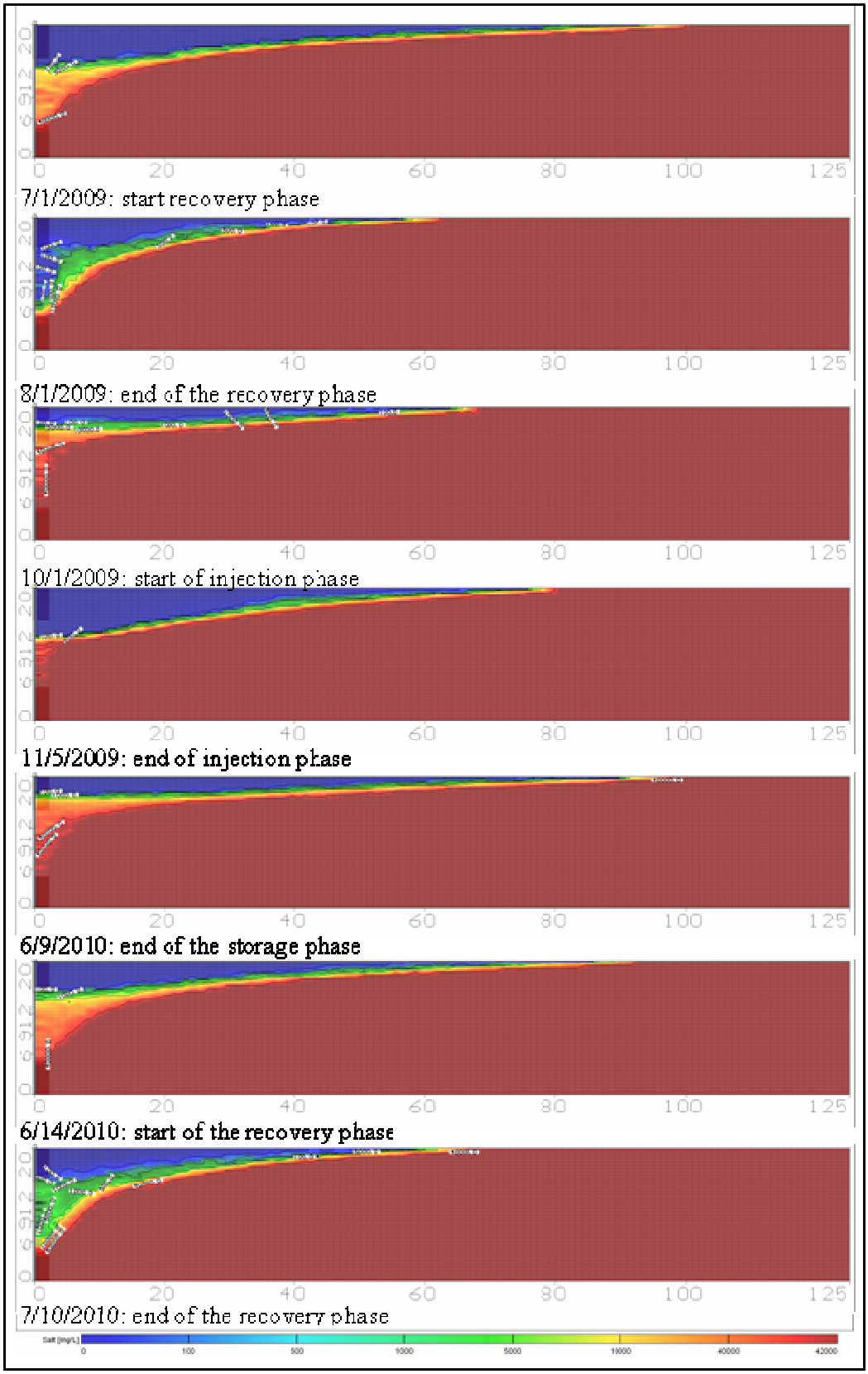
7/1/2009: start recovery phase
8/1/2009: end of the recovery phase
10/1/2009: start of injection phase
11/5/2009: end of injection phase
6/9/2010: end of the storage phase
6/14/2010: start of the recovery phase
7/10/2010: end of the recovery phase
0
20
40
60
80
100
125

Table 6: The operation scheme of a combined extraction-FSSE well field. The salt water demand and salt water extraction per month is given and the amount of FSSE-wells and extraction wells. In the last column the operation of the simulated FSSE-well are given (Figure 37).

Month	Salt water demand	Salt water production		FSSE wells		Extraction wells		Operation simulated FSSE-well
	m3/month	m3/month	m3/d	nr	m3/d	nr	m3/d	
Jan-08	41500	62000	2067	2	480	3	1587	Injection
Feb-08	44500	62000	2067	3	720	2	1347	Injection
Mar-08	48500	62000	2067	4	960	2	1107	Storage
Apr-08	50000	62000	2067	5	1200	2	867	Storage
May-08	52000	62000	2067	5	1200	2	867	Storage
Jun-08	67000	70000	2333	5	1200	2	1133	Storage
Jul-08	78000	70000	2333	5	1200	2	1133	Recovery
Aug-08	91000	70000	2333	5	1200	2	1133	Empty
Sep-08	79500	70000	2333	5	1200	2	1133	Empty
Oct-08	59500	65000	2167	5	1200	2	967	Injection
Nov-08	57000	65000	2167	5	1200	2	967	Injection
Dec-08	54000	65000	2167	5	1200	2	967	Storage
Jan-09	43500	65000	2167	7	1680	1	487	Storage
Feb-09	47000	65000	2167	8	1920	1	247	Storage
Mar-09	51000	65000	2167	9	2160	0	0	Storage
Apr-09	53000	65000	2167	9	2160	0	0	Storage
May-09	55000	65000	2167	9	2160	0	0	Storage
Jun-09	70500	70000	2333	9	2160	1	173	Storage
Jul-09	82000	70000	2333	9	2160	1	173	Recovery
Aug-09	95500	70000	2333	9	2160	1	173	Empty
Sep-09	83500	70000	2333	9	2160	1	173	Empty
Oct-09	62500	69000	2300	9	2160	1	107	Injection
Nov-09	60000	69000	2300	9	2160	1	107	Storage
Dec-09	57000	69000	2300	9	2160	1	107	Storage
Jan-10	46000	69000	2300	9	2160	1	107	Storage
Feb-10	50000	69000	2300	9	2160	1	107	Storage
Mar-10	53500	69000	2300	10	2400	0	0	Storage
Apr-10	55500	69000	2300	11	2640	0	0	Storage
May-10	57500	69000	2300	12	2880	0	0	Storage
Jun-10	74000	70000	2333	12	2880	0	0	Storage
Jul-10	86000	70000	2333	12	2880	0	0	Recovery
Aug-10	100000	70000	2333	12	2880	0	0	Recovery
Sep-10	88000	70000	2333	12	2880	0	0	
Oct-10	65000	65000	2167	12	2880	0	0	
Nov-10	63000	63000	2100	12	2880	0	0	
Dec-10	60000	60000	2000	12	2880	0	0	

8 Conclusions

8.1 Summary

This research is a feasibility study to determine whether fresh water storage in saline aquifers is possible by means of the Fresh Storage Saline Extraction (FSSE) well. The focus was on the situation prevailing along the Red Sea coast of Egypt.

The research question was whether fresh water can be stored in and recovered from a saline aquifer by means of a FSSE-well. The answer to the research question was sought by means of a mathematical solution to the problem followed by numerical modeling a representative situation using SEAWAT.

8.2 Conclusions

The results of the research show that it is possible to store fresh water in and recover fresh water from a saline aquifer by means of a FSSE-well.

The fresh water bubble can be kept in place around the well by continuous extraction of salt water at a limited rate of about 10% of normal extraction rates. Separate screens are necessary because with only one screen a seepage face will establish causing continuous mixing with salt water. The salt water extraction rate and the radius of the bubble can be calculated with an analytical formula derived in this research.

An interface is created between the injected fresh water and the salt water in the aquifer. During storage periods 4% fresh water is lost per month due to hydrodynamic dispersion for the case considered. After a storage period it is necessary to increase the rate of the salt water extraction some days before the onset of fresh water recovery to drive the fresh water closer to the well before recovery starts.

It is possible to infiltrate and recover the water in different cycles of injection and extraction. The mixing zone can be considered an investment and as such be added to the overall investment of the plant which can be used during successive storage-recovery periods. The mixing zone is equivalent to the walls of a storage basin above ground as it kind of prevents losses from subsequent injection-storage-recovery cycles. The recovery efficiency increases in successive cycles. The recovery efficiency in the first cycle is 50% in the second 67% and in the third 80% for the case considered.

The storable and recoverable volume is dependent on the characteristics of the aquifer: its thickness, hydraulic conductivity, heterogeneity and groundwater flow.

- In thicker aquifers, the salt water extraction can be larger than in thinner aquifers. Due to the larger possible salt water extraction flow more water can be kept in place. It is attractive to store the water in a thick aquifer if a FSSE-well is used. In thinner aquifers conventional ASR can be used by which the native salt water in the aquifer is completely displaced.

- A larger conductivity in the aquifer creates flatter more extended bubbles and so a larger radius is needed to store the same volume. To keep a bigger bubble in its place, a larger salt water extraction is needed.
- Heterogeneity of the aquifer needs to be determined in the field, it may be critical. When the aquifer is intersected by a gravel layer in the upper part, in the fresh water bubble, the mixing zone is increased and the recovery efficiency becomes very low (after a storage period of 90 days 8% for the case considered). But, when the aquifer is intersected by a clay layer in the middle of the aquifer, just below the fresh water bubble, the recovery efficiency becomes very high (after a storage period of 90 days 50% for the case considered).
- It is possible to recover the bubble after an unmanaged period of no pumping of the order of one week (calamity or maintenance) in which the bubble has floated to the ceiling of the aquifer for the case considered. But after a period of 1 month it is impossible to recover the fresh water with the normal salt water extraction rate.
- Ambient groundwater flow has a substantial influence on the recovery efficiency as well. For example a 15% recovery efficiency was obtained after a storage period of 80 days, with after 40 days, 40 days ambient specific groundwater flow of 0.53 m/d.

8.3 Recommendations

During this research interesting ideas have been raised that have to be studied in further detail. Due to time restrictions this has not been done in this thesis.

In this research the FSSE-wells have been analyzed from the point of view of groundwater hydraulics to examine their geohydrologic feasibility and to learn about the operations and design criteria necessary to make such systems a success in practice. A field experiment should be carried out before FSSE-wells can be used on large scale. The DEC ASR plans to carry out a pilot project in the next phase of the project, which is intended to start in January 2008. The results of a pilot project will give insight in well design, well construction and operation, recovery efficiency, mixing characteristics, water quality changes and the effect of storage time on water quality and recovery efficiency.

It is useful to have some idea of expected overall cost to compare with other water management alternatives that may achieve some or all of the same objectives. The DEC ASR has done a preliminary investigation on the savings per unit production cost by introducing ASR in relation to desalination plant capacity [Lamei, 2007]. It is advisable to develop a new estimate of the capital and operating costs of FSSE-well operation with the efficiency figures from this research. Such cost estimates can be confirmed upon completion of the testing phase.

It is to be recommended to investigate the advantages of fresh water storage combined with subsurface energy storage or wastewater storage.

It will be interesting to explore the application of FSSE-wells in other situations, i.e. to bridge weekly or day-night demand variations in drinking water companies or to prevent salt water upconing.

References

Aliewi, A.S., Mackay, R., Jayyousi, A., Nasereddin, K., Mushtaha, A., Yaqubi, A., 2001. Numerical simulation of the movement of salt water under skimming and scavenger pumping in the Pleistocene aquifer of Gaza and Jericho areas, Palestine. Transport in Porous Media, 43 (2001) 195-212.

Asghar, M.N., Prathapar, S.A., Shafique, M.S., 2002. Extracting relatively-fresh groundwater from aquifers underlain by salty groundwater. Agricultural Water Management 52 (2002) 119-137.

Attia, F.A.R. and E.H. Smidt, 1999. Contributions to environmental management of Egypt's groundwater resources. Final report EMGR project, 1994-1999. RIGW/Iwaco, 1999.

DEC ASR – Desalination and Aquifer Storage Recovery, 2007. Eindrapportage Desalinisatie en ASR (D-ASR) in Egypte (projectcode PVW06053), september 2007.

BBC weather centre, 2007: www.bbc.co.uk/weather.

Bear, J, 1978. Hydraulics of groundwater, Keterpress Enterprises, Jeruzalem, Israel.

Bloetscher, F., Muniz, A., Witt, G.M., 2005. Groundwater injection, modeling, risks, and regulations. The McGraw-Hill Companies, USA.

Boekelman, R.H., Bolier, G., van Dijk, M.J., van Genuchten, C.C.A., 2002. Lecture notes Geohydrology 1, TU Delft.

Bouwer, H., 2002. Artificial recharge of groundwater: hydrologeology and engineering. Hydrogeology Journal (2002) 10:121-142

Buros, O.K., Pyne, R.D.G., 1994. Extending water supplies in water short areas. Desalination 98 (1994), p437-442.

Chenaf, D., Chapuis, R.P., 2007. Seepage face height, water table position and well efficiency at steady state. Groundwater vol 45-2 (2007) 168-177.

Dabbagh, T.A., 2001. The management of desalinated water. Desalination 135 (2001) 7-23.

De Moel, P.J., Verberk, J.Q.J.C., van Dijk, J.C., 2006. Drinking water, Principles and Practices. World Scientific Publishing, p348-349.

Dillon, P. Pavelic, P., Toze, S., Rinck-Pfeiffer, S., Russell, M., Knapton, A., Pidsley, D., 2006. Role of aquifer storage in water reuse. Desalination 188 (2006) 123-134

El-Sadek, S., Mabrouk, B., 1992. Tourism development and desalination systems: comparative analysis of systems' suitability for coastal areas of the Red Sea and Gulf of Aqaba, Egypt. Desalination, 88 (1992) 161-177.

FAO: fao/org/ag/Agl/swlwpnr/reports/y_nf/Egypt/e_clim8.htm.

Fitts, C.R., 2002. Groundwater Science, Academic Press, San Diego, California, USA.

Google, Google earth.

Guo, W., Langevin, C.D., 2002. User's guide to SEAWAT: a computer program for simulation of three-dimensional variable density groundwater-flow. USFS Open file report 01-434.

Hafez, A., El-Manharawy, S., 2002. Economics of seawater RO desalination in the Red Sea region, Egypt, part 1, a case study. Desalination 153 (2002) 335-347.

Integral-transformer: integrals.wolfram.com/index.jsp.

Lamei, A., van der Zaag, P., von Munch, E., 2007. Basic cost equations to estimate unit production costs for RO desalination and long-distance piping to supply water to tourism-dominated arid coastal regions of Egypt. Desalination, 6-8-2007.

McDonald, M.G., Harbough, A.W., 2000. User's documentation for the U.S. Geological Survey modular finite-difference groundwater flow model, USGS.

Ministry of Tourism, Egypt, 2007: www.touregypt.net.

Olsthoorn, Th.N., 2007. Modeling the phreatic surface with a density model and verifying the results using the Dupuit solution and what is known about the relation between flow and head at the base of the aquifer and the velocities at the well face. TU Delft, Water Resources Section, Waternet.

Oude Essink, G.H.P., 2001. Density dependent groundwater flow – Salt water intrusion and heat transport. University of Utrecht, Interfaculty Centre of Hydrology Utrecht, Institute of Earth Sciences, Department of Geophysics.

Pollock, D.W., 1994. User's guide for Modpath/Modpathplot, version 3: a particle tracking post-processing package for MODFLOW, the U.S. Geological survey finite-difference groundwater flow model. USGS open-file report 94-464. USGS: Reston, Virginia, USA.

Pyne, R.D.G., 2007. Aquifer Storage Recovery: a guide to groundwater recharge through well. ASR systems LLC, Gainesville, Florida, USA.

Rientjes, T.H.M., Boekelman, R,.H., 2001. Lecture notes Hydrological Models, TU Delft.

Saeed, M.M., Ashraf, M., Asghar, M.N., Bruen, M., Shafique, M.S., 2002. Farmers' skimming well technologies: practices, problems, perceptions and prospects. Working Paper No. 40: Root zone salinity management using fractional skimming wells with pressurized irrigation. Lahore, Pakistan: International Water Management Institute, p6.

Saeed, M.M., Ashraf, M., Asghar, M.N., 2003. Hydraulic and hydro-salinity behavior of skimming wells under different pumping regimes. Agricultural Water Management 61 (2003) 163-177.

Schlumberger Water Services, Visual MODFLOW Premium, A professional application for 3D groundwater flow and contaminant transport modeling. User's Manual, 4.2.

Sedighi, A., Klammler, H., Brown, C., Hatfield, K., 2006. A Semi-analytical model for predicting water quality from an aquifer storage and recovery system. Journal of Hydrology (2006) 329, 403-412.

Shalaan, I.M., 2005. Sustainable tourism development in the Red Sea of Egypt threats and opportunities. Journal of Cleaner Production 13 (2005) 83-87.

Shata, A., 2007. Hydrogeologic information Egypt and Red Sea Area (see final PvW report on Desalination and ASER, 2007).

Sufi, A.B., Latif, M., Skogerboe, G.V., 1998. Simulating skimming well techniques for sustainable exploitation of groundwater. Irrigation and Drainage Systems, 12 (1998) 203-226, p207.

WHO, 2006. Guidelines for drinking water quality. Electronic version for the Web. ISBN 92 4 154696 4

World Bank, 2007: www.worldbank.org.

Zheng, C., Wang, P.P., 1998. MT3DMS Reference Manual, University of Alabama, USA.

Appendices

A. Related techniques.

B. Area descriptions.

C. Matlab script analytical solution.

D. Method of Characteristics.

E. Model settings.

F. Sensitivity analyses.

Appendix A Related techniques

Aquifer Storage and Recovery

Aquifer storage recovery is a practical, cost-effective and environmentally acceptable water management technique which is applicable to many water short areas that use seawater desalination, long pipelines, or other high capital cost facilities as part of the source of supply [Buros and Pyne, 1994]. Aquifer storage recovery (ASR) may be defined as the storage of water in a suitable aquifer through a well during times when water is available, and subsequent recovery of the water from the same well during times when it is needed [Pyne, 2007].

The principle component of an ASR system is an injection/extraction well which operates in cycles. Each cycle includes periods of water injection (recharge), storage and extraction (recovery) and each period lasts from several days to months. During injection, fresh water is introduced into an aquifer where it displaces ambient groundwater to form a reservoir or bubble of stored water. An interface develops between injected water and ambient groundwater which is not sharp, but a manifestation of hydrodynamic dispersion, i.e. a transition or mixing zone reflecting differences in solute concentrations between injected and ambient waters [Sedighi, et al., 2006].

ASR feasibility has been demonstrated at a growing number of operational sites in the USA and Australia in the past years. In Florida, for example, the City of Cocoa has been operating an ASR system since 1987. They are using this to reduce the need to expand their well field, 80 km of transmission pipeline and the treatment plant capacity to meet increasing seasonal peak demands. The water is being transported to the city during low use season and is withdrawn during the peak winter season. The goal is to build an ASR storage volume of 4 million m^3 in a brackish limestone aquifer at a depth of 100 m below ground surface [Buros and Pyne, 1994]. ASR has been used in Manatee County, Florida, where seasonally available water from Lake Manatee is stored underground using ASR. This is during months when flows are high and the demand low. This water is removed in spring, disinfected and pumped to the distribution system when the river flow is low and the demands high [Buros and Pyne, 1994]. Another application is in the Florida Keys, where water is brought down an island chain in the Gulf of Mexico through a 200 km pipeline to serve the islands along the chain. This pipeline is very vulnerable to disruption of its water supply through hurricanes or accidents. An ASR well has been tested with initial volumes of 60,000 m^3 in a saline aquifer that extends under the Gulf of Mexico [Buros and Pyne, 1994].

ASR wells make it possible to design and operate water-treatment plants for mean daily demand. The use of ASR wells to store seasonal surplus water and meet seasonal peak demands is often cheaper than the use of treatment plants and surface reservoirs with capacities based on peak demands without ASR [Bouwer, 2002]. When compared to surface water storage reservoirs, aquifer storage is very low cost, since land requirements are minimal and the storage capacity is provided by nature for the relatively low cost of a few ASR wells [Pyne, 2007]. Aquifer storage reservoirs do not harbor mosquitoes

or algal bloom, and there are no evaporation losses that can increase the salinity of the remnant water [Dillon et al., 2006].

The recovery efficiency of an ASR plant is defined as the percentage of water volume stored that is subsequently recovered while meeting a target water quality criterion in the recovered water [Pyne, 2007]. The recovery efficiency is controlled by a wide variety of factors, including ambient hydraulic gradient, aquifer permeability, porosity, heterogeneity, thickness and confinement; ambient groundwater density and quality, injected water density and quality; and ASR operation [Sedighi et al., 2006].

100% recovery efficiency is attainable at most ASR sites [Pyne, 2007], however a transition zone between injected water and ambient groundwater must be developed. The water needed for this transition zone can be seen as an investment analogous to constructing a reservoir above ground.

Skimming Wells

Worldwide, intrusion and upconing of saline water in fresh water aquifers are considered critical concerns in coastal and inland areas [Sufi et al., 1998]. Excessive over-pumping is the most common cause of salt water intrusion in coastal and inland fresh saline aquifers. In coastal aquifers, there is a direct contact between inland fresh water and marine saline water at a sloping interface. In inland aquifers, the fossil saline groundwater is overlain by fresh water accumulated as a result of recharge from precipitation, irrigation systems and natural streams. Exploitation and mining of fresh water resources in these aquifers take place regularly for irrigation purposes and to mitigate droughts, especially in (semi) arid regions [Saeed et al., 2003]. Extraction of water from inappropriate depths and at inappropriate rates will cause upconing of the interface between the relatively fresh groundwater lens and saline groundwater layer, and draw marginal quality water to the root zone or into the extraction well, resulting in an increase in salinity [Asghar et al., 2002].

One solution is the installation of horizontal subsurface drains below the water table, and an alternative method is the installation of shallow skimming wells [Asghar et al., 2002]. Skimming wells were first designed in the early 1970s. Skimming well is a general term to represent any well in which the depth of the well is defined by taking into consideration the underlying saline water layer and with an intention to extract relatively fresh water. Skimming wells are partially penetrating wells and screened in the upper fresh water layer of the aquifer [Saeed et al., 2002]. Different types of skimming wells are being used, including skimming tubewells (single strainer, multi strainer and centrifugal), radial wells, compound or scavenger wells and recirculation wells, Figure 38.

The objective of any skimming technique would be to extract fresh water with minimal disturbance of underlying saline water. The pumped water quality in skimming wells mainly depends upon the hydrogeological conditions of the aquifer, design and operation of wells. Among the hydrological conditions, the thickness of the fresh water lens, the source of fresh water recharge, the hydraulic parameters of the aquifer, and the existence of a natural barrier to prevent saline upconing are important [Saeed et al., 2003]. In the long term the operation of skimming wells may pose salinity hazards even if the well is properly designed and operated.

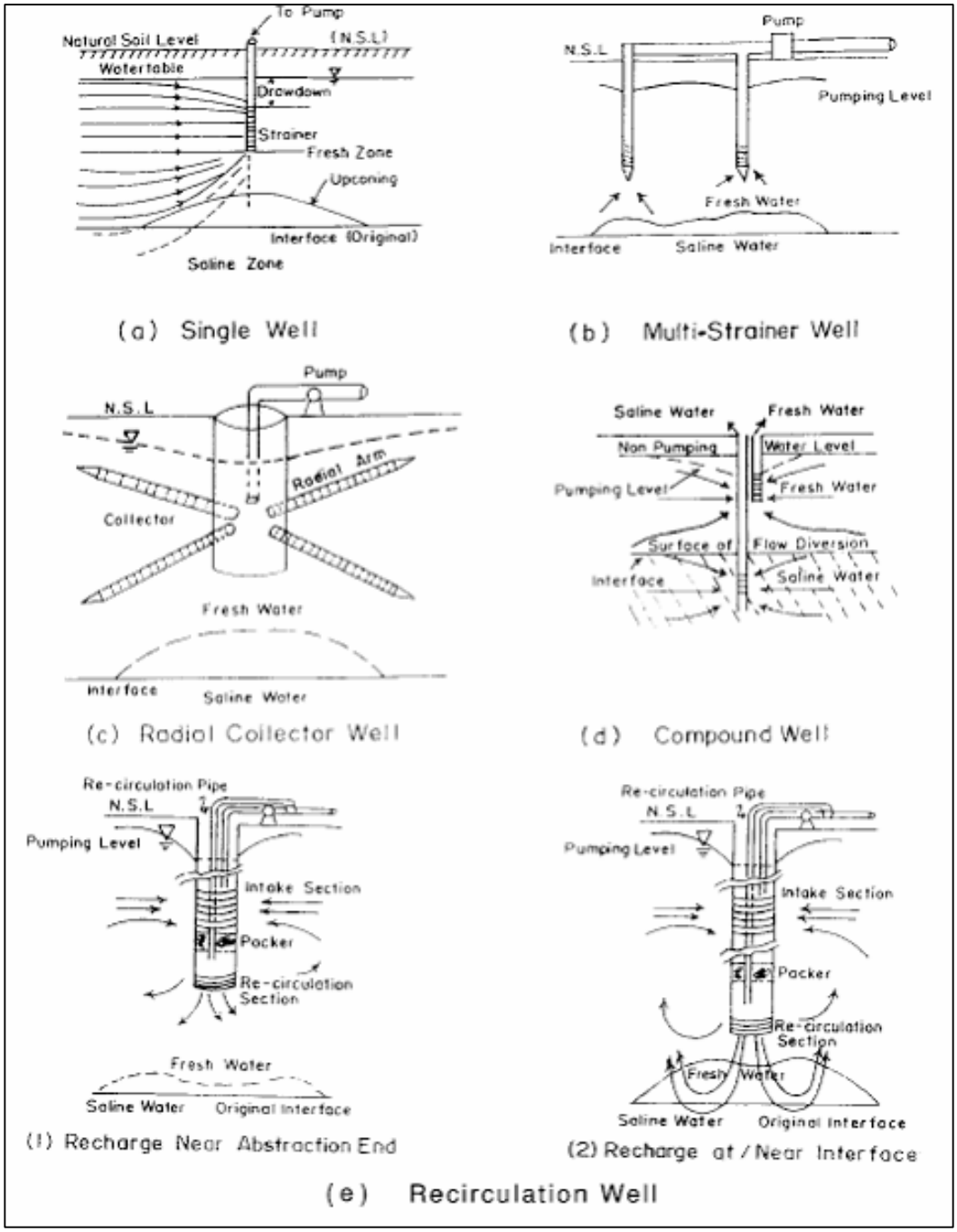

Figure 38: Different types of skimming wells [Sufi et al., 1998]

Scavenger wells both pump the fresh and saline groundwater to extract water from thin fresh groundwater lenses overlying saline water. Two casings are lowered in either a single borehole or in closely spaced boreholes. One casing is screened at the upper fresh water layer while the second is screened just below the fresh-saline interface. The fresh and saline water are extracted separately and simultaneously [Aliewi et al., 2001]. The concept of a scavenger well relies on the fact that interface

upconing is the result of pumping in the fresh water zone while interface downconing is caused by pumping saline water. These two processes can be balanced by varying the pumping rates from the two zones [Aliewi et al., 2001].

In the study of Aliewi et al., 2001 in which the movement of salt water under skimming and scavenger pumping in the Pleistocene aquifer of Gaza and Jericho, Palestine, was modeled numerically, the simulations show that the most important and sensitive parameters affecting the movement of saline water under scavenger pumping are:

- The relationship between recharge and fresh water abstraction rates, provided that the saline water pump is not in operation. This ratio plays a big role in determining the deficit that may come from deep salt water when the recharge rate is less than fresh water abstractions.
- The location of the well screen with respect tot the initial position of the fresh saline water interface. It is shown that if the fresh water well screen is closer to the initial position of the fresh saline water interface, then the mixing process will happen sooner and the overall abstracted water will have relatively higher values of salinity.
- The aquifer vertical permeability K_z. Higher values of K_z means more mixing between saline and fresh water.
- The transverse dispersivity. Increasing values of transverse dispersivity means more mixing and faster movement of the top of the transition zone.

It was also shown in the study of Aliewi et al, 2001, that the following parameters did not play a significant role in the process of vertical mixing between fresh and saline water under different operational conditions: lateral flow, horizontal permeability, longitudinal dispersivity, well screen length (although its position is important).

The mobilization of deep salts, the disposal of saline water, and the seepage of saline water during disposal are the main disadvantages of scavenger wells, which define the long-term negative impacts of these scavenger wells [Ali et al., 2004].

Appendix B Area descriptions

Five desalination plants along the Egyptian Red Sea coast were visited by the researcher in April and May 2007, during data collection field trips with the DEC ASR. These plants were El Gouna, Nefertary, Port Ghalib, Equinox and Cataract. The location of the plants is visualized in Figure 39.

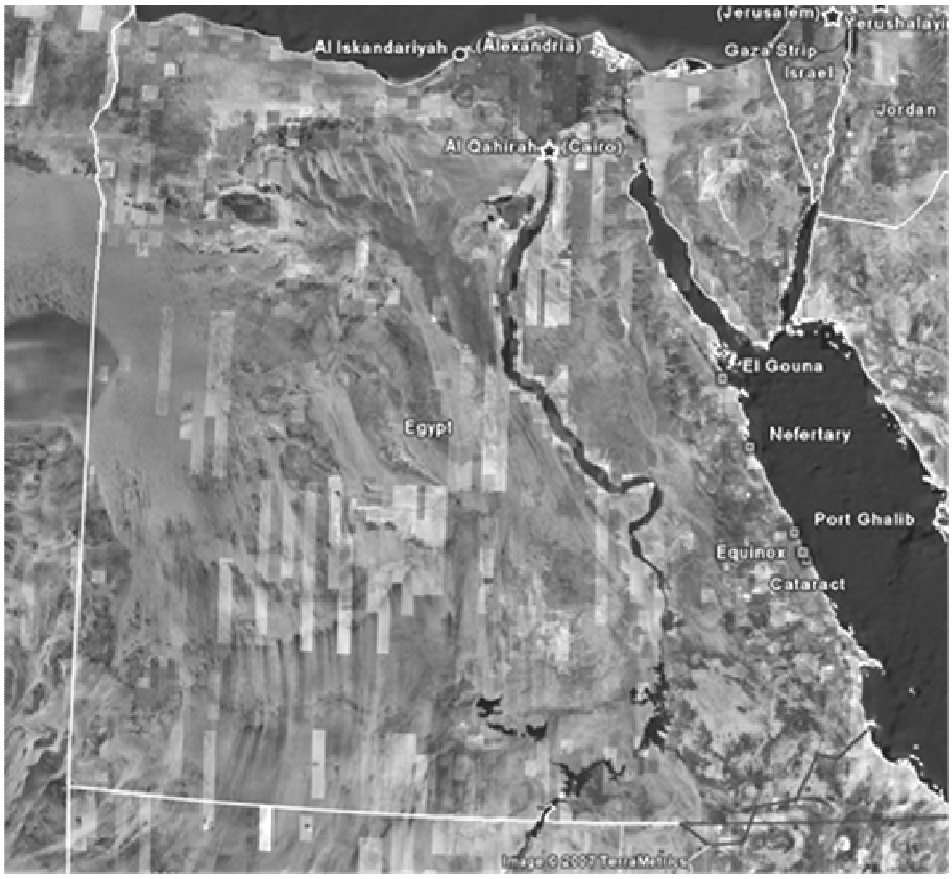

Figure 39: Egypt and the location of the five desalination plants El Gouna, Nefertary, Port Ghalib, Equinox and Cataract [Google Earth].

During the field trips the following data was collected: detailed description of the location (GPS measurements and sketches), lithology, salinity rate, well design, treatment scheme, production rate, demand figures and transmissivity assumptions. Besides, measurements were done in the well with CTD divers [Van Essen Instruments]. CTD divers were used to obtain a profile along the entire length of the well screen. This was done by lowering the diver slowly to the bottom of the well screen, while the registration frequency was high, i.e. once every 5 seconds. The researcher constructed several preliminary numerical models of the locations in close cooperation with Safaa Soliman of the Egyptian Research Institute on Groundwater in Cairo. The information in this appendix is classified information of clients in Egypt. For information on the project the reader is referred to Mr. E. Smidt, team leader DEC-ASR, smidt.sg@inter.nl.net or Mr. P. Westerhuis, project director DEC-ASR, pwesterhuis@slb.com.

Appendix C Matlab script analytical solution

```
clear;
close all;

%define constants
D = 20;
k = 30;
rho_s = 1025;
rho_f = 1000;
nu_s = (rho_s-rho_f)/rho_s;
Qs = [10:1:240];
r0 = 2.5;
R = [10:1:100];
delta_r = 1;
n= 0.15;

%create empty matrices
V=zeros(length(Qs),length(R));
W=zeros(length(Qs),length(R));

%define the functions b and g used in the analytical solution
b = @(Qs) (Qs/(pi()*k*nu_s));
g = @(Qs,R) ((exp(D^2/ (Qs/(pi()*k*nu_s)) ))/R);

%calculation
   %calculate for R=[10:1:100]
    for i=1:length(R);
       %calculate for Qs=[10:1:240]
        for j=1:length(Qs);
        r = [r0:delta_r:R(i)];
       %numerical solution
        h = sqrt(D^2+Qs(j)*(log(r/R(i)))/(pi()*k*nu_s));
        V (j,i) = sum((n*2*pi()*r.*(D-h)*delta_r),2);
       %analytical solution
        W (j,i) = ...
            1/4*pi()*n*...
            ( (D - sqrt(b(Qs(j))*log(g(Qs(j),R(i))*R(i)) ))*4*R(i)^2  +...
            (2*sqrt(2) * mfun('dawson',sqrt(2*(log(g(Qs(j),R(i))*R(i))))))...
              *R(i)^2 * sqrt(b(Qs(j))) ) ) - ...
            1/4*pi()*n*...
            ( (D - sqrt(b(Qs(j))*log(g(Qs(j),R(i))*r0) ))*4*r0^2  +...
            (2*sqrt(2) * mfun('dawson',sqrt(2*(log(g(Qs(j),R(i))*r0) ) ))...
              *r0^2 * sqrt(b(Qs(j))) ) );
        end
    end

%plot(r,h); ylabel('h(m)');xlabel('r(m)')
[cs,h]=contour(R,Qs,V,[100 200 500 1000 2000 4000 6000]),xlabel'R[m]',
ylabel 'Qs[m3/day]', title 'Volume [m3], D=20m, K=30m/d'
hold on
[cs,h]=contour(R,Qs,W,[100 200 500 1000 2000 4000 6000])

clabel(cs,h);
grid on
```

Appendix D Method of Characteristics

In this research the Method of Characteristics (MOC) is used as the numerical method to solve the transport equation. In this Appendix the method is described in detail. The information on the numerical method was found in the MT3DMS Reference Manual [Zheng and Wang, 1998].

The partial differential equation describing the fate and transport of contaminants of species *k* in 3D transient groundwater flow systems can be written as follows:

$$\frac{\partial\left(nC^k\right)}{\partial t}=\frac{\partial}{\partial x_i}n\left(D_{ij}\frac{\partial C^k}{\partial x_j}\right)-\frac{\partial}{\partial x_i}\left(nv_iC^k\right)+q_sC_s^k+\sum R_n \tag{46}$$

Where C^k is dissolved concentration of species k [ML^{-3}], n is the porosity of the subsurface medium [-], t is time [T], x_i is the distance along the respective Cartesian coordinate axis [L], D_{ij} is the hydrodynamic dispersion coefficient tensor [L^{2}T^{-1}], v_i is linear pore water velocity [L T^{-1}]; v_i is related to the specific discharge through the relationship, $v_i=q_i/n$, q_s is the volumetric flow rate per unit volume of aquifer representing fluid sources (positive) and sinks (negative) [T^{-1}], C_s^k is concentration of the source or sink flux for species k [ML^{-3}] and $\sum R_n$ is the chemical reaction term [ML^{-3} T^{-1}].

The MOC method uses a conventional particle tracking technique based on a mixed Eulerian-Lagrangian method for solving the advection term. The dispersion, sinks/source mixing and chemical reaction terms are solved with the finite difference method.

To use the Eulerian-Lagrangian approach, the transport governing equation needs to be transformed in Lagrangian form. First we can expand the advection term as follows:

$$\frac{\partial}{\partial x_i}\left(nv_iC\right)=nv_i\frac{\partial C}{\partial x_i}+C\frac{\partial\left(nv_i\right)}{\partial x_i}=nv_i\frac{\partial C}{\partial x_i}+Cq_s \tag{47}$$

Substituting this equation in the transport governing equation and dividing both sides by the retardation factor, the governing equation becomes:

$$\frac{\partial C}{\partial t}=\frac{1}{Rn}\frac{\partial}{\partial x_i}\left(nD_{ij}\frac{\partial C}{\partial x_j}\right)-\bar{v}_i\frac{\partial C}{\partial x_i}-\frac{q_s}{Rn}\left(C-C_s\right)-\frac{\lambda_1}{R}C-\frac{\lambda_2}{R}\frac{\rho_b}{n}\bar{C} \tag{48}$$

Where $\bar{v}_i=v_i/R$ represents the retarded velocity of a contaminant particle, λ_1 is the first-order reaction rate for the dissolved phase [T^{-1}], λ_2 is the first-order reaction rate for the sorbed (solid)

phase [T^{-1}], ρ_b is the bulk density of the subsurface medium [ML^{-1}] and $\bar{C}$ is the concentration of species sorbed on the subsurface solids [MM^{-1}].

This equation is an Eulerian expression in which the partial derivative, $\partial C / \partial t$, represents the rate of change in solute concentration at a fixed point in space. This equation can also be expressed in Lagrangian form as:

$$\frac{DC}{Dt} = \frac{1}{Rn}\frac{\partial}{\partial x_i}\left(nD_{ij}\frac{\partial C}{\partial x_j}\right) - \frac{q_s}{Rn}\left(C - C_s\right) - \frac{\lambda_1}{R}C - \frac{\lambda_2}{R}\frac{\rho_b}{n}\bar{C} \tag{49}$$

Where the substantial derivative, $DC/Dt = \partial C/\partial t + \bar{v}_i \partial C/\partial x_i$, represents the rate of change in solute concentration along the path line of a contaminant particle.

By introducing the finite-difference algorithm, the substantial derivative in the previous equation can be approximated as:

$$\frac{DC}{Dt} = \frac{C_m^{n+1} - C_m^{n*}}{\Delta t} \tag{50}$$

So that the equation becomes:

$$C_m^{n+1} = C_m^{n*} + \Delta t * RHS \tag{51}$$

Where C_m^{n+1} is the solute concentration for node *m* at new time level *n+1*, C_m^{n*} is the solute concentration for node *m* at new time level *n+1* due to advection alone, also referred to as intermediate time level n*, Δt is the time step between old time level *n* and new time level *n+1*, and RHS represents the finite-difference approximation to the terms on the right-hand side of equation 1. The finite-difference approximation is explicit if the concentration at the old time level C^n is used in the calculation of the RHS and it is implicit if the concentration at the new time level C^{n+1} is used.

Equation 51 constitutes the basic algorithm of the mixed Eulerian-Lagrangian methods. In these methods, the term C_m^{n*} in equation 51, which accounts for the effect of advection, is solved with a Langrangian method in a moving coordinate system. The second term $\Delta t * RHS$ of equation 51, which accounts for the effects of dispersion, sink/source mixing, and chemical reactions, is solved with either the explicit or implicit finite-difference method on a fixed Eulerian grid.

A conventional particle tracking technique is used to solve the advection term. At the beginning of the simulation, a set of moving particles is distributed in the flow field. A concentration and a position in the Cartesian coordinate system are associated with each of these particles. Particles are tracked forward through the flow field using a small time step. At the end of each time step, the average concentration at cell *m* due to advection alone over the time step, i.e. C_m^{n*}, is evaluated from the concentrations of

moving particles which are located within that cell. If a simple arithmetical averaging algorithm is used, this average concentration is expressed by the following equation:

$$C_m^{n*} = \frac{1}{NP_m} \sum_{p=1}^{NP_m} C_p^n \text{ if } NP_m > 0$$

Where NP_m is the number of particles within cell *m*, and C_p^n is the concentration of the p^{th} particle at the old time level (*n*). This equation is applicable only if the model grid is regular.

After completing the evaluation of C_m^{n*} for all cells, a weighted concentration $C_m^{\hat{n}}$ is calculated based on C_m^{n*} and the concentration at the old time level C_m^n:

$$C_m^{\hat{n}} = \omega C_m^{n*} + (1-\omega) C_m^n$$

Where ω is a weighting factor between 0.5 and 1.

The First-order Euler algorithm is used for particle tracking. A uniform step size is used for all moving particles during each transport step in the particle tracking calculations. For particles located in areas of relatively uniform velocity, the First-order Euler algorithm is sufficiently accurate. However, for particles in areas of strongly converging or diverging flows (for example near sources or sinks), a higher-order algorithm, the Fourth-order Runge Kutta algorithm, is used to provide a more accurate solution.

$C_m^{\hat{n}}$ is then used to calculate the second term in equation 51, or the changes in concentration due to dispersion, sink/source mixing, and chemical reactions (the terms on the right hand side of equation 49) with either the explicit or implicit finite-difference method. If the explicit finite difference method is used, then:

$$\Delta C_m^{n+1} = \Delta t * RHS\left(C_m^{\hat{n}}\right)$$

The use of the weighted concentration represents an averaged approach because the processes of dispersion, sink/source mixing, and/or chemical reactions occur throughout the time step. The concentration for cell *m* at the new time level (*n+1*) is then the sum of the C_m^{n*} and ΔC_m^{n+1} terms. The concentrations of all moving particles are also updated to reflect the change due to dispersion, sink/source mixing, and chemical reactions. This completes the calculation of one transport step for the Method of Characteristics. The procedure is repeated until the end of the desired time period is reached.

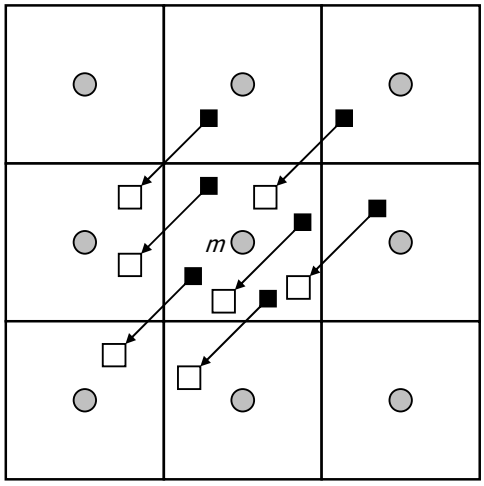

Figure 40: Illustration of the MOC technique. A set of moving particles are tracked forward during each time period. An intermediate concentration for cell *m*, equal to the weighted average of the concentrations of all particles in the cell, is computed. This intermediate concentration accounts for the effect of advection alone during a time step Δt, and is used to calculate changes in concentration due to dispersion and other processes over that time step.

The main advantage of the MOC technique is that it is virtually free of numerical dispersion caused by spatial truncation errors. The major drawback of the MOC technique is that it can be slow and requires large amount of computer memory. The MOC technique can also lead to large mass balance discrepancies under certain situations, because the discrete nature of the particle tracking based mixed Eulerian-Lagrangian solution techniques does not guarantee local mass conservation at a particular time step. In the computer code the memory requirement for the MOC technique is reduced through the use of a dynamic approach for particle distribution. The mass balance discrepancy problem is also mitigated to some degree through the use of consistent velocity interpolation schemes and higher-order particle tracking algorithms.

Appendix E Model settings

Parameters

Parameter	Value	Unit
Conductivity K_x	30	m/d
Conductivity K_y	30	m/d
Conductivity K_z	3	m/d
Specific storage S_s	1e-4	1/m
S_y	0.20	-
Effective porosity n_{eff}	0.15	-
Total porosity n_{tot}	0.30	-
Recharge	0	-
Evapotranspiration	0	-
Extinction Depth	0	-
Longitudinal dispersivity α_L	0.1	-
Horizontal/longitudinal dispersivity α_H	0.1	-
Vertical/longitudinal dispersivity α_V	0.01	-
Diffusion coefficient D	0	-
Salinity groundwater	42000	Mg/l
Salinity drinking water	0	Mg/l

Calculation settings

VDF settings	Initial time step	0.1
	VDF and IMT	explicitly coupled
	Internodal density calculation algorithm	Upstream weighted
	Variable density water table correction	not applied
Flow settings	Solver	SAMG
	Max iterations	100
	Max cycles	50
	Budget closure criterion	1e-4
	Damping factor	1
	Max damping factor	1
	Min damping factor	0.2
Transport settings	Solution option advection	MOC
	Dispersion, reaction, sinks and sources	Explicitly solved
	Initial step size	0.1
	Max step size	10
	Multiplier	1.2
	Porosity	Effective porosity
	Min saturation thickness	0.01
	Courant number	0.75
MOC settings		
Particle tracking method	4^{th} order Runge Kutta for sinks and sources, Euler elsewhere	
Particle parameters	Concentration weighting factor	0.5
	Max number of particles	1.000.000
	Min number of particles per cell	2
	Max number of particles per cell	30
	Number of planes	2
	Negligible gradient	1e-5
	Particles for C<negligible gradient	0
	Particles for C>negligible gradient	16
	Critical concentration gradient	0.001
	Particle pattern	Random
Flow settings		
Flow	Layers	0: Confined, constant S,T
	Rewetting	Active cell rewetting
Transport settings		
Transport	Max transport time steps	100.000

Appendix F Sensitivity analyses

In this appendix the results of sensitivity analyses are given. The heads for flow to a well in a confined aquifer in a radial symmetric cross section model (SEAWAT) are compared to the analytical solution. The optimal grid size, calculation method and calibration criterion were sought.

Grid size

The head results of model simulations with a grid size of 0.5 m and of 1 m are compared to the analytical solution. The results are given in Table 7 and Figure 41.

Table 7: RMSE analytical vs numerical (SEAWAT).

	With first point	Without first point
Grid size 0.5 m	4.68e-3	4.44e-3
Grid size 1.0 m	3.90e-3	3.85e-3

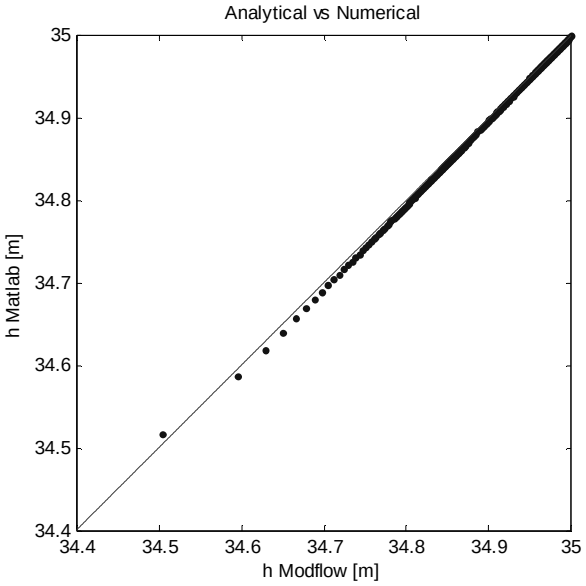

Figure 41: The dots are the SEAWAT numerical result and the line is the analytical solution with a grid size of 1 m.

The error is smaller than for the model with a grid size of 0.5 m. The velocity is too high, the particles pass more than one cell per time step. It is better to use a grid size of 1.0 m instead of 0.5 m.

Calculation method

The heads calculated with the TVD method and the MOC method, are compared to the analytical solution. The results are given in

Table 8, and in Figure 42 and Figure 43.

Table 8: RMSE analytical vs numerical (SEAWAT).

	With first point	Without first point
Modflow with MOC	4.68e-3	4.44e-3
Modflow with TVD	4.73e-3	4.48e-3

The TVD method has a larger error than the MOC method, as was already found in theory. The MOC method will be used for the modeling effort.

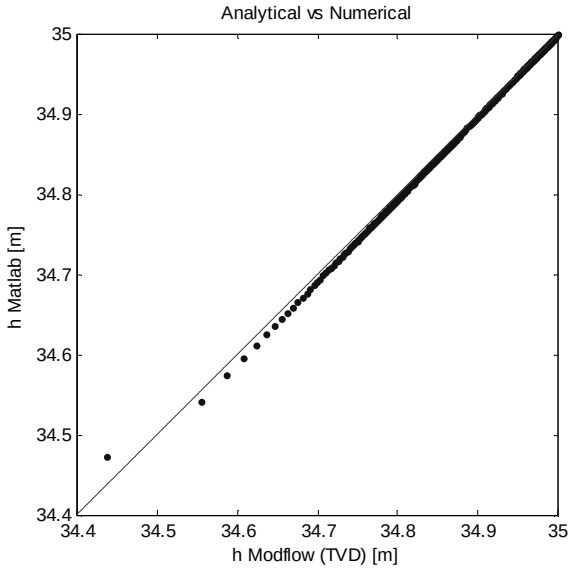

Figure 42: Analytical vs Numerical (TVD). The dots are the SEAWAT numerical result with the TVD method as numeric engine and the line is the analytical solution.

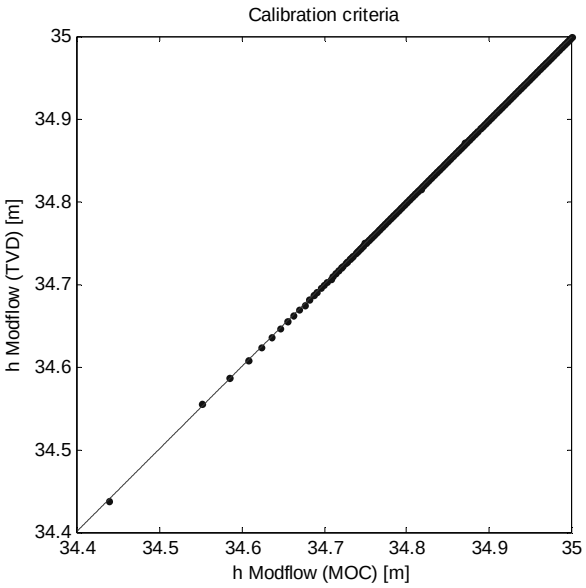

Figure 43: TVD vs MOC.

Calibration criterion

The heads calculated with a calibration criterion of 1e-4 and 1e-2 are compared to the analytical solution. The results are given in Table 9, and in Figure 44 and Figure 45.

Table 9: RMSE analytical vs numerical (SEAWAT).

	With first point	Without first point
1e-4	4.68e-3	4.44e-3
1e-2	4.11e-3	3.85e-3

The error with the analytical solution is smaller with a calibration criterion of 1e-2 instead of 1e-4. This is strange. When models with two density fluids were made, a calibration criterion of 1e-4 appeared to be necessary to give a good representation of the mixing zone. A calibration criterion of 1e-4 is used in the modeling effort.

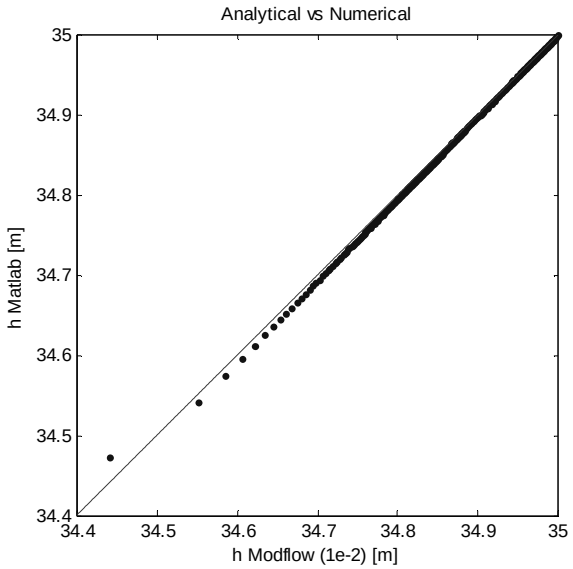

Figure 44: Analytical vs Numerical (1e-2). The dots are the SEAWAT numerical result with a calibration criterion of 1e-2 and the line is the analytical solution.

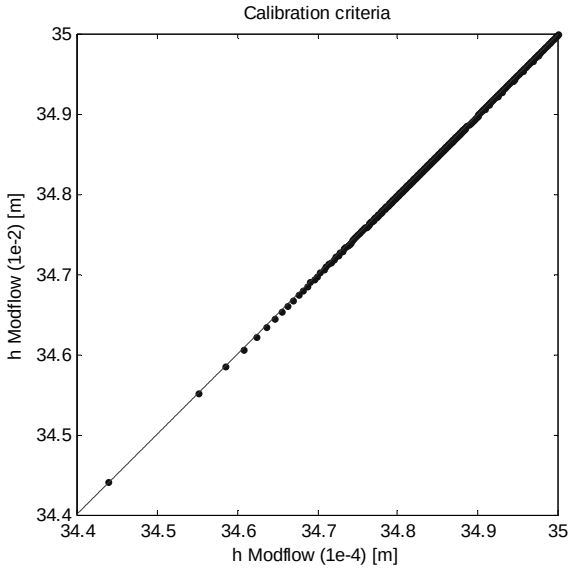

Figure 45: Calibration criterion 1e-4 vs calibration criterion 1e-2.